The Pennsylvania State University

The Graduate School

Eberly College of Science

FRACTIONAL QUANTUM HALL EFFECT IN HIGHER LANDAU LEVELS AND IN GRAPHENE

A Thesis in Physics

by

Csaba Tőke

Submitted in Partial Fulfillment
of the Requirements
for the Degree of

Doctor of Philosophy

May 2007

The thesis of Csaba Tőke was reviewed and approved* by the following:

Jainendra K. Jain
Erwin Müller Professor of Physics
Thesis Adviser
Chair of Comittee

Gerald D. Mahan
Distinguished Professor of Physics

Vincent H. Crespi
Professor of Physics
Professor of Materials Science and Engineering

Lyle N. Long
Distinguished Professor of Aerospace Engineering and Mathematics

Jayanth R. Banavar
Professor of Physics
Department Head

*Signatures are on file in the Graduate School.

Abstract

In this dissertation I try to extend the composite fermion model, the key to our understanding of the fractional quantum Hall effect (FQHE), beyond its primary domain (media with quadratic dispersion relation, lowest Landau level).

The poor performance of the standard composite fermion wave functions in the $\frac{1}{5}$ to $\frac{4}{5}$ filling factor range of the second Landau level of media with quadratic dispersion is caused by the significant residual interaction between composite fermions. A perturbative improvement to the composite fermion wave function describes the exact ground state very accurately for small systems in the disk geometry in this range. Using the same approach in the spherical geometry the excitation gap is estimated at filling factor $\frac{7}{3}$.

The FQHE at half-filled second Landau level ($\frac{5}{2}$ and $\frac{7}{2}$) has been a long standing enigma. The popular Pfaffian model of Moore and Read is reviewed and scrutinized. In an exact diagonalization study on finite systems it is shown that the Pfaffian model provides an inadequate description of the excitations, whose non-Abelian braiding statistics has been exploited in several proposals for quantum computing. An alternative understanding of the $\frac{5}{2}$ FQHE within the composite fermion theory is presented. The residual interaction between composite fermions is found to play a crucial role in establishing incompressibility at $\frac{5}{2}$. The low-energy spectrum and the activation gap are estimated with the help of a perturbative procedure that incorporates inter-composite-fermion interactions. This approach is amenable to systematic improvement, and produces ground as well as excited states. It, however, does not relate to non-Abelian statistics in any obvious manner.

Graphene, a single-layer hexagonal form of carbon, provides a two-dimensional electron system with two unusual properties: the low-energy electronic states have a linear dispersion, and the two sublattices of the hexagonal lattice introduce a valley degree of freedom.

Both have consequences for the FQHE, which remains to be observed.

For large Zeeman energy, the low-energy electronic states still have an SU(2) valley symmetry. Phenomena formerly discussed for the vanishing Zeeman energy limit in GaAs are predicted to occur here: purely interaction-induced integer plateaus, large pseudoskyrmions, fractional sequences, even/odd numerator effects, composite fermion pseudoskyrmions, and a pseudospin-singlet composite-fermion Fermi sea. As a consequence of the linear dispersion of the low-energy carriers the $|n| = 1$ Landau level is predicted to show more robust FQHE than the $n = 1$ Landau level of GaAs.

If the Zeeman energy is much smaller than the interaction energy scale, the system is approximately SU(4) symmetric. New FQHE states are predicted at fractions $\frac{n}{2pn\pm1}$ with $n \geq 3$, which involve an essential interplay between the spin and valley degeneracies. Conditions for the observation of these states are outlined, and the structure of these states and their excitations is described. Zero-temperature phase transitions are predicted to occur between these states when the SU(4) symmetry is weakly broken by external fields.

Contents

List of Figures

List of Tables

Abbreviations

CF	Composite fermion
FQHE	Fractional quantum Hall effect
IQHE	Integer quantum Hall effect
LL	Landau level
MOSFET	Metal-oxide-semiconductor field-effect transistor
PfQH sector	Pfaffian quasihole section. Cf. definition below Eq. (3.8) on p. 52
2DEG	Two-dimensional electron gas
ODLRO	Off-diagonal long range order
p-h	particle-hole

List of symbols

$H^{\mathrm{qu.}}$	Hamiltonian for media with quadratic dispersion (GaAs), Eq. (2.1)
$H^{\mathrm{gr.}}$	Hamiltonian for media with linear dispersion (graphene), Eq. (2.14)
H_{K}	Kinetic energy, Eq. (2.1)
$V^{(\mathrm{C})}$	Coulomb interaction energy, Eq. (2.1)
$B_\perp$	Perpendicular magnetic field
$B_\parallel$	In-plane magnetic field
R_{xx}	Longitudinal magnetoresistance
R_{xy}	Hall resistance
ϕ_0	Magnetic flux quantum (hc/e)
l_B	Magnetic length, Eq. (2.4)
N	Number of electrons
N_h	Number of holes
ν	Filling factor, Eq. (2.10)
$\tilde{\nu}$	Filling factor with IQHE baseline removed, Eq. (4.2)
$\nu^{(n)}$	Filling factor in Landau level n
$\eta_{n,m}$	Single-particle state for GaAs, Eq. (2.6)
Q	Monopole strength, p. 16
Y_{Qlm}	Monopole harmonics, Eq. (2.20)
$\Psi_{p,s}^{(n,m)}$	Single-particle state for graphene, Eqs. (2.15) to (2.17)
Φ_1	Jastrow factor, Eqs. (2.11) and (2.21)
V_m	Haldane pseudopotential, Eq. (2.22)
$V_m^{(n)}$	Haldane pseudopotential in LL n, Eqs. (2.24) and (2.31)
$V_m^{(n)\mathrm{gr.}}$	Haldane pseudopotential in LL n of graphene, Eq. (2.33)

$\mathcal{P}_{\rm LLL}$	Projection to the lowest Landau level, p. 23
B^*	Effective magnetic field for CF's, p. 22
Q^*	Effective monopole strength for CF's, Eq. (2.36)
L^*	Effective total angular momentum for CF's, Eq. (2.37)
^{2p}CF	CF with $2p$ bound vortices, Sec. 2.5
$\chi^{(J)}$	Wave function in J-th order CF diagonalization, p. 27
$E^{(J)}$	The energy of $\chi^{(J)}$
$\chi^{(J)}(L)$	Wave function in J-th order CF diagonalization for given L, p. 27
$E^{(J)}(L)$	The energy of $\chi^{(J)}(L)$
$V^{\rm eff}(r)$	Effective real-space interaction, c.f. Eqs. (3.1), (3.10), and (3.11)
$\Psi^{\rm Pf}$	Pfaffian wave function for the ground state, Eqs. (3.2) and (3.5)
$\Psi^{\rm Pf}_{\rm 2-qh}$	Pfaffian wave function for two quasiholes, Eqs. (3.3) and (3.6)
$\Psi^{\rm Pf}_{V}$	Pfaffian wave function for a vortex, Eqs. (3.4) and (3.7)
$V^{\rm (Pf)}$	Three-body model interaction, Eq. (3.8)
E_Z^S	Zeeman energy, p. 92
E_Z^P	Pseudo-Zeeman energy, p. 92
$E_Z^{S'}$	Effective Zeeman energy, Eq. (4.7)

Acknowledgements

This dissertation is based on my work done under the supervision of my advisor, Jainendra K. Jain. The results of this work have been published as Refs. [1, 2, 3, 4, 5, 6, 7]. (Ref. [2] is not used here.) I am greatly indebted to my advisor, as well as my coauthors: Michael R. Peterson, Gun-Sang Jeon and Chiachen Chang (Penn State University at the time of collaboration), Paul E. Lammert and Vincent H. Crespi (Penn State University), and Nicolas Regnault (Laboratoire Pierre Aigrain, Ecole Normale Supérieure).

The following figures are reproductions from other publications:

- Fig. 1.1 is taken from Paalanen, Tsui, and Gossard [9]. © 1982 The American Physical Society.
- Fig. 1.2 is taken from Störmer [11]. © 1998 The Nobel Foundation.

The data presented and analyzed in this study was mostly calculated by the author, except for the following parts:

- Figs. 3.8 and 3.9, and Table 3.3 present data obtained by Michael R. Peterson,
- Figs. 3.12 to 3.16 were produced by Nicolas Regnault. The data in Tables 3.10, 3.6, and 3.7 was partly obtained by Nicolas Regnault.
- Fig. 2.4 was drawn by Gun-Sang Jeon.

For most calculations I used parts of software codes developed by my predecessors in prof. Jain's group.

Chapter 1

Introduction

1.1 The quantum Hall effects

The quantum Hall effect is observed when a two-dimensional electron gas (2DEG), implemented in high mobility samples, is subjected to a high perpendicular magnetic field ($B_\perp$) at low temperatures. The effect consists of quantized plateaus superimposed on the semiclassical line $R_{xy} = \frac{B_\perp}{ec}$ of the Hall resistance [33], and a concomitant vanishing longitudinal magnetoresistance (R_{xx}) at the center of the plateaus (c.f. Figs. 1.1 and 1.2). The plateaus are quantized as

$$R_{xy} = \frac{h}{fe^2}, \tag{1.1}$$

for characteristic integer and fractional values of f, and occur when the so-called filling factor,

$$\nu = \frac{\rho hc}{eB_\perp} \approx f.$$

(ρ is the electron density.) We speak about the integer quantum Hall effect (IQHE, von Klitzing, Dorda, and Pepper [8]) when f is an integer (Fig. 1.1), and about the fractional quantum Hall effect (FQHE, Tsui, Störmer, and Gossard [10]) when f is a rational fraction (Fig. 1.2).

The quantum Hall effect is understood as a consequence of the incompressibility (excitation gap) of the 2DEG at certain parameters values ($B_\perp$, ρ) and the localization of a macroscopic fraction of states by disorder. By Laughlin's classical argument [48] (c.f. also

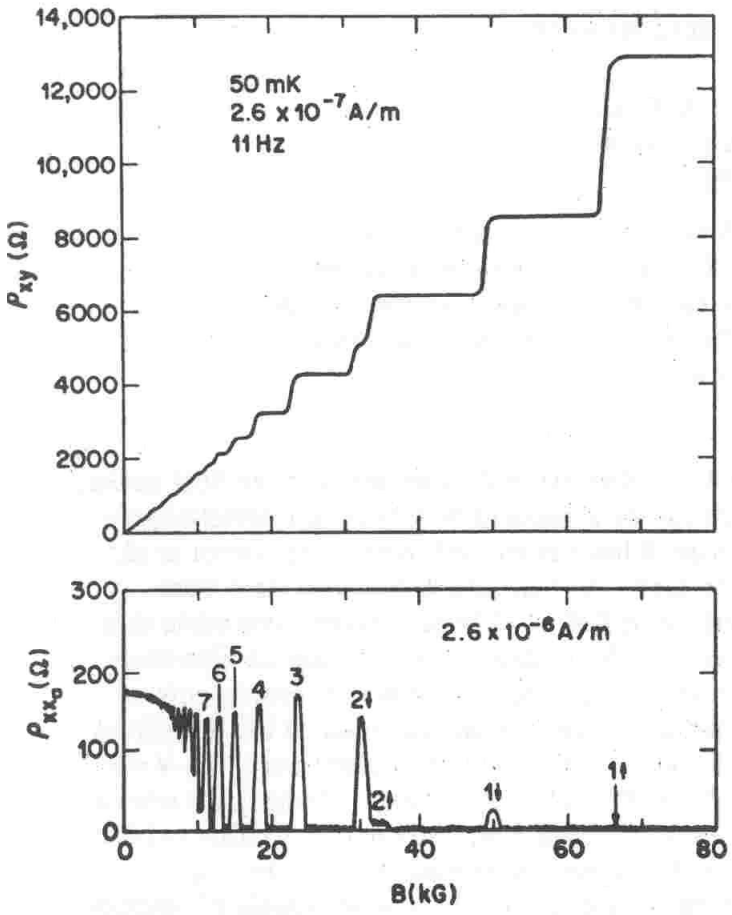

Figure 1.1: Integer quantum Hall effect in an GaAs/$Al_xGa_{1-x}As$ heterojunction sample. From Paalanen, Tsui, and Gossard [9]. The $n = 1$ and $n = 2$ plateaus are spin-resolved. The authors estimate that in the $n = 1$ Landau level 93% of the states are localized, which they extrapolate to 97% in the $T \to 0$ limit.

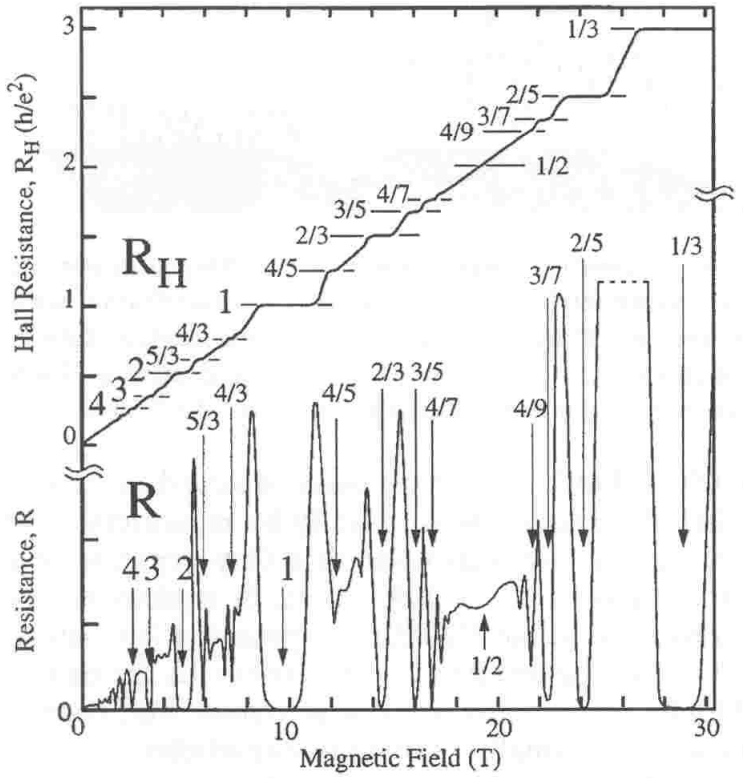

Figure 1.2: Fractional quantum Hall effect in an GaAs/$Al_xGa_{1-x}As$ heterojunction sample. From Horst Störmer's Nobel lecture [11].

Halperin [49]), if the disorder-free system has an excitation gap, after the introduction of a weak disorder the states localized by it will not contribute to the transport, thus keeping R_{xy} constant. Disorder induces a nonzero density of states in the gap, but still there remains a mobility gap, i.e., a gap for charged, delocalized excitations in the bulk.

The excitation gap for the IQHE is simply due to the well-known Landau quantization of the kinetic energy: the IQHE occurs when the electrons fill an integral number of Landau levels, and the charged excitations are electron-hole pairs with a gap corresponding to the cyclotron energy in the noninteracting picture. On the other hand, as the FQHE occurs at partially filled Landau levels, the gap here is due to the interparticle interaction.

Most of the observed FQHE states are in the lowest Landau level, which, taking the electron spin into account, means the $\nu < 2$ range; but there are some known plateaus in the second ($2 < \nu < 4$) [23, 25] and some hints in the third ($4 < \nu < 6$) Landau level [26]. The states belonging to the standard sequence

$$\nu = \frac{n}{2pn \pm 1}, \tag{1.2}$$

(with integers n, p) and their particle-hole conjugates ($\nu \to 1-\nu$ for the effectively spinless, $\nu \to 2-\nu$ for the spinful case), and their spin-reversed twins ($\nu \to 1+\nu$) are explained by the composite fermion theory (Jain [51]), which proceeds by variational wave function constructions for the ground state and the excited states, just like Laughlin's earlier theory [50].[1] Together with superfluidity and superconductivity, the fractional quantum Hall effect is one of the paradigmatic examples of emergent collective behavior due to quantum mechanical correlations.

This dissertation is an attempt to extend the applicability of the composite fermion model beyond the standard sequence (1.2) and the media where it is usually applied (media with quadratic dispersion, described by an effective Schrödinger's equation). In Chapter 3 I will address the problem of FQHE states in higher Landau levels, still assuming a standard medium. In particular, the state at $\nu = \frac{5}{2}$, the only well-established even denominator FQHE state, has received much recent attention because a paired composite fermion state [77] has been suggested [78, 80, 67] to occur at $\nu = \frac{5}{2}$, which would sustain excitation with

[1] The FQHE cannot be accounted for by Hartree-Fock, density functional, or perturbative methods.

non-Abelian braiding statistics [77, 81, 82, 83], that could be used in quantum computers [88, 90, 92, 93]. The origin of several states, e.g., at $\frac{12}{5}$ and $\frac{13}{5}$, is still unclear [86, 87]. In Chapter 4 I will study the peculiarities of the FQHE in graphene,[2] a single-layer hexagonal lattice of carbon, which was first produced a few years ago [42] and received much attention because of its simplicity, beauty, and its potential for demonstrating fundamental physics and implementing practical applications. In particular, I study the consequences of the linear dispersion of low-energy carriers in graphene, and the possible effects of the spin and valley degrees of freedom. The composite fermion theory provides insight and new predictions in this setting, too.

1.2 Implementations of the two-dimensional electron gas

The 2DEG can be implemented experimentally (i) in the inversion layer of silicon metal-oxide-semiconductor field-effect transistors (MOSFETs) (Fig. 1.3), (ii) at heterointerfaces and in quantum wells of GaAs/$Al_xGa_{1-x}As$ modulation-doped heterostructures (Fig. 1.4) built by molecular-beam epitaxy,[3] (iii) in similarly manufactured AlAs quantum wells [38] (iv) in single-layer hexagonal carbon lattices called graphene [42, 43], and (v) at the surface of liquid Helium. As the electron density in (v) is strongly bounded from above, the regime where quantum effects become important has not been approached. I review (i)-(iv) only as far it is helpful for understanding where the cited data comes from.

1.2.1 In silicon metal-oxide-semiconductor field-effect transistors

In the channel of Si MOSFETs the potential of the metallic gate is tuned so that, assuming a p-doped channel, the conduction band edge bends below the Fermi energy in the proximity of the oxide-semiconductor interface (Fig. 1.3). The resulting inversion layer is about 10 nm wide, a small fraction of the depletion layer (about 1 μm), where the band bending is such that the acceptor impurities, whose states are only slighltly above the top of the valence band, are negatively charged. Electrons are trapped in the triangular well in the inversion layer. The mobility Si MOSFET devices at low temperatures is limited by the

[2] When I write these lines, the FQHE in graphene has not been observed experimentally.

[3] Heterointerfaces can also be manufactured out of other semiconductors [13], but the carrier mobility in such structures is too low for FQHE experiments.

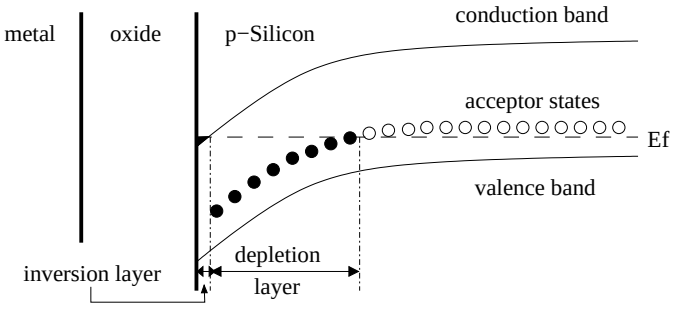

Figure 1.3: The emergence of an inversion layer in a silicon MOSFET. A detailed study of the electronic states in the inversion layer is provided by Stern and Howard [45].

scattering due to ionized acceptors in the depletion layer, and the surface states at the oxide-semiconductor interface. (Notice SiO_2 is an amorphous material, therefore the roughness of the surface cannot be eliminated.) The highest mobility reported for Si MOSFET's is about 4 m^2/Vs. It was in such a device that the integer quantum Hall effect was discovered [8]. If the MOSFET is grown on the (100) surface of Si, the carriers will occupy two valleys.

1.2.2 In semiconductor heterostructures

Much higher mobilities can be achieved in modulation doped GaAs/$Al_xGa_{1-x}As$ heterostructures. The goals are to decrease the scattering due to surface states, and to separate carriers from the ionized parent impurities in order to radically reduce disorder [14, 15]. One can exploit the fact that GaAs and AlAs have almost identical lattice constants (difference about 0.15%) and widely different band gaps 1.42 eV and 2.163 eV, respectively) and electroaffinities. For $Al_xGa_{1-x}As$ the lattice constant interpolates linearly, and the band gaps change monotonically, with a cusp at $x \approx 0.45$. For $x < 0.45$ the band gap is direct, for $x > 0.45$ it is indirect. At the interface of $Al_xGa_{1-x}As$ and $Al_yGa_{1-y}As$, with $x < y < 0.45$, both the conduction and the valence bands are shifted as shown in Fig. 1.4(a). A typical value is $\Delta E_c \approx 0.33$eV (conduction band) and $\Delta E_v \approx -0.04$eV (valence band) on the interface between GaAs and $Al_{0.3}Ga_{0.7}As$. Thus both electrons and holes are trapped on the GaAs side of the interface. If the $Al_xGa_{1-x}As$ side is n-doped, electrons migrate to the GaAs side of the interface, an electric field builds up; the conduction band bends so as to bind the electrons in an almost triangular quantum well.

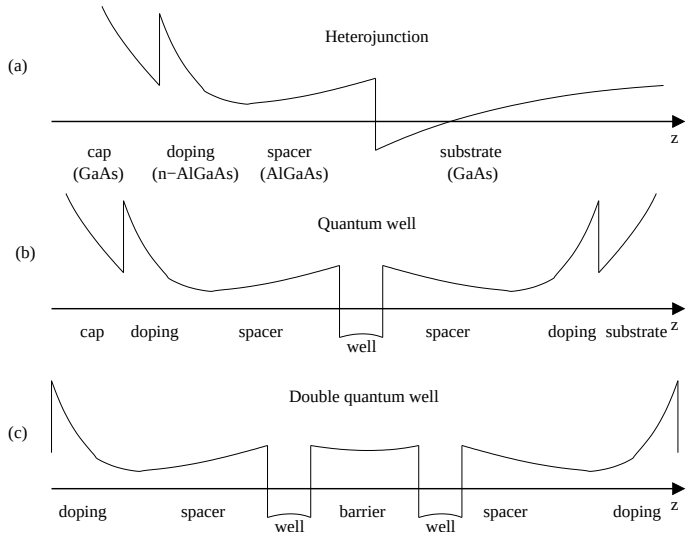

Figure 1.4: Typical $GaAs/Al_xGa_{1-x}As$ heterostructures used in quantum Hall experiments. The line shows the conduction band edge for n-channel case. (a) Simple heterointerface: the 2DEG forms on the GaAs side of the barrier-channel interface. (b) Simple quantum well doped symmetrically on both sides. (c) Bilayer implemented in double quantum well. A detailed study of the electronic states in the heterointerface (a) is given by Stern and Das Sarma [46].

This method increases the mobility by orders of magnitude at $\sim$ 10mK temperatures (recent publications [24, 25] cite $\mu = 3100$ m^2/Vs at $T = 9$mK), and by at least an order of magnitude at intermediate temperatures ($\mu \approx 15$ m^2/Vs reported [14] at $T < 100$K). With the flexibility of molecular beam epitaxy heterojunction and quantum well structures can be built in a highly controlled manner. See Fig. 1.4 for some typical applications.

1.2.3 In graphene

Graphene is a recently realized two-dimensional form of carbon [42, 43]. The carbon atoms are in a densely packed hexagonal (honeycomb) crystal structure. Graphene can be viewed as a monolayer extracted from graphite, or an unrolled single-walled carbon nanotube. Currently it is manufactured by a micromechanical cleavage of graphite on a SiO_2 surface, followed by the identification of monolayers by optical microscopy and atomic force microscopy [40]. Recently mobilities up to 5 m^2/Vs have been reached in the $T < 100$ K temperature range on graphene flakes a few microns wide by this method [44]. Efforts are being made to grow graphene by epitaxial methods, with the prospect of achieving higher mobilities and sample areas.[4] The low-energy carriers in graphene have a linear dispersion, as can be checked theoretically in the tight-binding approximation [103, 104], or experimentally by analyzing the Shubnikov-de Haas oscillations [42]. Carriers with linear dispersion are described by an effective massless Dirac equation with the Fermi velocity replacing the speed of light. Theoretically, it has been clarified that these carriers form a Fermi liquid (marginal Fermi liquid if the Fermi energy is at the Dirac points) in the absence of a magnetic field [94]. While the IQHE, including several probably interaction-induced odd-integer plateaus, has been demonstrated very accurately in graphene [42, 43, 44], the FQHE has not yet been observed so far. This may be due to the relatively low mobilities, or some properties of graphene that is still not properly understood.

1.3 Probes of spin physics in the quantum Hall regime

Part of this thesis is about spin-related physics in the fractional quantum Hall regime. This is a brief survey of our sources of information on spin physics.

[4] Graphene multilayers have been reported in the literature [41].

Tilted field experiments

As the filling factor is determined by the perpendicular magnetic field $B_\perp$, and the Zeeman energy is proportional to the total field

$$B = \sqrt{B_\perp^2 + B_\parallel^2},$$

introducing a nonzero in-plane $B_\parallel$ (i.e., tilting the total B) is a good probe. This method was used in several beautiful experiments, for example (i) Eisenstein *et al.* demonstrated a phase transitions between unpolarized and fully polarized states at even-numerator fractions [12]; (ii) Schmeller *et al.* [35] showed that the relevant excitation at $\nu = 1$ filling are skyrmions (with about seven filled spins), while they are single spin flip at $\nu = 3$ and 5. One should note, however, that because of the finite thickness of the 2DEG an in-plane field $B_\parallel$ may also deform the single-particle states, causing a weaker effective interparticle interaction. (The cited experiments were implemented in narrow GaAs quantum wells.) Thus the weakening of a FQHE state by the tilt angle does not necessarily imply that the state is not fully polarized [20, 21, 22, 80, 67].

Hydrostatic pressure

The Landé g-factor of GaAs can be tuned by hydrostatic pressure: starting from $g = -0.44$, it increases monotonically, changing sign at ~ 18 kbar. By measuring the excitation gap as a function of g, Leadley *et al.* observed small skyrmionic excitation consisting of about three reversed spin at $\nu = \frac{1}{3}$. They could also show that the excitations at $\nu = \frac{2}{5}$ are spin-reversed, and involve one spin only.

Optically pumped nuclear magnetic resonance

Nuclear magnetic resonance (NMR) [33] is an efficient probe of the magnetic structure of bulk materials, but as the NMR signal is detectable only for a large number of nuclei, its application in microscopic samples or thin films needs consideration. The signal can be enhanced by increasing the average spin polarization of the nuclei (^{71}Ga in the relevant case) via polarized optical pumping [31, 32]. Measuring the Knight shift (the difference of the nuclear fine structure resonance frequencies in the sample and in non-paramagnetic

compounds of the same element) gives direct information on the spin inbalance of the conduction bands. This technique yielded the first results on skyrmions at $\nu = 1$ filling by Barrett *et al.* [34].

Polarized absorption spectroscopy

By measuring the absorption of left- and right circularly polarized light in interband optical transitions, one can infer the relative occupancy of the spin-up and spin-down subbands of a Landau level, assuming a small but not negligible Zeeman energy. This measurement admits the estimation of the total spin per flux quantum with about 10% accuracy [36]. Using this method, Aifer *et al.* [36] can trace the spin polarization in the $0.6 < \nu < 1.6$ range, and analyzing the fast demagnetization in the neighborhood of $\nu = 1$ they can estimate the number of flipped spins in the skyrmionic excitations as ≈ 3.7 in their samples.

$Al_xGa_{1-x}As$ quantum wells

In $Al_xGa_{1-x}As$, the Landé g-factor depends on the Aluminum content: g changes monotonically from $g = -0.44$ to 0.5 as x goes from 0 to 0.35; g vanishes about $x \approx 0.13$. This fact can be exploited assuming that impurity scattering dominates over alloy scattering. By measuring the energy gap as a function of the tilt angle in a $Al_{0.13}Ga_{0.87}As$, Skhula *et al.* [37] observed skyrmions involving about fifty spin flips at $\nu = 1$ filling. (They estimate $g \approx 0.043$ in their experiment, slightly deviating from the ideal case.)

Valley-degenerate systems

Whenever two valleys are degenerate (AlAs, graphene, Si MOSFET's grown on the (100) plane of silicon), a pseudospin physics arises, which gives insights into how the real spin systems should behave in the elusive zero Zeeman energy limit. See, for example, Refs. [38].

Chapter 2

Theoretical basics

2.1 Media with quadratic dispersion

2.1.1 Hamiltonian

The single-layer Hamiltonian for the 2DEG is

$$H^{\mathrm{qu.}} = H_{\mathrm{K}} + V^{(\mathrm{C})} + g\mu_B \mathbf{B}\cdot\mathbf{S}; \tag{2.1}$$

$$H_{\mathrm{K}} = \frac{1}{2m_b}\sum_j \left(\mathbf{p}_j + \frac{e}{c}\mathbf{A}(\mathbf{r}_j)\right)^2, \tag{2.2}$$

$$V^{(\mathrm{C})} = \frac{e^2}{\epsilon}\sum_{i<j}\frac{1}{|\mathbf{r}_i - \mathbf{r}_j|}, \tag{2.3}$$

where m_b is the band mass of the electron and ϵ is the dielectric constant of the host semiconductor; $E_Z^S = g\mu_B\mathbf{B}\cdot\mathbf{S}$ is the Zeeman energy. In bulk GaAs, $m_b = 0.067m_e$, $\epsilon = 12.8$ and $g = -0.44$, where m_e is the electron mass. We use complex coordinates $z = x - iy$ on the plane. The distance is measured in units of the magnetic length

$$l_B = \sqrt{\hbar c/eB_\perp} \tag{2.4}$$

and interaction energy in units of $e^2/\epsilon l_B$.

2.1.2 Single-particle states

Single-particle states can be found conveniently in the symmetric gauge vector potential

$$\mathbf{A} = \left(\frac{-B_\perp y}{2}, \frac{B_\perp x}{2}, 0 \right). \tag{2.5}$$

In this gauge the angular momentum L_z commutes with both $H_{\rm K}$ and $V^{(\rm C)}$, and the common eigenfunctions of L_z and $H_{\rm K}$ may be written as

$$\begin{aligned} \eta_{n,m}(z) &= \frac{1}{\sqrt{2\pi n!(n+m)!}} (a^\dagger)^n (b^\dagger)^{n+m} e^{-|z|^2/4} \\ &= \frac{(-1)^n \sqrt{n!}}{\sqrt{2^{m+1}\pi (m+n)!}} z^m L_n^m \left(\frac{|z|^2}{2} \right) e^{-|z|^2/4}. \end{aligned} \tag{2.6}$$

where the raising and lowering operators are defined as

$$a = \frac{\alpha + \beta}{\sqrt{2}}, \qquad b = \frac{\alpha^\dagger - \beta^\dagger}{\sqrt{2}}, \tag{2.7}$$

$$\alpha = \frac{z}{2}, \qquad \beta = \partial_x + i\partial_y = 2\partial_{z^*},$$

where $n \geq 0$, $n + m \geq 0$. The (kinetic) energy levels

$$E_n = \hbar\omega_c \left(n + \frac{1}{2} \right) \tag{2.8}$$

are called Landau levels (LL's), and each has a macroscopic degeneracy

$$\frac{AB_\perp}{\phi_0}, \tag{2.9}$$

where $\phi_0 = hc/e$ is the quantum of magnetic flux and A is the area of the sample. One can introduce the dimensionless filling factor ν as the ratio of the electron number and the degeneracy of a Landau level:

$$\nu = \frac{N_e}{AB_\perp/\phi_0} = \frac{\rho hc}{eB_\perp} = 2\pi l_B^2 \rho, \tag{2.10}$$

where $\rho = N_e/A$ is the electron density. The problem of diagonalizing $H^{\text{qu.}}$ is difficult, as for $k_B < \hbar\omega_c$ the kinetic energy is quenched and $V^{(\text{C})}$ is the only relevant term; there is no small parameter.

2.1.3 Many-body states, disk geometry

The Fock space over single-particle states $\eta_{n,m}$ (Eq. (2.6)) can be made finite by fixing the Landau level n and the total angular momentum L. This effectively confines the electrons to a disk. (This approach is sometimes called "disk geometry".) The filling factor can be tuned by varying L. Unfortunately, the filling factor is in general not a well-defined quantity for a finite disk system. For certain wave functions, however, it is possible to write a relation between L and ν for a finite N. The Fock state with all single-particle states filled up to a certain limit, the finite representation of the $\nu = 1$ IQHE state, takes the form

$$\Phi_1 = \prod_{i<j}(z_i - z_j)e^{-|z|^2/4}, \tag{2.11}$$

and occurs at $L = \binom{N}{2}$. Laughlin's ground state wave function [50] for $\nu = \frac{1}{2p+1}$ (where p is an integer),

$$\Psi_{1/(2p+1)} = \prod_{i<j}(z_i - z_j)^{2p+1}e^{-|z|^2/4}, \tag{2.12}$$

satisfies the relation

$$\nu = \frac{1}{2p+1} = \binom{N}{2}\frac{1}{L}. \tag{2.13}$$

We thus know what L value corresponds to $\nu = \frac{1}{2p+1}$ in the disk geometry (including $p = 0$), and it is natural to assume that the filling factor decreases monotonically with L. From Eq. (2.10) the radius of the disk can be estimated as

$$R = \sqrt{\frac{2N}{\nu}}l_B.$$

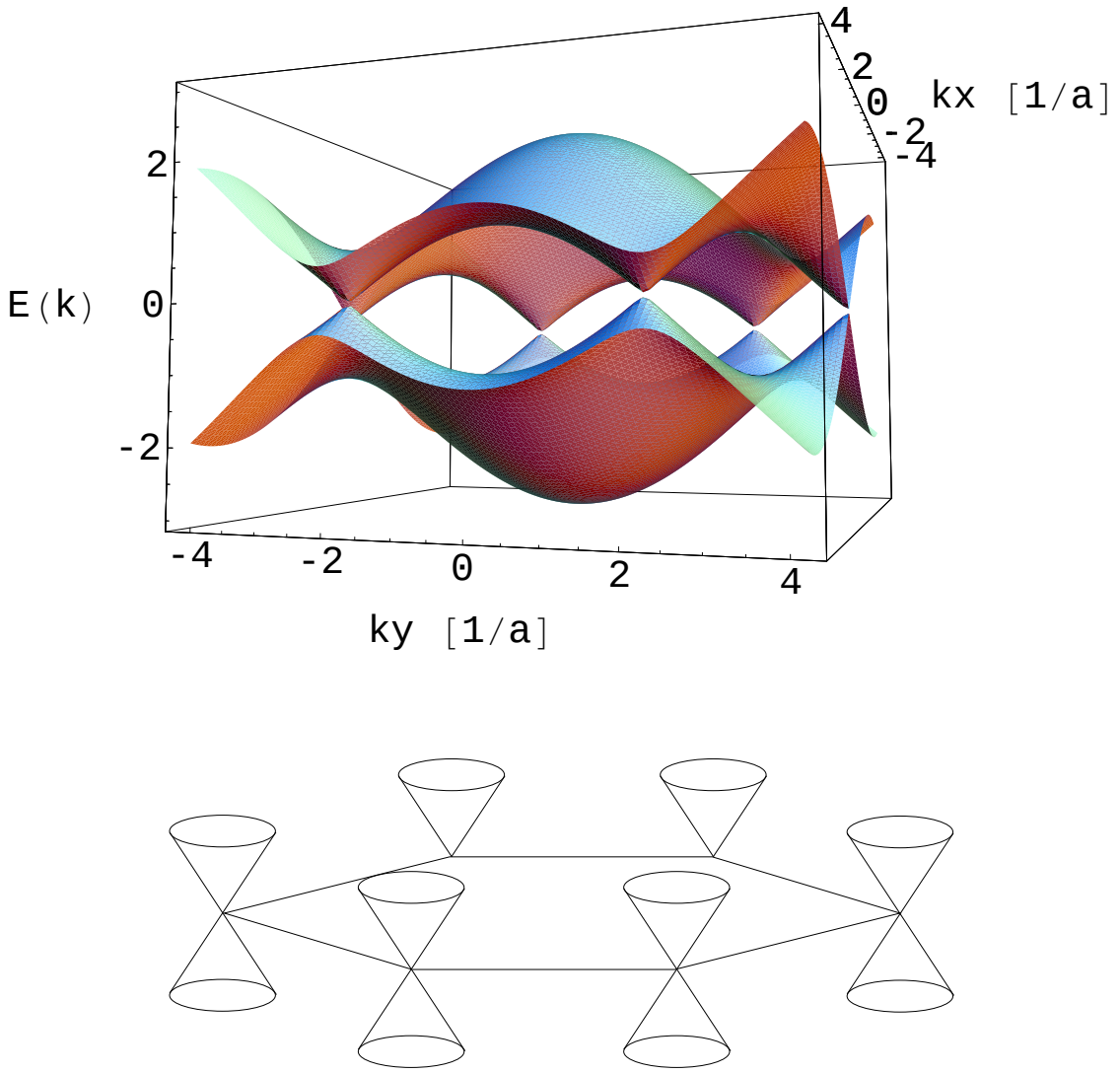

Figure 2.1: Top: the band structure of graphene from the tight-binding approximation [103, 104]. The valence and conductance bands touch at the corners of the hexagonal first Brillouin zone, called Dirac or Fermi points. Around the Dirac points the dispersion is linear up to very high energies ($\sim$ 1000 K). Bottom: simplified low-energy band structure.

2.2 Media with linear dispersion

2.2.1 Hamiltonian

The electronic structure of graphene is well described by a tight binding model [103, 104], which gives a vaulted band structure with the valence and conductance bands touching in the symmetry protected Dirac (or Fermi) points at the six corners of the hexagonal first Brillouin zone (Fig. 2.1). The low energy states, in particular, occupy double cones [105] with apices at the corners. Only two of these six double cones are inequivalent, giving rise to a valley degree of freedom, which is conveniently described as a pseudospin. Denoting spin by $\mathbf{S}$ and pseudospin by $\mathbf{P}$, the low energy states are described in the continuum approximation by an effective Hamiltonian [103]

$$H^{\text{gr.}} = v_F \begin{pmatrix} \sigma \cdot \mathbf{\Pi} & 0 \\ 0 & (\sigma \cdot \mathbf{\Pi})^{\mathrm{T}} \end{pmatrix} + \Delta P_z + g\mu_B \mathbf{B} \cdot \mathbf{S}, \tag{2.14}$$

that acts on 4-spinor Hilbert space. Here $v_F \approx 10^6$ m/s is the Fermi velocity [42, 43], $\mathbf{\Pi} = \mathbf{p} + \frac{e}{c}\mathbf{A}$, Δ is the on-site energy difference between the two sublattices, $E_Z^P = \Delta p_z$ is the pseudo-Zeeman energy, $P_i = 1 \otimes \frac{1}{2}\sigma_i$ is the pseudospin operator, and $\mathbf{S}$ is the spin. In this formalism the first and third elements of the 4-spinors are amplitudes on the A sublattice, the second and the fourth elements are amplitudes on the B sublattice; $\Sigma = \frac{1}{2}\sigma_z \otimes 1$ is the sublattice index operator.

2.2.2 Single-particle states

In the symmetric gauge (2.5) the Hamiltonian $H^{\text{qu.}}$ is diagonalized by the eigenvectors

$$\Psi^{(0,m)}_{p=1/2,s} = \begin{pmatrix} 0 \\ \eta_{0,m} \\ 0 \\ 0 \end{pmatrix} \otimes \alpha_s, \qquad \Psi^{(0,m)}_{p=-1/2,s} = \begin{pmatrix} 0 \\ 0 \\ \eta_{0,m} \\ 0 \end{pmatrix} \otimes \alpha_s, \tag{2.15}$$

$$\Psi^{(n\neq 0,m)}_{p=1/2,s} = \frac{1}{\sqrt{2}} \begin{pmatrix} -\mathrm{sgn}(n) i \eta_{|n|-1,m} \\ \eta_{|n|,m} \\ 0 \\ 0 \end{pmatrix} \otimes \alpha_s, \tag{2.16}$$

$$\Psi^{(n\neq 0,m)}_{p=-1/2,s} = \frac{1}{\sqrt{2}} \begin{pmatrix} 0 \\ 0 \\ \eta_{|n|,m} \\ -\mathrm{sgn}(n) i \eta_{|n|-1,m} \end{pmatrix} \otimes \alpha_s, \tag{2.17}$$

where $\alpha_{1/2} = \begin{pmatrix} 1 \\ 0 \end{pmatrix}$, $\alpha_{-1/2} = \begin{pmatrix} 0 \\ 1 \end{pmatrix}$ are spinors, and $\eta_{n,m}$ is defined in Eq. (2.6). The energy levels are

$$E_{nps} = \mathrm{sgn}(n) \sqrt{\frac{2\hbar v_F^2 eB|n|}{c}} + \Delta p + g\mu_B B s. \tag{2.18}$$

The degeneracy is still given by Eq. (2.9). Notice that restricted to the $n = 0$ Landau level the sublattice and pseudospin operators Σ and P_z are equivalent.

2.3 Spherical geometry

Bulk properties are conveniently studied in the spherical geometry, introduced by Wu and Yang [61] and first applied to quantum Hall problems by Haldane [57]. In this geometry, electrons are constrained to move on the surface of a sphere and a radial magnetic field is produced by placing a magnetic monopole of strength Q at the center, where $2Q\phi_0$ is the magnetic flux through the surface of the sphere. $2Q$ is an integer according to Dirac's quantization condition [60].

The orbital angular momentum L and its z-component L_z are good quantum numbers. The single particle solution of Schrödinger's equation (relevant for carriers with quadratic

dispersion relation) Y_{qlm} are called monopole harmonics [61] and are given by

$$\begin{aligned} Y_{Qlm}(\theta,\phi) &= (-1)^{l+m}\sqrt{\frac{2l+1}{4\pi}\frac{(l+m)!(l-m)!}{(l+Q)!(l-Q)!}}e^{iQ\phi}u^{Q-m}v^{Q+m} \\ &\times\sum_{s=0}^{l-Q}\binom{l-Q}{s}\binom{Q+l}{l+m-s}(v^*v)^{l-Q-s}(u^*u)^s, \end{aligned} \tag{2.19}$$

where Q is the monopole strength, $l = Q + n$ is the single particle angular momentum, $n = 0, 1, \ldots$ is the LL (or shell) index, $m = -l, -l+1, \ldots, l$ is the z-component of angular momentum, and

$$u = \cos\left(\frac{\theta}{2}\right)e^{-i\phi/2}, \qquad v = \sin\left(\frac{\theta}{2}\right)e^{i\phi/2}. \tag{2.20}$$

The eigenvalues of the kinetic energy are

$$E_{Qlm} = \frac{l(l+1)-Q^2}{2|Q|}\hbar\omega_c,$$

which converges to E_n of Eq. (2.8) in the $Q \to \infty$ limit with $l - Q = n$ fixed. The degeneracy of the n-th landau level is $2l + 1$. Thus one can unambigously define sequences of finite systems to represent any integer filling factor. Let Φ_m be the Fock state in which m Landau levels are completely filled. In particular, Φ_1 takes the simple form

$$\Phi_1 = \prod_{i<j}(u_iv_j - u_jv_i). \tag{2.21}$$

For Φ_m, $N = 2Qm + \binom{N}{2}$. This state corresponds to $\nu = m$, because

$$\nu = \lim_{N\to\infty}\frac{N}{2(Q+n)+1}.$$

Finite representations of fractional fillings are provided by composite fermion theory (Sec. 2.5 below).

For the Coulomb interaction the distance between particles r_{ij} is taken to be the chord distance $r_{ij} = 2R|u_iv_j - v_iu_j|$, where the radius of the sphere is $R = \sqrt{Q}$ in units of the magnetic length.

The single-particle solutions of the massless Dirac equation on the sphere are not known

to the author.

2.4 Pseudopotentials

2.4.1 Quadratic dispersion, planar geometry

Two-body interactions are characterized by the Haldane pseudopotentials [57, 58] V_m, which are the energies of two electrons in relative angular momentum m state,

$$\begin{aligned} V_m &= \frac{\langle \eta_{0,m}|V(z_1-z_2)|\eta_{0,m}\rangle}{\langle \eta_{0,m}|\eta_{0,m}\rangle} \\ &= \frac{1}{2^{2m+1}m!}\int rdrV(r)r^{2m}e^{-r^2/4} = \int qdq\tilde{V}(q)L_m(q^2)e^{-q^2}, \end{aligned} \tag{2.22}$$

where $V(\mathbf{r}) = 1/r$ is the Coulomb interaction, $\tilde{V}(\mathbf{q}) = \frac{2\pi}{q}$ is its Fourier transform, and L_m is a Laguerre polynomial. The Coulomb interaction can be written in terms of the pseudopotentials:

$$V^{(\mathrm{C})}|\psi\rangle = \sum_{i<j}\sum_m V_m P_m^{ij}|\psi\rangle, \tag{2.23}$$

where P_m^{ij} projects the wave function of the i,j-th particles into the state of relative angular momentum m. If the spatial part of the fermion wave function is fully antisymmetric (full spin polarization), only the odd m projections are nonzero. In spinful and multi-layer problems all V_m's are relevant.

When studying a state in the n-th LL we typically assume that the $0,\ldots,(n-1)$ LL's are completely filled and inert, and therefore one can diagonalize the interaction in the Hilbert subspace of the n-th LL. The existence of LL raising operators (2.7) in the planar geometry lets us map this problem to the lowest LL by using effective pseudopotentials $V_m^{(n)}$:

$$V_m^{(n)} = \frac{\langle \eta_{n,m}|V(z_1-z_2)|\eta_{n,m}\rangle}{\langle \eta_{n,m}|\eta_{n,m}\rangle}. \tag{2.24}$$

where $\eta_{n,m}$ is defined in Eq. (2.6). One can show that

$$\tilde{V}^{(n)}(\mathbf{q}) = \left(L_n\left(q^2/2\right)\right)^2\tilde{V}(q), \tag{2.25}$$

where $\tilde{V}^{(n)}(\mathbf{q})$ is the Fourier transform of the effective interaction for LL n. Then $V_m^{(n)}$ can

be calculated in a closed form by Eqs. (2.22) and (2.25) in a straightforward manner. For the first few Landau levels, for example,

$$V_m^{(0)} = \frac{\Gamma(m+\frac{1}{2})}{2\Gamma(m+1)}, \tag{2.26}$$

$$V_m^{(1)} = \frac{(m-\frac{3}{8})(m-\frac{11}{8})\Gamma(m-\frac{3}{2})}{2\Gamma(m+1)}, \tag{2.27}$$

$$V_m^{(2)} = \frac{(2^7m^2-608m+585)(2^7m^2-352m+105)\Gamma(m-\frac{7}{2})}{2^{15}\Gamma(m+1)}, \tag{2.28}$$

$$V_m^{(3)} = (2^{10}m^3-10368m^2+30680m-24801)\times (2^{10}m^3-7296m^2+13016m-3465)\frac{\Gamma(m-\frac{9}{2})}{2^{21}\Gamma(m+1)}. \tag{2.29}$$

The pseudopotentials of the lowest three LL's are shown in Fig. 2.2. With increasing LL index the short-range part of the interaction weakens, while the long-range behavior hardly changes.

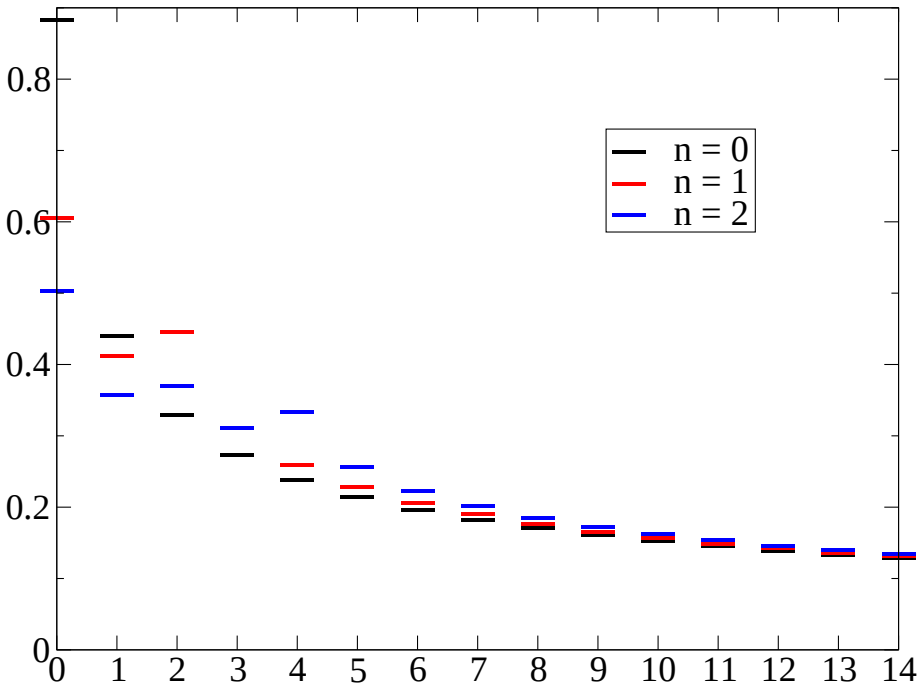

Figure 2.2: Pseudopotentials for $n \leq 2$ Landau levels in media with quadratic dispersion.

2.4.2 Quadratic dispersion, spherical geometry

The matrix elements can be expanded as [59]

$$\langle n, m_1; n, m_2 \mid V^{(\mathrm{C})} \mid n, m_3; n, m_4 \rangle = \sum_{j=0}^{2l} \langle l, m_1; l, m_2 \mid j, m_1 + m_2 \rangle \langle l, m_3; l, m_4 \mid J, m_3 + m_4 \rangle V_j^{(l)},$$

where $V_j^{(l)}$ is the energy of two electrons in the relative angular momentum $2l - j$ state ($l = Q + n$), and it can be calculated for highest weight states as [59]

$$\begin{aligned} V_j^{(l)} &= {}_2\left\langle j, j \left| \frac{1}{|r_1 - r_2|} \right| j, j \right\rangle_2, \\ |l, l\rangle_2 &= (u_1 v_2 - u_2 v_1)^{2l-J} u_1^j u_2^j. \end{aligned} \tag{2.30}$$

Then, with the help of the identities proven by Wu and Yang [61], the Coulomb pseudopotentials in the spherical geometry in the n-th LL are given by

$$\begin{aligned} V_m^{(n)} = \frac{1}{R} \sum_{m_1, m_2 = -l}^{l} \sum_{j = |m_1 - m_2|}^{2l} (-1)^{j + m_2 - m_1} \times \\ \langle 2l - m, 0 \mid l, m_1; l, -m_1 \rangle \langle 2l - m, 0 \mid l, m_2; l, -m_2 \rangle \times \\ \left| \langle l, m_1; j, m_2 - m_1 \mid l, m_2 \rangle \langle l, Q; j, 0 \mid l, Q \rangle \right|^2, \end{aligned} \tag{2.31}$$

where m is the relative angular momentum of two particles, $l = Q + n$, and $R = \sqrt{Q}\, l_B$ is the radius. Eq. (2.31) reduces to the expression in Fano, Ortolani and Colombo [59] for the lowest LL:

$$V_m^{(0)} = \frac{\binom{4Q-2J}{2Q-J}\binom{4Q+2J+1}{2Q+J+1}}{2R\binom{4Q+2}{2Q+1}^2},$$

with $J = 2Q - m$.

When working with effective interactions defined via power series, the pseudopotentials

of a monomial r^n in the lowest LL will prove useful[1]:

$$V_m[r^n] = \frac{1}{R}\frac{2^{n+4}\pi^2}{(2Q+n/2+1)!(2J+1)!}\sum_{k=0}^{J}\frac{(J!)^2(J+k)!(2Q+n/2-k)!}{k!(J-k)!}. \tag{2.32}$$

2.4.3 Linear dispersion, planar geometry

Let us evaluate the Coulomb matrix elements within the $n \neq 0$ Landau level of graphene. Write $|n_1, m_1; n_2, m_2; \ldots; n_N, m_N\rangle$ for the product state $\eta_{n_1,m_1} \otimes \eta_{n_2,m_2} \otimes \cdots \otimes \eta_{n_N,m_N}$ and $\| n_1, m_1; n_2, m_2; \ldots; n_N, m_N\rangle\!\rangle$ for $\Psi^{(n_1,m_1)} \otimes \cdots \otimes \Psi^{(n_N,m_N)}$. Then, by Eqs. (2.16) and (2.17),

$$\begin{aligned} 4\langle\!\langle n, m_1; n, m_2 \parallel V \parallel n, m_3; n, m_4\rangle\!\rangle = \langle n, m_1; n, m_2|V|n, m_3; n, m_4\rangle + \\ \langle n-1, m_1; n, m_2|V|n-1, m_3; n, m_4\rangle + \langle n, m_1; n-1, m_2|V|n, m_3; n-1, m_4\rangle + \\ \langle n-1, m_1; n-1, m_2|V|n-1, m_3; n-1, m_4\rangle. \end{aligned}$$

By angular momentum conservation, these matrix elements are proportional to $\delta_{m1+m2,m3+m4}$. The problem of interacting electrons in the n-th graphene LL thus formally maps into that of the lowest GaAs LL with an effective interaction defined by the pseudopotentials

$$\begin{aligned} V_m^{(n)\mathrm{gr.}} &= \frac{1}{4}\left(V_m^{(n)} + V_m^{(n-1)} + 2V_m^{(n,n-1)}\right), \\ V_m^{(n,n-1)} &= \int \frac{d^2q}{(2\pi)^2}\frac{2\pi}{q}L_n\left(\frac{q^2}{2}\right)L_{n-1}\left(\frac{q^2}{2}\right)e^{-q^2}L_m(q^2), \end{aligned} \tag{2.33}$$

where $V_m^{(n)}$ was defined in Eq. (2.25). As seen in Fig. 2.3, $V_m^{(1)\mathrm{gr.}}$ lies between $V_m^{(0)}$ and $V_m^{(1)}$, except for $m = 1$.[2]

2.4.4 Linear dispersion, spherical geometry

Not knowing the single-particle states of the massless Dirac equation on the sphere, I cannot calculate the pseudopotentials for this case. One can, however, use the pseudopotentials $V_m^{(n)\mathrm{gr.}}$ for the *planar* geometry on the sphere; this procedure gives the exact result for very

[1] This formula was derived by Chia-Chen Chang.

[2] The same result is derived in Refs. [96, 97, 98] in a slightly different formalism.

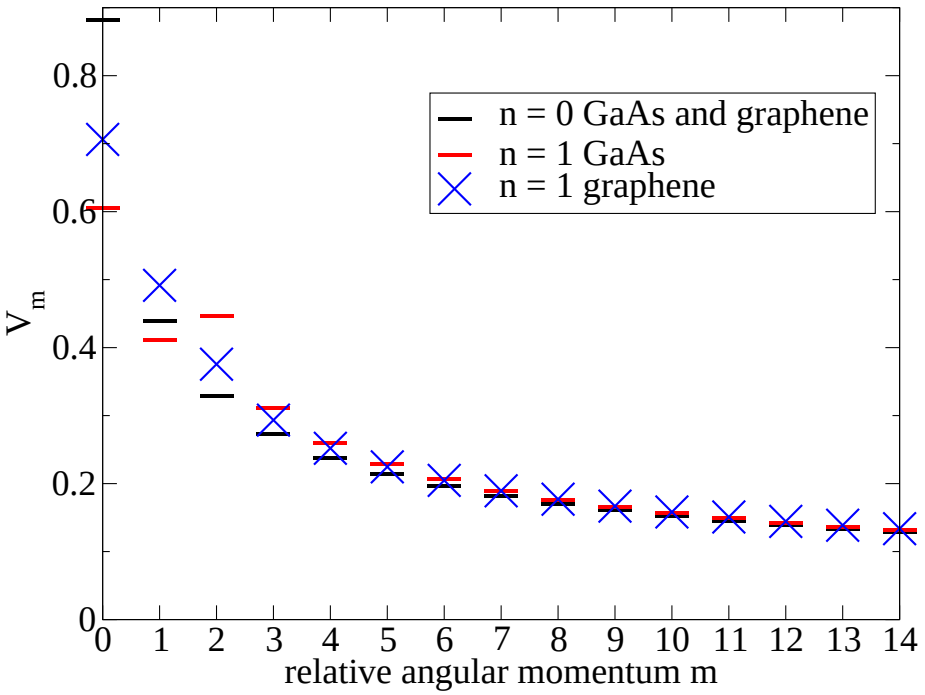

Figure 2.3: Pseudopotentials for $|n| = 1$ Landau levels in media with linear dispersion.

large systems and is generally a reasonable approximation. This method will be used in Secs. 4.2.2 and 4.3.2 below.

2.5 Composite fermions

2.5.1 Variational wave functions

Composite fermion (CF) theory [51, 52, 54, 56] describes the two-dimensional electron system in terms of composite fermions, which are electrons bound to an even number ($2p$) of quantized vortices. It was proposed [51] as a nonperturbative microscopic theory of the electron correlations in the lowest LL of the 2DEG in the fractional quantum Hall regime. The attached vortices partly cancel the Aharonov-Bohm phase, thus on the mean-field level CF's feel a reduced field $B^* = B_\perp - 2p\rho\phi_0$. The lowest LL splits into "Λ-levels" of composite fermions, which are analogous to Landau levels of electrons in the reduced field B^*. If B and B^* point in the same direction (parallel flux attachment), CF formation is

defined microscopically by the mapping

$$\Psi_Q = \mathcal{P}_{\rm LLL}\Phi_1^{2p}\Phi_{Q^*}, \tag{2.34}$$

$$\Psi_L = \mathcal{P}_{\rm LLL}\Phi_1^{2p}\Phi_{L^*}, \tag{2.35}$$

where Φ_{Q^*} (Φ_{L^*}) is a wave function for N electrons at monopole strength Q^* (total angular momentum L^*), the Jastrow factor Φ_1^2 attaches two vortices to them, and $\mathcal{P}_{\rm LLL}$ projects its argument into the lowest LL[3]. Φ_1 coincides with the wave function of a completely filled Landau level, which are given by Eqs. (2.11) (apart from the Gaussian part) and (2.21) for the disk and the sphere, respectively. The monopole strengths (total angular momenta) are related by

$$Q = Q^* + p(N-1), \tag{2.36}$$

$$L = L^* + pN(N-1). \tag{2.37}$$

^{2p}CF denotes a composite fermion with flavor $2p$.

By Eqs. (2.36) and (2.37) that the filling factors of composite fermions (ν^*) and electrons (ν) are related as

$$\nu = \frac{\nu^*}{2p\nu^* + 1}. \tag{2.38}$$

I.e., whenever composite fermions fill an integral number of Landau levels, the electronic filling factor has the value of the quantized FQHE plateaus (Eq. (1.2) with + sign). Thus, if the gap due to the Landau quantization of the kinetic energy survives composite fermionization (Eqs. (2.34) and (2.35)), the FQHE of electrons is explained in an intuitively transparent manner as the IQHE of composite fermions. Various numerical studies show that this is indeed the case.

If B and B^* point in opposite directions (reverse or antiparallel flux attachment), the wave function construction and the relation between CF and electronic parameters

[3]For parallel flux attachment the projection procedure for CF wave functions was elaborated by Jain and Kamilla [54]. direction), and by Möller and Simon for antiparallel (or reverse) flux attachment (when B^* and B point in opposite directions).

(Eqs. (2.34) to (2.38) change as:[4]

$$\begin{aligned}
\Psi_Q &= \mathcal{P}_{\rm LLL}\Phi_1^{2p}\overline{\Phi_{Q^*}}, && (2.39)\\
\Psi_L &= \mathcal{P}_{\rm LLL}\Phi_1^{2p}\overline{\Phi_{L^*}}, && (2.40)\\
Q &= -Q^* + p(N-1),\\
L &= -L^* + pN(N-1),\\
\nu &= \frac{\nu^*}{2p\nu^* - 1}.
\end{aligned}$$

States obtained by reverse flux attachment generate the other stardard fractions (Eq. (1.2) with $-$ sign).

Composite fermion theory recovers Laughlin's ground state wave function of Eq. (2.12) as a special case, justifies his quasihole wave function and improves upon [52, 53] his quasiparticle wave function proposed originally [50]. It gives a ground state with no free parameters at all fractions in the standard sequence $\nu = \frac{n}{2pn\pm 1}$, as well as quasihole, quasiparticle and exciton wave functions. The variational wave functions (2.34), (2.35), (2.39), (2.40) proved to be extremely accurate in numerical studies, and, as many consequences of this model been corroborated in experiments [56], one can safely regard composite fermions the true emergent particles in the fractional quantum Hall regime. The CF ground state and quasihole wave functions can be justified as the exact zero-energy solutions of a short range hard-core interaction, which in the pseudopotential representation takes the form

$$V_m = \delta_{1,m},$$

and, in real-space, becomes

$$V(z_1, z_1) = \nabla^2\delta(z_1 - z_2).$$

Thus composite fermions may form in two-dimensional systems where the kinetic energy is quenched and the inter-particle interaction is sufficiently sharp at short-range.

[4]For antiparallel flux attachment the projection procedure for CF wave functions was elaborated by Möller and Simon.

2.5.2 Composite fermions with nonorbital degrees of freedom

The composite fermion model easily generalizes to the spinful case [118, 117, 102, 119], and it provided an understanding of the singlet and partially polarized FQHE states. Here I give a generalization for the case of electronic states with SU(n) symmetric internal (nonorbital, spinlike) degree of freedom. The SU(4) symmetric CF model will be used in Sec. 4.3 for graphene in the spin and valley degenerate limit.

With a SU(n) symmetry, only those wave functions are legitimate which are eigenstates of the Casimir operators of SU(n) and the $n-1$ generators of the Cartan subalgebra [134] of SU(n). (For SU(2) these operators are simply S^2 and S_z.) These satisfy, for the so-called highest weight state [134], the Fock's cyclic condition [108]. The idea is to construct valid Hartree-Fock-like IQHE wave functions Φ, and then show that their "composite fermionization" (Eq. (2.34), (2.35), 2.39), and (2.40)) produces legitimate wave functions.

We are using the Young tableau notation $[m_1, \ldots, m_{n-1}]$ for the SU(n) multiplets: $m_1 \geq m_2 \geq \ldots m_{n-1} \geq 0$ are integers, m_i being the length of the i-th line of the Young tableau of the representation. (The last m_i's are omitted if zero.) Recall that Young tableaux are generated from the direct products of the fundamental representation (a single box) with symmetrization in the rows and antisymmetrization in the columns.

Let $\{\alpha^t\}$ be a basis of the (n-dimensional) fundamental representation of SU(n), and let M_t be the number of particles in the α^t internal state. Let

$$\Phi'(\{\vec{r}_j\}) = \mathcal{A}\left(\Phi(\{\vec{r}_j\})\prod_{t=1}^{n}\prod_{i=\min_t}^{\max_t}\alpha_i^t\right),$$

where $\min_1 = 1, \max_1 = M_1, \min_2 = M_1 + 1, \max_2 = M_1 + M_2, \ldots$, and $\mathcal{A}$ is the antisymmetrizer. Assume $\Phi(\{\vec{r}_j\})$ is antisymmetric in each subset $\{\min_t, \ldots, \max_t\}$ of its variables. $\Phi'(\{\vec{r}_j\})$ is a highest weight state (w.r.t. a choice of positive roots) if and only if it is annihilated by any attempt to antisymmetrize an electron l of type u ($\min_u \leq l \leq \max_u$) with respect to the electrons of type $t < u$, i.e.

$$\left(1 - \sum_{k=\min_t}^{\max_t}(k,l)\right)\Phi(\{\vec{r}_j\}) = 0, \tag{2.41}$$

where (k, l) permutes indices k and l.

Consequently, any orbital wavefunction

$$\Phi = \Phi_1 \Phi_2 \cdots \Phi_n, \tag{2.42}$$

where Φ_s's are Slater determinants such that any state (n, m) in Φ_s is also filled in Φ_{s-1} (conversely, if (n, m) is unfilled in Φ_s it is also unfilled in Φ_{s+1}), is a legitimate highest weight wave function for SU(n). This class includes IQHE states (Ψ_s has the lowest l_s Landau level completely filled; l_s's are in decreasing order), Fermi sea states, and single particle, single hole, and particle-hole pair states above the IQHE and Fermi sea states, provided that no hole is created in spin state s in a LL that is filled in Φ_{s+1}, and, conversely, no particle is created in spin state s in a LL that is unfilled in Φ_{s-1}.

If state Φ satisfies Fock's condition (2.41), so does Ψ given by Eqs. (2.34), (2.35) (2.39), or (2.40), and Ψ is therefore a legitimate state. Thus composite fermion states with parallel or antiparallel flux attachment can be constructed from electronic Hartree-Fock states as usual. CF variational wave functions for SU(2) systems thus generalizes trivially to SU(n) systems.

2.5.3 Composite fermion diagonalization

The wave functions generated from a single Slater determinant by Eqs. (2.35) and (2.34) can be regarded as a mean-field treatment of composite fermions. One can improve these wave functions by treating the residual inter-composite-fermion interaction successively by the procedure first described in Ref. [124]. The is to include successive order of Λ-level mixing caused by the residual interaction. Instead of the full lowest LL basis space, as is done in exact diagonalization studies, the Hamiltonian is diagonalized in a restricted basis of correlated states produced by the CF theory. In the n-th order of CF diagonalization, all basis states with at most n units of kinetic energy above the minimum possible for the given N, p and L^*/Q^* are collected:

$$\left\{ \{\Phi_\alpha^{(0)}\}, \{\Phi_\beta^{(1)}\}, \{\Phi_\gamma^{(2)}\}, \ldots, \{\Phi_\zeta^{(n)}\} \right\}.$$

A correlated CF basis at Q/L, of dimension $D^{(n)}$, is obtained through Eqs. (2.34) or (2.35),

$$\left\{\{\Psi_\alpha^{(0)}\},\{\Psi_\beta^{(1)}\},\{\Psi_\gamma^{(2)}\},\ldots,\{\Psi_\zeta^{(n)}\}\right\}, \tag{2.43}$$

with $n_i = l_i - Q^*$ now interpreted as the Λ-level index, and $\sum_i n_i$ as the total "CF kinetic energy." The Coulomb interaction $V^{(\mathrm{C})}$ is diagonalized in this basis. That requires a Monte Carlo evaluation of the direct product and interaction matrices

$$\langle\Psi_\alpha^{(n)}|\Psi_\beta^{(m)}\rangle \quad \text{and} \quad \langle\Psi_\alpha^{(n)}|V^{(\mathrm{C})}|\Psi_\beta^{(m)}\rangle, \tag{2.44}$$

respectively, orthogonalization by the standard Gram-Schmidt procedure, and numerical diagonalization. One can regard CF diagonalization as analogous to the "configuration interaction" method of quantum chemistry.

A diagonalization in this basis incorporates the effect of Λ-level mixing perturbatively. Fig. 2.4 gives an example of CF basis construction in the disk geometry. $\chi^{(J)}$ and $E^{(J)}$ wil denote the ground state wave function and the ground state energy obtained by CF diagonalization. $E^{(J)}$ is a strict upper bound on the exact energy. In the spherical geometry, $\chi^{(J)}(L)$ and $E^{(J)}(L)$ will refer to the ground state wave function and its energy obtained by CF diagonalization in the orbital angular momentum L sector.

For many values of the monopole strength Q (total angular momentum L) a unique state is obtained at the lowest level (i.e., $\Psi^{(0)}$ is unique), which gives a variational state with no free parameters. In the spherical geometry this happens only when ν^* is an integer. On the disk there are many such states (c.f. Table 3.2 below for example), called compact states [73]. Of course, by increasing J one will eventually obtain the exact state (although through an unnecessarily complicated route), but often a good approximation is obtained with at low orders. CF diagonalization results are nontrivial if the dimension of the correlated basis is much smaller than the dimension of the complete Hilbert space; then one can claim that CF formation captures the essential part of the electron correlation.

In the spherical geometry, excitations are obtained by promoting a CF from the highest filled Λ-level to the lowest empty Λ-level, leaving behind a hole. Thus in $\Psi_\eta^{(J)}$, at most J CF particle-hole pairs may exist. In the disk geometry, once a CF is raised to a higher Λ-level, its angular momentum is no longer fixed, and one can redistribute the angular

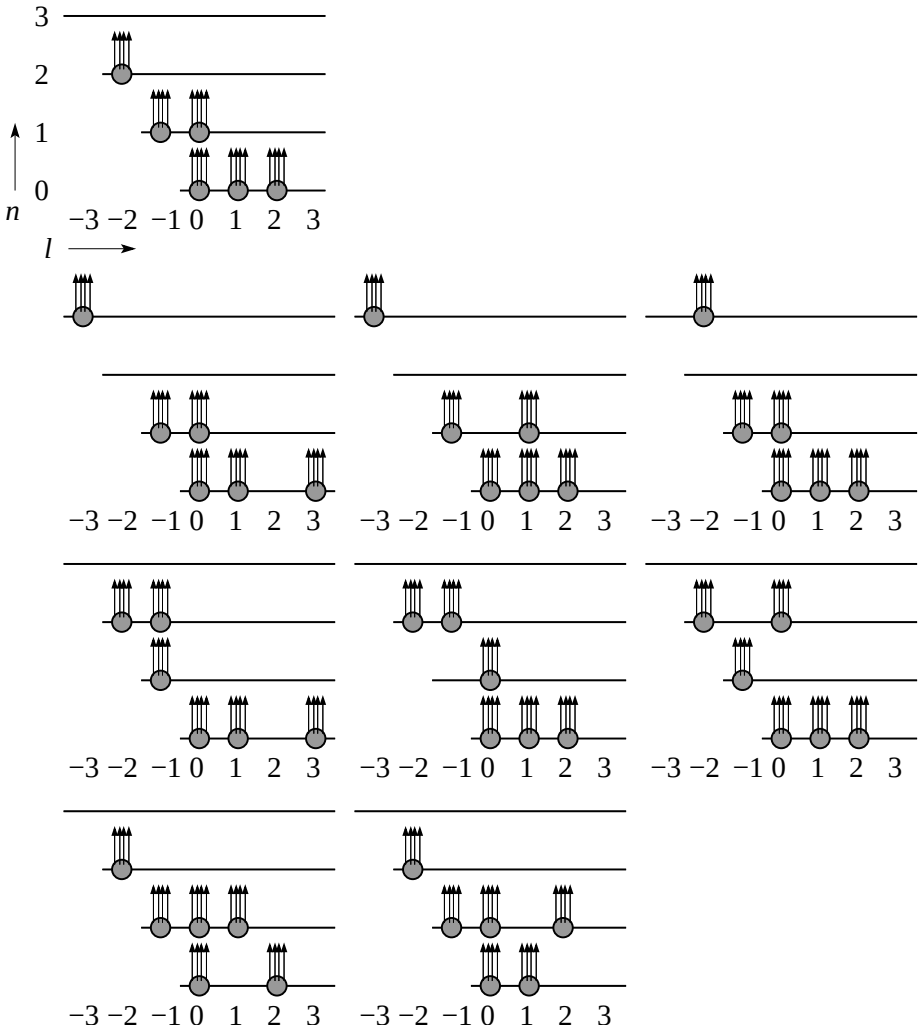

Figure 2.4: The CF basis states (schematically) for $N = 6$ electrons at $L = 60$ in the disk, which maps into $L^* = 0$ of ^{4}CF's. The y-axis shows the Λ-level index, and the x-axis the single-particle angular momentum. The top row shows the unique state with the smallest (4) effective cyclotron energy. The remaining figures show all the linearly independent configurations with one additional unit of kinetic energy. (There are a total of 10 distinct electron states in the $J = 1$ basis at $L^* = 0$, which produce 9 linearly independent CF basis states.)

momenta of the particles in the lowest Λ-level. This additional variational freedom lets us investigate edge effects as well [71, 125].

2.6 Landau level mixing

We will neglect Landau level mixing throughout this study. In GaAs systems this is a good approximation at high magnetic fields, because the interaction strength scales as $\frac{e^2}{\epsilon l_B} \propto \sqrt{B}_\perp$ while the spacing between LL's goes as $\hbar\omega_c \propto B_\perp$. In graphene, the above scaling argument does not apply, as the gap between LL's (c.f. Eq. (2.18)) also scales with $\sqrt{B}_\perp$. Even though both LL separation and Coulomb interaction have the same $B_\perp$-dependence, the relative strengths can be controlled by variation of other parameters (Fermi velocity, dielectric constant, etc.), and we will assume that the LL separation is large enough to suppress LL mixing.

2.7 Finite thickness

The 2DEG with Coulomb interaction is an ideal limit. The extended nature of the electronic states in the perpendicular direction can be taken into account by several approximations [45, 46, 47], which are specific to the particular implementation of the 2DEG. Assuming translational invariance and that only the lowest state of the (self-consistently handled) perpendicular confining potential in is filled, finite thickness in general causes an effective interparticle interaction that is weaker in the short range than the pure Coulomb interaction $V^{(\mathrm{C})}$. Acknowledging this fact, the consequences of finite thickness will be neglected throughout this study.

Chapter 3

Fractional quantum Hall effect in the second Landau level

3.1 Introduction

Given that more than 50 fractions have been observed in the lowest LL, one might expect a large number of fractions in the second LL as well, but FQHE is relatively scarce in the second or higher LL's. However, with improved experimental conditions (higher mobilities and lower temperatures), many fractions have been observed outside of the lowest LL. As seen in the experiments of Xia *et al.* [25], the observed fractions are $\nu^{(1)} = \frac{1}{3}, \frac{1}{5}, \frac{2}{5}, \frac{2}{3}$, and $\frac{4}{5}$, where $\nu^{(1)}$ is the filling factor of the second LL. (The total filling factor is $\nu = 2 + \nu^{(1)}$ or $\nu = 3 + \nu^{(1)}$, with each LL contributing two to the filling factor, taking the spin degree of freedom into account.) Gervais *et al.* [26] have also seen evidence for FQHE at $\frac{1}{5}$ and $\frac{4}{5}$ in the *third* LL at intermediate temperatures 80 to 120 mK. There is, however, an FQHE state state that occurs only in the second Landau level: the enigmatic state at $\nu = \frac{5}{2}$ and $\frac{7}{2}$ [19, 20], i.e., at half-filled second LL.

The decreasing stability of CF formation (Sec. 2.5) has been suggested on theoretical grounds [63], and charge-density wave phases are known to be dominant in $n \geq 2$ LL's [64]. The competition between many nearly degenerate ground states in the second LL is illustrated by the observation of the so-called re-entrant integer quantum Hall effect: the system goes back and forth between the IQHE and the FQHE state several times (see, for

example, Eisenstein *et al.* [24] and Xia *et al.* [25]), with the re-entrant IQHE interpreted in terms of a localization of a correlated bubble crystal proposed theoretically by Koulakov, Fogler, and Shklovskii [64].

3.2 Fractional quantum Hall effect at $\nu = \frac{7}{3}$ and $\nu = \frac{8}{3}$

Because the observed odd-denominator fractions are consistent with the expectation from a trivial generalization of the CF model to the second LL, it is natural to attempt an explanation in terms of composite fermions. However, the microscopic description of the observed fractional states in the second LL has not been as successful as in the lowest LL. As noted by Haldane [57] and by d'Ambrumenil and Reynolds [62], a generalization of the Laughlin wave function for the ground state at $\nu = \frac{1}{3}$ to the second LL [65] has rather poor overlaps with the exact second LL ground state (from 0.47 to 0.61 for $4 \leq N \leq 9$ particles), which is to be contrasted with near unity overlaps in the lowest LL. Exact diagonalization studies [57, 62] on small systems have been unable to capture conclusively the incompressibility of $\nu^{(1)} = \frac{1}{3}$: the system is compressible for some particle numbers and incompressible for others, and when incompressible, the gap varies widely with the number of particles [62]. The observation of many FQHE states in the filling factor range $2 < \nu < 4$ has motivated us to seek a better quantitative understanding of the FQHE in the second LL.

Another motivation arises from certain new FQHE states within the lowest Landau level. Pan *et al.* [23] have observed several fractions ($\frac{4}{11}$, $\frac{5}{13}$, $\frac{6}{17}$, $\frac{4}{13}$, $\frac{5}{17}$, $\frac{7}{11}$) that fall outside the standard sequences $\nu = \frac{n}{2pn \pm 1}$. Although these sequences exhaust the possible fractions for a system of *noninteracting* composite fermions, the residual interaction between the CF's can generate more fractions, in perfect analogy to the appearance of the FQHE for electrons because of the Coulomb interaction. The new fractions are interpreted in terms of the *higher* Λ-level *fractional* quantum Hall effect of composite fermions [23, 120, 121, 122, 123]. In particular, $\nu = \frac{4}{11}$ is related to the FQHE at $\nu^* = \frac{4}{3}$ of CF's, i.e., $\frac{1}{3}$ of CF's in the second Λ-level. (Here full spin polarization is assumed, which is reasonable in the second LL [80]. The filling factor $\nu^{(1)}$ in the second LL corresponds to $\nu = 1 + \nu^{(1)}$ for spinless electrons, but to $\nu = 2 + \nu^{(1)}$ for the real "spinful" electrons of experiment.) It was shown

by Chang and Jain [121] that the actual $\frac{4}{11}$ state is extremely well described quantitatively by analogy to the $\frac{1}{3}$ state in the *second* LL, but not to the $\frac{1}{3}$ state in the lowest LL. That further underscores the need for a better quantitative understanding of the FQHE in the second LL.

Wójs and Quinn [66] have argued that the difference between the lowest LL and the second LL physics is due to some kind of pairing in the second LL. They study the occupation number of various relative angular momentum m channels in the exact ground states for $8 \leq N \leq 14$ electrons in the spherical geometry and find that as the filling factor is varied (tuned by the monopole strength Q, c.f. Sec. 2.3), there are peaks in the occupation of the $m = 5$ channel at certain flux values that they identify with $\nu = \frac{7}{3}, \frac{5}{2}, \frac{8}{3}$. These findings are taken as evidence for pairing of electrons in the $m = 5$ channel.[1] Wójs and Quinn thus assign a *qualitatively* different physics to FQHE in the second LL than that in the lowest LL, as reflected in the fact that, in the spherical geometry, their paired state at $\frac{1}{3}$ in the second LL occurs at the LL degeneracy $N_d = 3N - 4$ as opposed to $N_d = 3N - 2$ for the $\frac{1}{3}$ state in the lowest LL. (Here $N_d = 2Q + 3$ in the second LL.) No explicit wave functions have been constructed for the conjectured paired states which could be compared to the exact wave functions.

Our approach is different. We attribute the same *qualitative* physics to the odd-denominator FQHE in the lowest and the second LL's and argue that the *quantitative* differences arise because of substantial Λ-level mixing in the second LL. The Λ-level mixing is a signature of the residual interaction between CF's. The negligibility of Λ-level mixing for the lowest LL FQHE states is taken to imply that the CF's are weakly interacting. We will see that composite fermions are more strongly interacting in a range of filling factor in the second LL, although not so strongly as to destabilize all FQHE completely.

We will restrict electrons to the second LL, assuming an inert lowest LL, and neglect LL mixing (Sec. 2.6) and finite thickness. We map the second LL problem into an effective lowest LL problem (c.f. Eqs. (2.25) and (2.26)), and work within the lowest LL. The interaction between composite fermions is taken into account by CF diagonalization (Sec. 2.5.3).

[1] It is noted pairing of CF's may be significant [68] for the FQHE at $\nu = \frac{5}{2}$ [19], which is often discussed in terms of the Pfaffian wave function of Moore and Read [77, 78, 80, 67]. See Secs. 3.3.1 to 3.5 for review and analysis.

With minimal Λ-level mixing, CF diagonalization produces explicit wave functions which, when tested against exact wave function, are found to be excellent approximations to the ground states, thus demonstrating that Λ-level mixing captures the physics of the second LL FQHE. This will be seen to hold for the entire filling factor range where the second LL behaves differently from the lowest LL. In particular, at $\nu^{(1)} = \frac{1}{3}$, the overlap with the exact wave function increases from 0.71 to 0.95 (for six particles in the disk geometry) upon lowest-order Λ-level mixing.

Sec. 3.2.1 compares the exact ground states in the lowest three Landau levels for six electrons on a disk, and shows that there exists a filling factor range where the LL's behave differently. Sec. 3.2.2 includes the effect of Λ-level mixing at the lowest order to obtain improved variational ground states in the second LL, and finds high overlaps, between 0.94 and 0.98, with the exact ground state. The same method is applied in the spherical geometry to estimate the excitation gap at $\nu^{(1)} = \frac{1}{3}$ in Sec. 3.2.3.

3.2.1 Comparison of the state in the lowest Landau levels

As we work technically in the lowest LL, the phrase "the ground state in the n-th LL" really means "lowest LL sibling of the n-th LL ground state." The actual n-th level ground state can be obtained by promoting the lowest LL wave function to the n-th LL by the raising operators (Eq. (2.7)). With that understanding, the ground states $|\Psi_{ex}^{(n)}\rangle$ of different LL's can be compared by calculating the overlap $\langle\Psi_{ex}^{(n)}|\Psi_{ex}^{(n')}\rangle$. (Of course, the real n-th LL ground state for $n > 0$ is orthogonal to the lowest LL ground state.)

Fig. 3.1 shows how the overlap between the second and lowest (upper panel) and the third and lowest (lower panel) Landau levels varies with L. It is apparent that there is an angular momentum range where the ground states in the lowest and the excited LL's are quite different. As one considers higher LL's, this range widens. Similar behavior is found for $N = 7$ and $N = 8$ (Figs. 3.2 and 3.3).

There are angular momenta where the ground states in different Landau levels are nearly orthogonal. For example, for $N = 6$ $\langle\Psi_{ex}^{(1)}|\Psi_{ex}^{(0)}\rangle = 0.00024, 0.005$ for $L = 41, 81$, respectively, and is 0 within numerical accuracy for $L = 46, 52$. This near orthogonality is most unexpected. We have found that, in most cases, the following simple explanation can be given for it. As known from quantum dot studies [126, 127, 128, 129, 71], two-

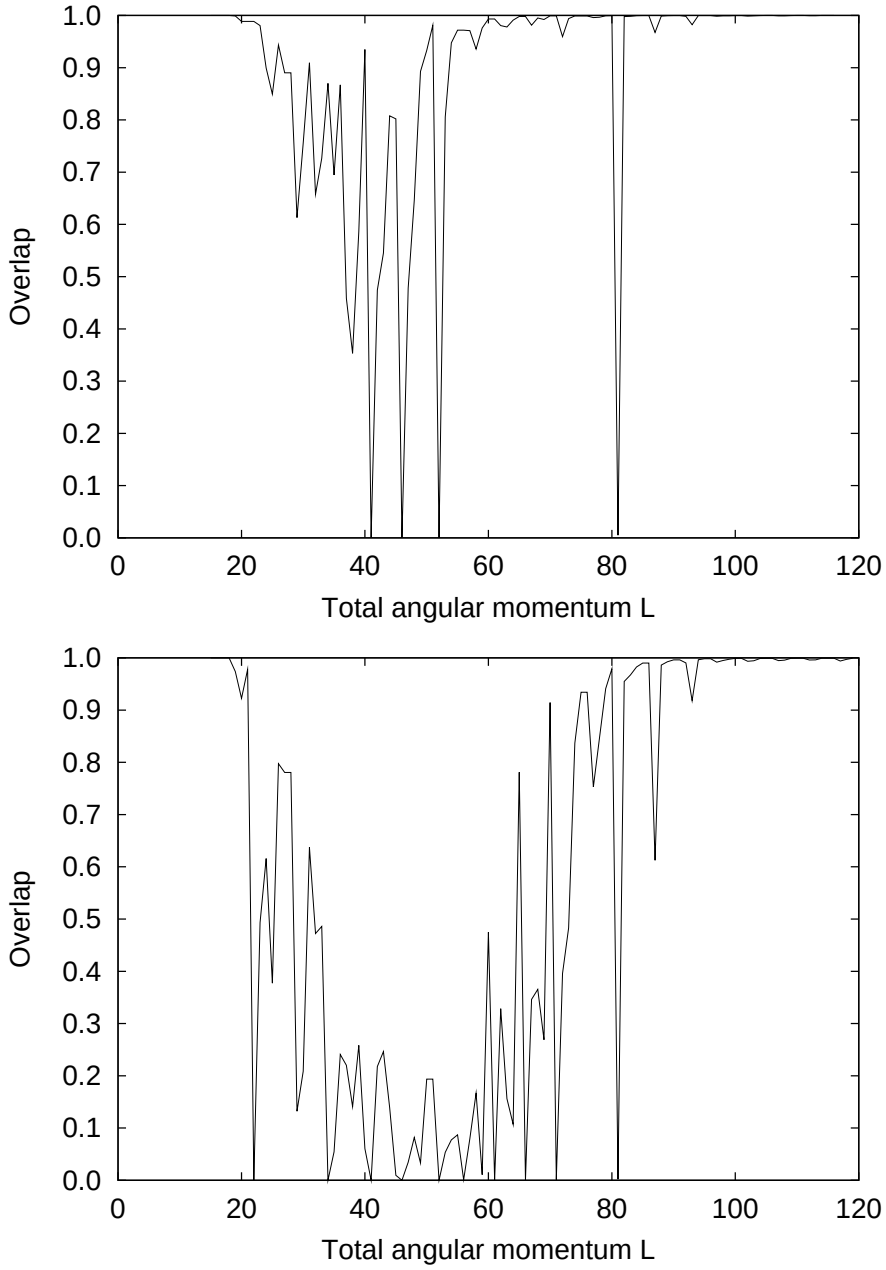

Figure 3.1: Overlap of the lowest LL ground state $|\Psi_{ex}^{(0)}\rangle$ with the second LL ground state $|\Psi_{ex}^{(1)}\rangle$ (top) and the third LL ground state $|\Psi_{ex}^{(2)}\rangle$ (bottom) for $N = 6$. L denotes the total angular momentum. The overlap $|\langle\Psi_{ex}^{(0)}|\Psi_{ex}^{(1)}\rangle|$ is almost zero for $L = 41, 46, 52, 81$, and $|\langle\Psi_{ex}^{(0)}|\Psi_{ex}^{(2)}\rangle|$ nearly vanishes for $L = 22, 34, 41, 46, 52, 56, 61, 66, 71, 81$. The fillings $\nu = \frac{1}{3}$ and $\frac{1}{5}$ occur at $L = 45$ and 75, respectively. The lines are a guide to the eye.

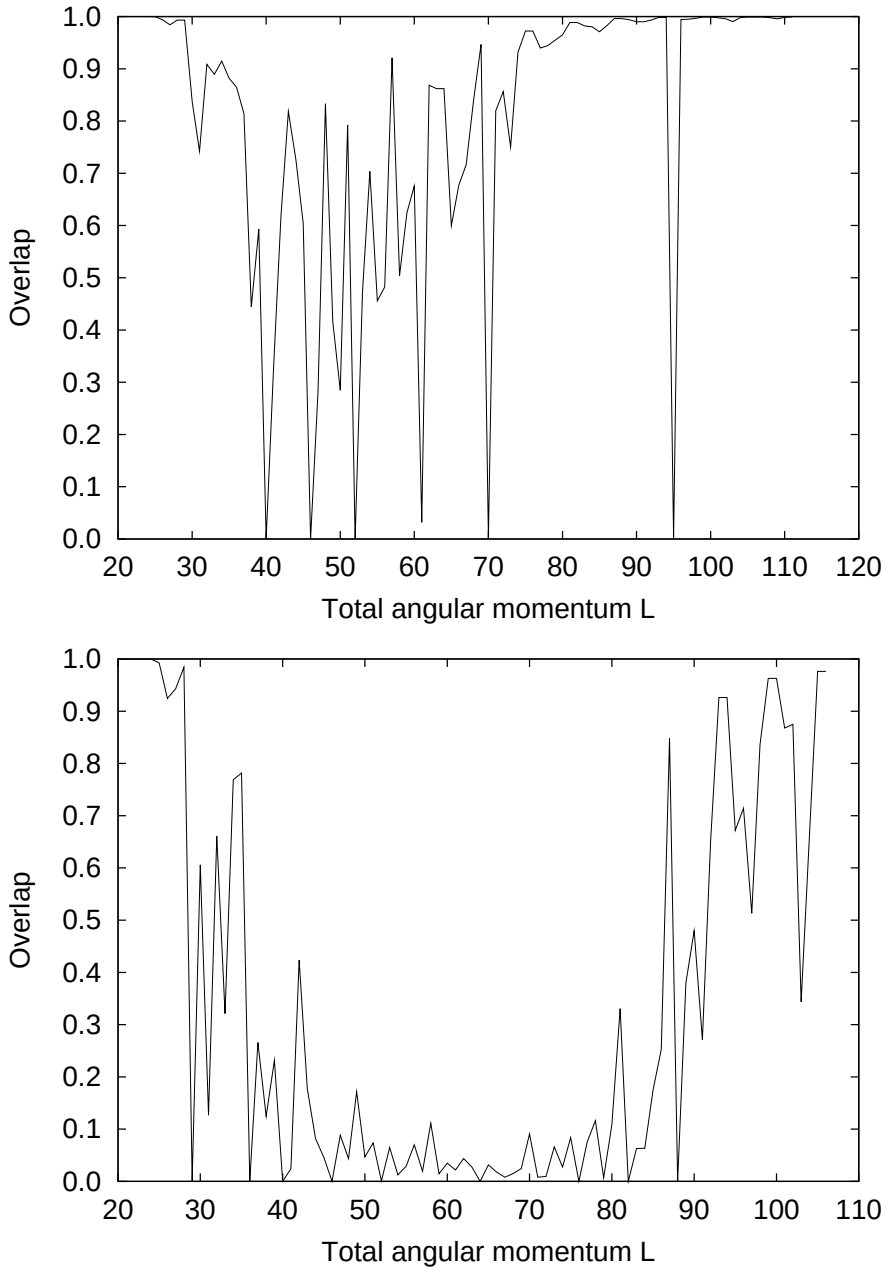

Figure 3.2: Overlap of the lowest LL ground state $|\Psi_{ex}^{(0)}\rangle$ with the second LL ground state $|\Psi_{ex}^{(1)}\rangle$ (top) and the third LL ground state $|\Psi_{ex}^{(2)}\rangle$ (bottom) for $N = 7$. The overlap $\langle\Psi_{ex}^{(0)}|\Psi_{ex}^{(1)}\rangle$ is near zero for $L = 40, 46, 52, 70, 95$ and quite low (≈ 0.03) for $L = 61$, where L is the total angular momentum. The overlap $\langle\Psi_{ex}^{(0)}|\Psi_{ex}^{(2)}\rangle$ is rather low over a range of L. The fillings $\nu = \frac{1}{3}$ and $\frac{1}{5}$ correspond to $L = 63$ and 105, respectively. The lines are a guide to the eye.

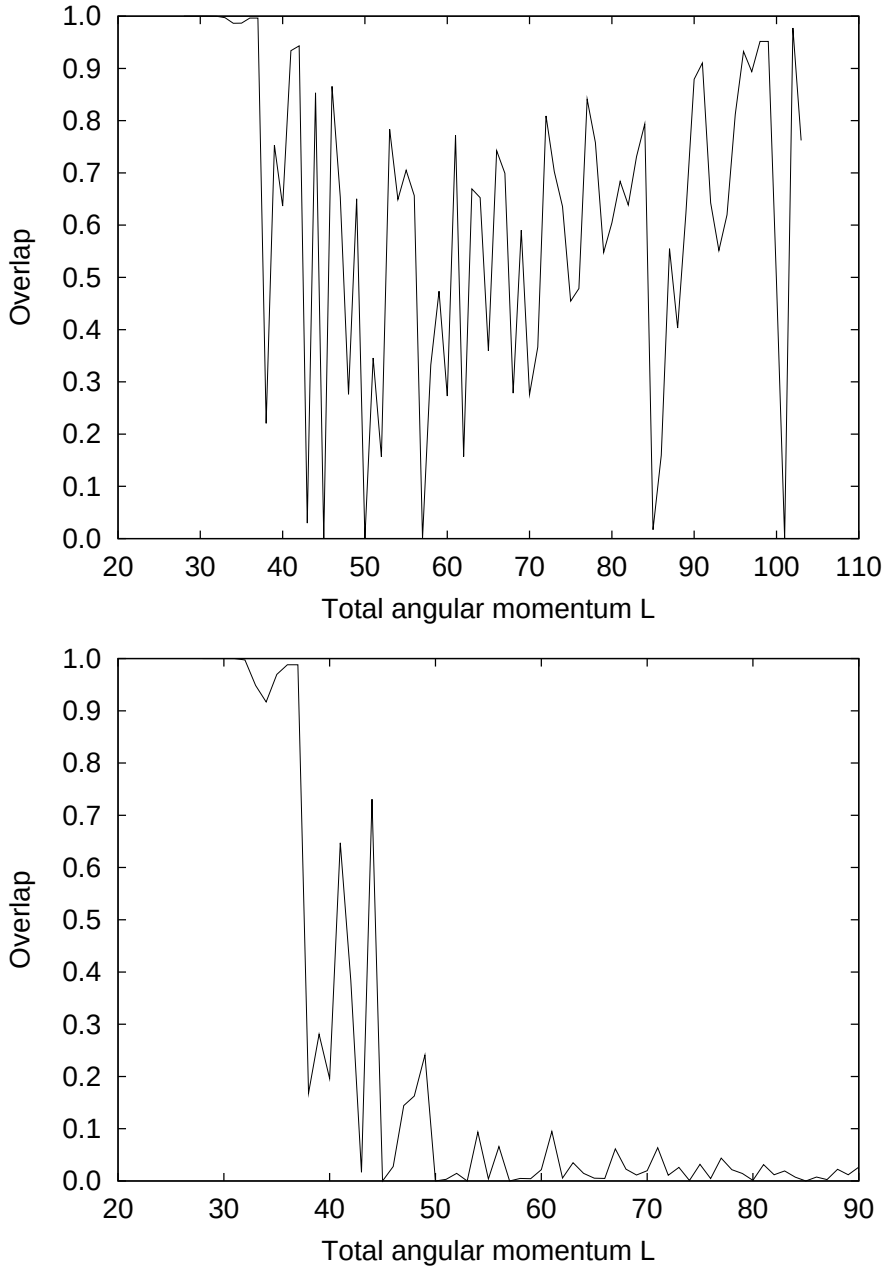

Figure 3.3: Overlap of the lowest LL ground state $|\Psi_{ex}^{(0)}\rangle$ with the second LL ground state $|\Psi_{ex}^{(1)}\rangle$ (top) and the third LL ground state $|\Psi_{ex}^{(2)}\rangle$ (bottom) for $N = 8$ particles. The overlap $\langle\Psi_{ex}^{(0)}|\Psi_{ex}^{(1)}\rangle$ is almost zero for $L = 45, 50, 57, 85, 101$, where L is the total angular momentum. The fillings $\nu = \frac{1}{3}$ and $\frac{1}{5}$ occur at $L = 84$ and 140, respectively. The lines are a guide to the eye.

dimensional few electron systems in a strong transverse magnetic field have a tendency to form crystallites. Crystallite structures with $N = 6$ fall into two classes of symmetry: the (1,5) crystallite resembles a rotating molecule with one particle at the center and five in a ring; the (0,6) crystallite has all particles on a ring. Although the density profile differentiates between the two groups, the pair correlation function contains more information about the crystallite structure. For $N = 6$ and $L = 41, 46, 52, 81$ the symmetry of the crystallites in the two LL's differ, as suggested by the "effective" density profiles $\rho^{\rm eff}(r)$ in Fig. 3.4 and demonstrated by the pair correlation functions $g^{\rm eff}(\mathbf{r})$ in Fig. 3.5. (The superscript "eff" reminds us that the density or the pair correlation function are for the lowest LL representation of the n-th LL states. The "real" density or the pair correlation function in the n-th LL can be obtained by elevating the wave functions to the n-th LL with the help of the raising operators (2.7).) For $L = 41$ and $L = 46$ the crystallite in the lowest LL has $(1, 5)$ symmetry while the one in the second LL has $(0, 6)$ symmetry; for $L = 52$ and $L = 81$ the opposite holds. Although the majority of cases of almost zero overlap can be understood this way, there are exceptions ($N = 7, L = 95$ and $N = 8, L = 101$). We have not explored this issue further.

Outside a range of L, the higher LL physics is similar to that in the lowest LL. It was shown earlier [62, 72] that for $\nu \leq \frac{1}{5}$ the lowest two LL's should show similar behavior. The difference at $N = 6, L = 81$ seems to violate this rule, but the system is so small that this exception can be attributed to finite size effects. We have found no such exception for $N = 7$ in the L range that we have investigated below $\nu = \frac{1}{5}$ ($105 < L \leq 111$); for $N \geq 8$ the total angular momentum corresponding to $\nu = \frac{1}{5}$ could not be reached.

3.2.2 Inter-composite-fermion interaction at $\nu^{(1)} = \frac{1}{3}$

The residual interaction between composite fermions is taken into account by composite fermion diagonalization (c.f. Sec. 2.5.3). As this procedure requires the evaluation of the overlap interaction matrix elements (2.44) between the CF basis vectors by Monte Carlo methods, we need to know the real-space interaction corresponding to the effective pseudopotentials $V_m^{(n)}$. The inverse Fourier transform of $\tilde{V}^{(n)}(\mathbf{q})$ in Eq. (2.25) is not defined (the integral is divergent). This, however, causes no problem. Because the pseudopotentials completely determine the interaction, any real-space interaction $V^{(n)}(r)$ that gives

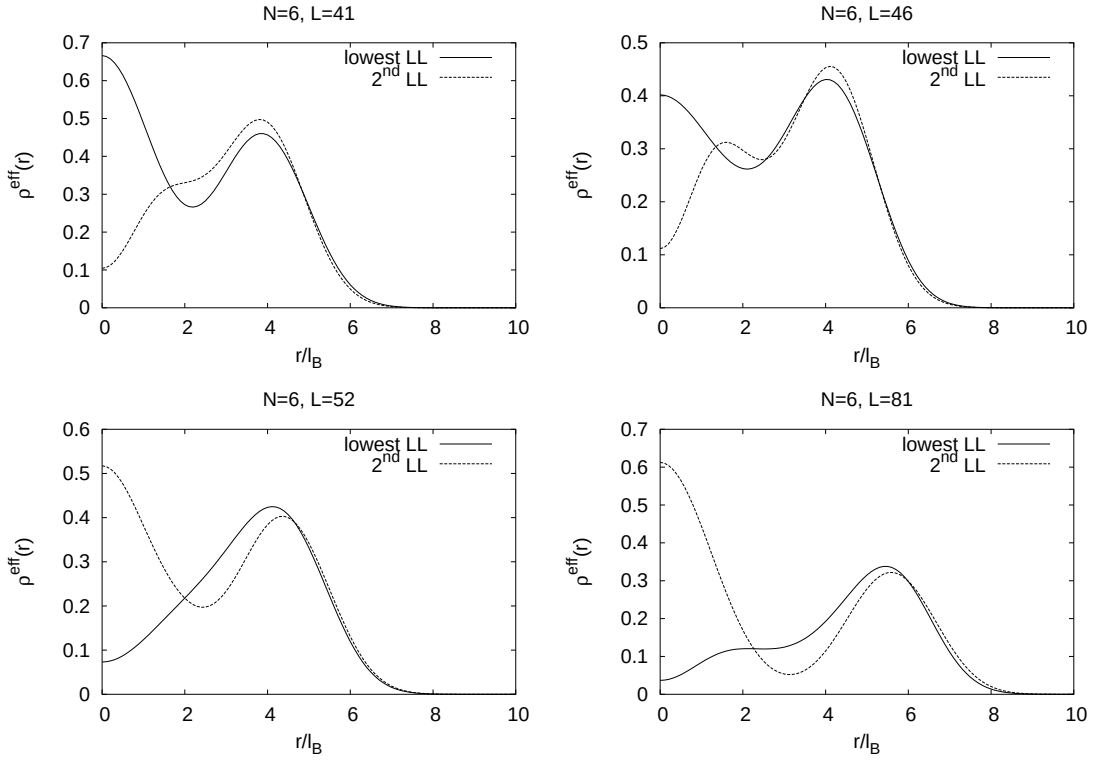

Figure 3.4: Comparison of the density profiles $\rho^{\text{eff}}(r)$ of the exact lowest LL and second LL ground states for the angular momentum (L) values for which the overlap between the two states is nearly zero. The reason for the superscript "eff" is that the density is calculated for the lowest LL sibling of the actual ground state. Note the different behaviors near the origin. The two Landau levels prefer crystallites with different symmetries at these L values.

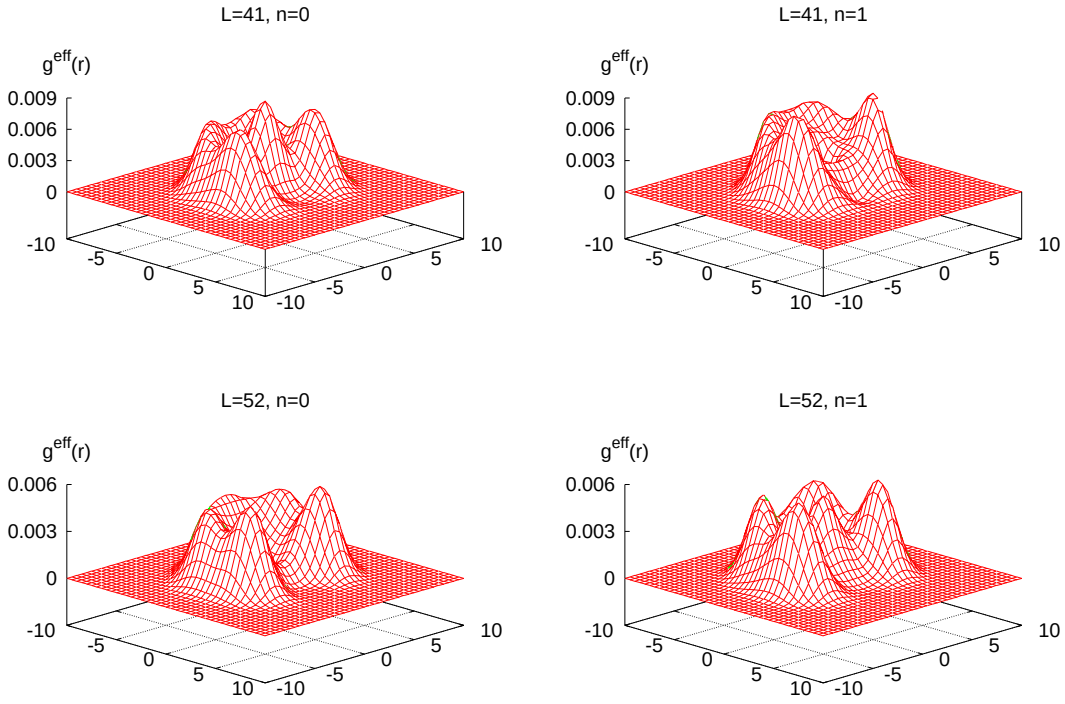

Figure 3.5: The "effective" pair correlation function $g^{\text{eff}}(\mathbf{r})$ of the ground state for total angular momenta $L = 41$ and $L = 52$ in the lowest ($n = 0$) and the second ($n = 1$) Landau levels. The reason for the superscript "eff" is that the pair correlation function is calculated for the lowest LL sibling of the actual higher LL ground state. Similar differences were found for $L = 46$ and $L = 81$.

Coefficient	Value
c_0	-50.36588
c_1	87.38159
c_2	-56.08439
c_3	17.76573
c_4	-2.97162
c_5	0.25132
c_6	-0.008435

Table 3.1: Coefficients in Eq. (3.1) to produce the effective interaction for the second Landau level. C.f. Table 4.5 for analogous parameters for graphene.

the same $V_m^{(n)}$ by Eq. (2.22) will be sufficient for our purposes. Thus we can use some convenient prescription for the analytic form of $V^{(n)}(r)$. The goal is that the Monte Carlo evaluation of the matrix elements of $V^{(n)}(r)$ should converge rapidly. In this section we will use the following form:

$$V^{\text{eff}}(r) = \frac{1}{r} + \sum_{i=0}^{M} c_i r^i e^{-r}. \tag{3.1}$$

This form is based on the observation that the long-range behavior of the effective interaction should approach the Coulomb interaction, hence all corrections must be short-range. Keeping enough number of terms in the sum will give as accurate a representation of the interaction as desired. For our purposes, it is enough to keep the first seven terms ($M = 6$). We calculate the first seven odd m pseudopotentials $V_1^{\text{eff}}, V_3^{\text{eff}}, \ldots, V_{13}^{\text{eff}}$ from Eq. (3.1) symbolically by MATHEMATICA, and determine c_i ($0 \le i \le M$) to satisfy

$$V_m^{\text{eff}} = V_m^{(1)} \ .$$

The obtained coefficients c_i are given in Table 3.1, and the resulting real-space interaction is shown in Fig. 3.6. Alternative prescriptions are available in the literature [74, 69, 63], and will also be used in subsequent sections (Eqs. (3.10) and (3.11)). The goal is the rapid convergence in Monte Carlo.

We comment on the validity of the truncated interaction, i.e., Eq. (3.1) with $M = 6$ and the coefficients in Table 3.1. First, the physics of the FQHE is governed by the first few relevant pseudopotentials. Since our truncated interaction reproduces correctly, by

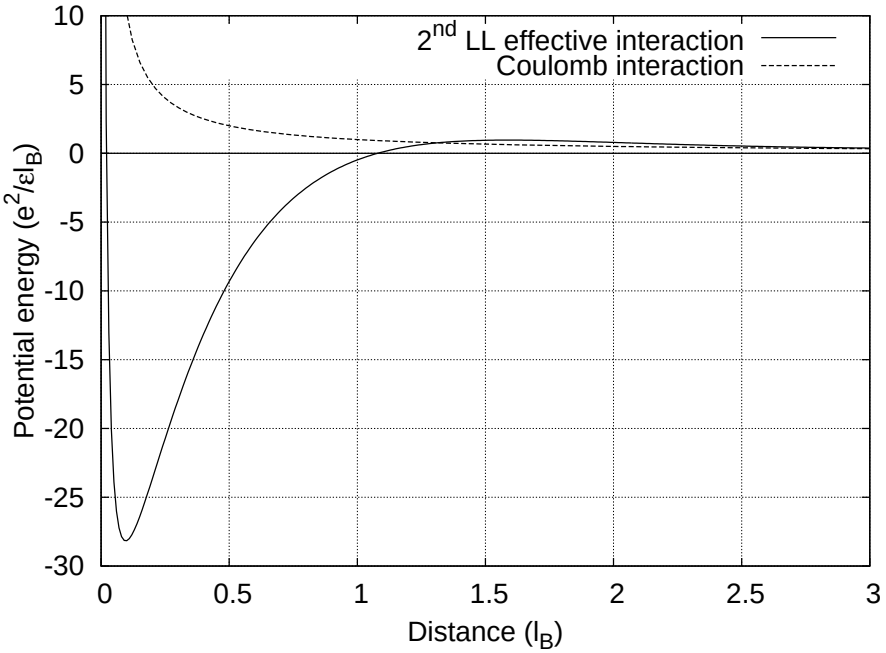

Figure 3.6: The effective real-space potential $V^{\text{eff}}(r)$ (defined in Eq. 3.1) which simulates the second LL physics in the lowest LL. In spite of the deep dip at $r < l_B$, where l_B is the magnetic length, it reproduces the second LL pseudopotentials to a very high accuracy (details in text).

construction, the first *seven* odd pseudopotentials, it is expected to be quite good. Second, $V^{\rm eff}(r)$ is also guaranteed to reproduce the pseudopotentials for very large m, where the interaction approaches $1/r$. We have found that the largest relative error in V_m is 5% at $m = 37$ up to $m \leq 49$. (For a given total angular momentum L, the greatest relative angular momentum is $m_{max} = L - \binom{N-1}{2}$; for our calculations, which go up to $L = 60$ for $N = 6$, the largest relevant relative angular momentum is $m = 49$.) At such large m, the pseudopotential is so small that such error is of no consequence. As a final test, we have compared the ground state of the truncated interaction with the ground state of the Coulomb interaction. In the $L \leq 75$ range the smallest overlap occurs at $L = 71$, which is 0.998303. To quote a typical number, at $L = 45$ the overlap is 0.99997. The truncated interaction is thus essentially exact.

To find $\langle \Psi_\alpha^{(j_1)} | \Psi_\beta^{(j_2)} \rangle$ and $\langle \Psi_\alpha^{(j_1)} | V^{(\rm C)} | \Psi_\beta^{(j_2)} \rangle$, typically 6.6×10^7 to 7.5×10^7 Monte Carlo steps were performed, where a Monte Carlo step is defined as a number of iterations during which each particle coordinate is expected to be updated once. Averages and error bars were calculated from five independent runs.

We have performed CF diagonalization in the $34 \leq L \leq 60$ range. The dimensions of various bases are given in Table 3.11. This encompasses $\nu = \frac{1}{3}$ (which occurs at $L = 45$). The flavors ^{2}CF's are used for $L \leq 48$, ^{4}CF's for $L \geq 49$. (This choice ensures the smallest CF basis.) The results are shown in Table 3.2 and Fig. 3.7. The zeroth-order variational energies and overlaps are given for all $34 \leq L \leq 60$. The first-order wave function is evaluated for all L's except for $L = 43, 44$; for these cases the correlated CF basis is too big ($D^{(1)} = 83$ and 111, respectively) preventing an evaluation of the matrix elements of $V^{(\rm C)}$ with sufficient accuracy.

Our principal result, as shown in Table 3.2 and Fig. 3.7, is that CF theory without Λ-level mixing is not satisfactory, but very good agreement is obtained once Λ-level mixing is incorporated at the lowest order. In particular, at $\nu = \frac{1}{3}$ ($L = 45$) the zeroth-order variational wave function $\chi^{(0)}$ is the Laughlin wave function (Eq. (2.12)), whose energy ($E_{CF}^{(0)} = 3.0796(3)$) significantly overestimates the exact energy 3.05354. The overlap is 0.712(2), which is similar to the values found in the spherical geometry [62]. The first-order CF diagonalization yields $E_{CF}^{(1)} = 3.0621(1)$ and $\langle \Psi_{ex} | \chi^{(1)} \rangle = 0.9467(8)$.

As noted in Sec. 3.2.1, for certain L values the ground states of different LL's have

Table 3.2: Comparison of the energies (in units of $e^2/\epsilon l_B$) of the exact ground state and the states obtained from zeroth- and first-order CF diagonalization. We are using the Coulomb interaction for the exact calculation and the truncated interaction for the CF diagonalization. Even though they have almost identical pseudopotentials, sometimes the latter produces a very slightly lower energy than the energy of the exact ground state. To avoid confusion, the energies $E_{CF}^{(J)}$ in Table 3.2 are the expectation values of the second LL *Coulomb* interaction with respect to $\chi^{(J)}$. D_{ex}, $D_{CF}^{(0)}$ and $D_{CF}^{(1)}$ are the dimensions of the full Hilbert space, of the CF basis in the zeroth order calculation, and of the CF basis in the first order calculations, respectively. A few numbers were omitted due to computational limitations.

L	E_{ex}	$E_{CF}^{(0)}$	$E_{CF}^{(1)}$	D_{ex}	$D_{CF}^{(0)}$	$D_{CF}^{(1)}$
34	3.57207	3.5801(1)	3.5748(7)	235	4	27
35	3.48739	3.5144(1)	3.49786(2)	282	1	10
36	3.44351	3.47805(2)	3.4476(2)	331	2	18
37	3.39199	3.42079(1)	3.3962(1)	391	5	31
38	3.37222	3.3899(3)	3.3770(5)	454	9	47
39	3.31020	3.3403(1)	3.3174(3)	532	1	17
40	3.25712	3.27476(2)	3.2616(1)	612	2	26
41	3.22851	3.2647(3)	3.2330(5)	709	4	41
42	3.18755	3.2206(3)	3.1933(9)	811	7	59
43	3.15253	3.1761(1)	-	931	12	83
44	3.12831	3.1379(4)	-	1057	18	111
45	3.05354	3.0796(3)	3.0621(1)	1206	1	28
46	3.04126	3.0805(5)	3.0484(6)	1360	1	39
47	3.01108	3.0561(3)	3.0235(5)	1540	2	55
48	2.97252	3.02019(8)	2.9860(8)	1729	3	74
49	2.94205	2.94937(4)	2.9443(2)	1945	4	46
50	2.87713	2.88772(2)	2.8805(2)	2172	2	32
51	2.87227	2.8786(6)	2.8790(2)	2432	1	19
52	2.85393	2.8667(3)	2.8597(6)	2702	10	65
53	2.82087	2.8375(3)	2.827(1)	3009	5	44
54	2.77835	2.79440(4)	2.7881(5)	3331	2	26
55	2.72364	2.737(2)	2.7289(2)	3692	1	13
56	2.72364	2.7457(2)	2.7383(2)	4070	5	39
57	2.69540	2.70221(2)	2.7018(1)	4494	2	21
58	2.68363	2.7054(7)	2.6979(7)	4935	9	48
59	2.64022	2.65914(2)	2.6495(6)	5427	3	25
60	2.58918	2.603(7)	2.6034(4)	5942	1	9

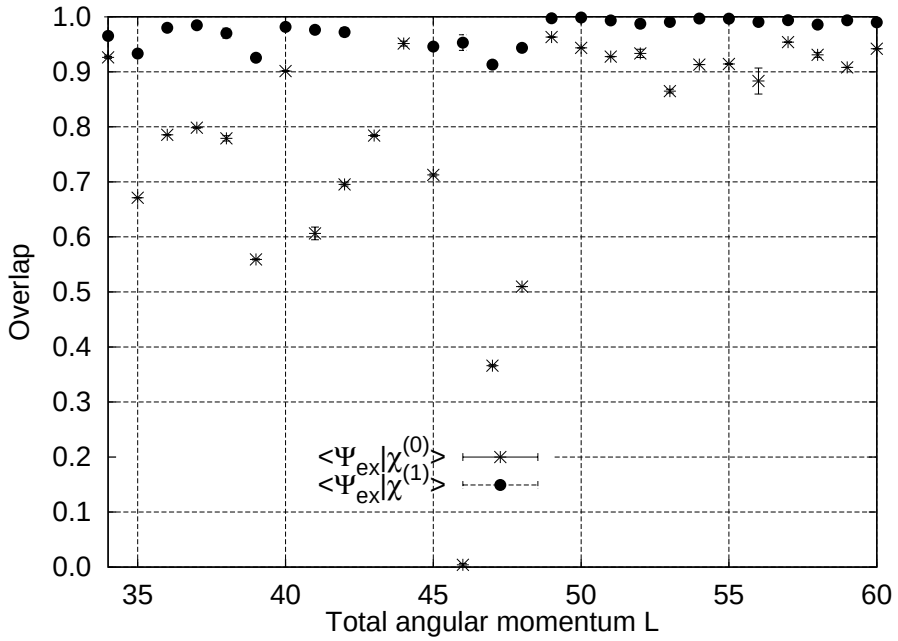

Figure 3.7: Overlap of the exact second Landau level ground state with the wave function obtained from CF diagonalization with and without Λ-level mixing (solid circles and stars, respectively).

anomalously low overlaps. Let us consider $L = 41$, 46, and 52 for $N = 6$. (We could not investigate $L = 81$ due to computational limitations.) At the zeroth order (i.e., without Λ-level mixing), the overlaps for these L are $\langle \Psi_{ex} | \chi^{(0)} \rangle = 0.614(2)$, 0.004(2) and 0.933(7), respectively. For $L = 46$ the small overlap follows because the zeroth order CF basis contains only one state, which is very close to the lowest LL ground state. In the other two cases, the zeroth order CF basis is larger (with 4 and 10 states); the greater flexibility results in better overlaps. With Λ-level mixing, the overlaps increase to $\langle \Psi_{ex} | \chi^{(1)} \rangle = 0.9814(2)$, 0.9695(7) and 0.987(7), respectively.

3.2.3 Estimation of the gap at $\nu = \frac{7}{3}$

The best estimate of the gap at $\nu = \frac{7}{3}$ so far is from the exact diagonalization calculation of Morf [80], where he obtained a gap of $\Delta_{7/3} \approx 0.02 e^2/\epsilon l_B$ for $N = 10$ particles, which gives a measure of the thermodynamic gap. Here we estimate the excitation gap at $\nu^{(1)} = \frac{1}{3}$ from CF diagonalization on the sphere.

Again, CF diagonalization was performed with the effective real-space interaction defined in Eq. (3.1), but now we will work in the spherical geometry (Sec. 2.3).[2] The zeroth order yields a unique $L = 0$ state. In the first order there is one additional state for each total angular momentum $L = 1, 2, \ldots, \frac{N+n^2+n}{n}$, of which $\mathcal{P}_{\rm LLL}$ annihilates the state at $L = 1$ [75]. The calculated excitation spectrum $E^{(1)}(L)$ for $\nu^{(1)} = \frac{1}{3}$ for $N = 16$ is shown by solid circles in Fig. 3.8. (Similar behavior occurs for other system sizes.) It has an $L = 0$ ground state ($\Psi^{(0)}$ in this case) separated from the other states by a gap. It may be tempting to calculate the excitation gap, but we know that $\Psi^{(0)}$ is a poor representation of the actual ground state in the second LL in the spherical geometry [62] and in the disk geometry (Sec. 3.2.1 and elsewhere [54]) and suspect that the excited states are also equally bad. Thus, we expand our basis for CF diagonalization (2.43) to $J = 2$.

The open diamonds in Fig. 3.8 show the spectra in second-order CF diagonalization for $N = 16$ at $\nu^{(1)} = \frac{1}{3}$. First, as expected, the lowest energy in each L sector has been lowered significantly. (Many new higher energy states are also created.) Second, the

[2] One could have constructed the effective real-space interaction directly in the spherical geometry, as will be done in Sec. 3.5 below. Using the real-space interaction that reproduces the pseudopotentials on the plane is an approximation that is justified in the $N \to \infty$ limit.

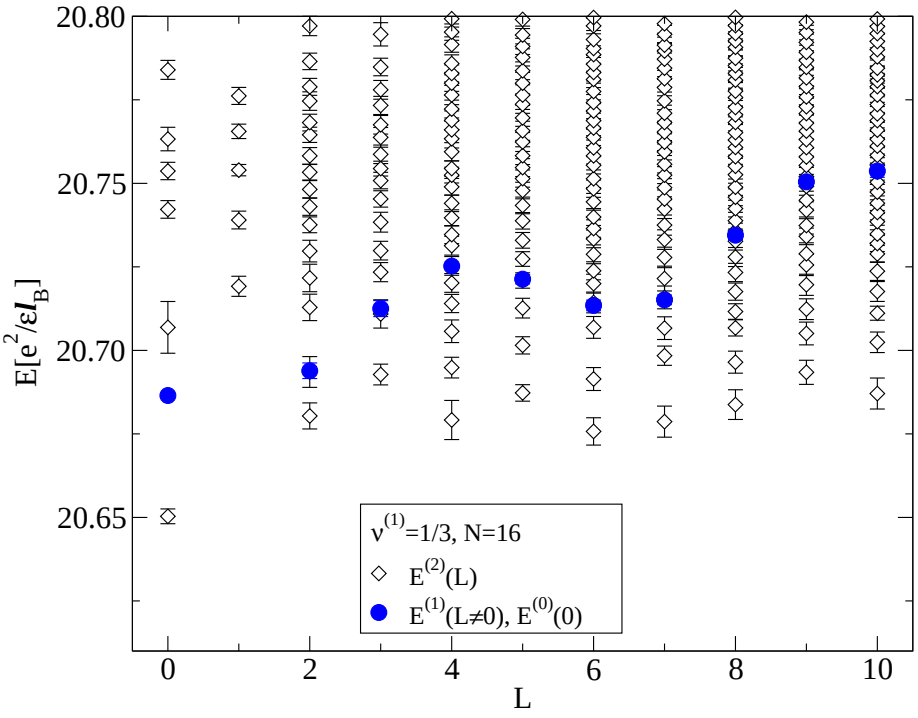

Figure 3.8: First-order (blue circles) and second-order (open diamonds) composite fermion diagonalization spectra for $N = 16$ electrons in the second Landau level. The energies have been corrected for the finite sized deviation in the density by the factor $\sqrt{\rho/\rho_N} = \sqrt{2Q\nu/N}$. The contribution from the uniform positive background has not been subtracted.

N	$\lvert\langle\chi^{(2)}\lvert\Psi^{(0)}\rangle\rvert^2$
10	0.82(1)
11	0.81(1)
12	0.82(2)
13	0.835(3)
16	0.77(4)

Table 3.3: The overlap between the improved variational ground state wave function and the Laughlin wave function at $\nu^{(1)} = \frac{1}{3}$ for $N = 10, 11, 12, 13$, and 16 particles.

gap is significantly enhanced. Both facts underscore the importance of Λ-level mixing for the second LL FQHE. Table 3.3 gives the overlap between $\chi^{(2)}$ at $L = 0$ and $\Psi^{(0)}$ for a number of system sizes. The relatively small overlaps give further evidence that the CF diagonalization in the $J = 2$ basis has significantly improved the ground state wave function.

The overall size of the basis for $J = 1$ consists of $\frac{N+n^2+n}{n} + 1$ states across the whole spectrum while for $J = 2$ it is approximately 500 states for $N = 16$ (9 states in the $L = 0$ channel up to $\sim$ 50 states in the $L = 10$ channel.) That should be compared to the dimension of the full Hilbert space, which is $\sim 10^{10}$. The overlap and interaction matrix elements were calculated from about 10^7 Monte Carlo iterations. The error bars were calculated from about ten distinct Monte Carlo configurations. Approximately 7200 CPU hours were utilized in the spherical to obtain the data in this section.

With the effective potential in Eq. (3.1) we found that the Monte Carlo error is on the order of ten times larger than the error when using the pure Coulomb potential when $\Psi^{(0)}$ is used as the sampling function. To save CPU time, we calculated the spectra using several different sampling functions. Figs. 3.8 and 3.9 gives the energy with the smallest statistical error for the choices of the different sampling functions.

Assuming that $J = 2$ order CF diagonalization is quantitatively accurate in the second LL, we proceed to calculate the excitation gap for FQHE at $\nu^{(1)} = \frac{1}{3}$. Fig. 3.9 shows the excitation energy Δ as a function of wave vector k, where $kl_B = L/R$. We show data for $N = 10, 11, 12, 13$, and 16 by the different symbols. The energies for different system sizes have roughly collapsed onto a single line indicating that we are close to the thermodynamic limit. The Monte Carlo error is $\sim$ 10 times what one is used to with gap calculations in

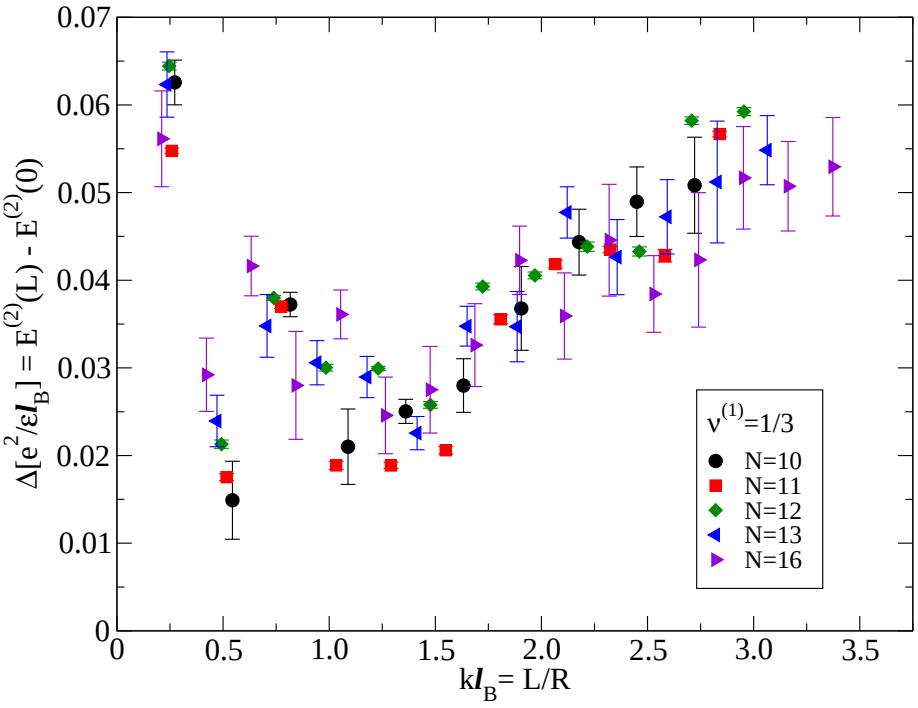

Figure 3.9: The excitation spectrum from second-order composite fermion diagonalization at $\nu^{(1)} = \frac{1}{3}$. The different symbols represent the excitation energy for $N = 10, 11, 12, 13,$ and 16 electrons as a function of $kl_B = L/R$, where R is the radius of the sphere and L is the total orbital angular momentum. For the finite size density correction see the caption to Fig. 3.8.

the lowest LL.

The dispersion somewhat differs from that of the lowest LL $\frac{1}{3}$ state, which has a single roton minimum. There seem to be two minima in the spectra, at $kl_B \approx 0.5$ and $kl_B \approx 1.25$. The value of roton gaps is crudely $\approx 0.02e^2/\epsilon l_B$ in both cases. This value is consistent with Morf's estimation [80], further supporting the CF model with lowest order Λ-level mixing as an explanation of the FQHE in the second LL. The transport gap is identified with the excitation energy at $L = N$ (maximal CF particle-hole separation), an is estimated as $\approx 0.05e^2/\epsilon l_B$. The theoretical gaps are much larger than the experimental gaps, however. In Ref. [23] the excitation gaps at $\frac{7}{3}$ and $\frac{8}{3}$ were measured as $\Delta_{7/3} = 0.10$ K and $\Delta_{8/3} = 0.055$ K, respectively. Using the experimental parameters our calculated gap for $\nu = \frac{7}{3}$ is $\Delta \approx 2$ K for the roton and $\Delta \approx 5$ K for the transport gap. The theoretical calculations quite generally overestimate the FQHE gap; we expect that our estimate would scale down once finite thickness, LL mixing, and disorder effects are taken into account. For comparison, the theoretical gap at $\nu = \frac{5}{2}$ estimated from exact diagonalization studies by Morf [80], $\Delta_{5/2} \approx 0.05e^2/\epsilon l_B$, is also large compared to the latest experimental gap by Eisenstein *et al.* [24], ≈ 0.31 K or $0.0027e^2/\epsilon l_B$ with their parameters. Our gap is significantly lower than $0.15e^2/\epsilon l_B$ quoted in Ref. [70].

3.3 Fractional quantum Hall effect at $\nu = \frac{5}{2}$ and $\frac{7}{2}$

Unlike the fractions that belong to the standard sequences $\nu = \frac{n}{2pn\pm1}$, the FQHE states at $\nu = \frac{5}{2}$ and $\frac{7}{2}$, i.e., at half-filled second Landau level, do not have a straightforward interpretation in the CF model. The state at $\nu = \frac{5}{2}$ was originally discovered by Willett *et al.* [19], and remains the strongest [24] of the few FQHE states in the second Landau level [24, 25, 26]. As the noninteracting composite fermion model fails here, other theories had to be sought. The Pfaffian wave function of Moore and Read [77] has been applied to the FQHE at $\nu = \frac{5}{2}$ by Greiter, Wen, and Wilczek [78]. This wave function describes state of p-wave paired composite fermions; full spin polarization is assumed. The FQHE at $\frac{5}{2}$, however, was widely believed to be partially polarized or unpolarized, due to the experiments [20, 21, 22] that show that the FQHE states at $\nu = \frac{5}{2}$ and $\frac{7}{2}$ develop a strong anisotropy (similar to states at half-filled higher Landau bands from $\nu = \frac{9}{2}$ to $\frac{21}{2}$) and the plateau dis-

appears very quickly when an in-plane magnetic field is applied. This view changed when Morf [80] showed in an exact diagonalization study that the states about $\nu = \frac{5}{2}$ prefer full spin polarization, and that the decay of the $\nu = \frac{5}{2}$ FQHE with a tilted field can be explained with the weakening of the interparticle interaction between electrons due to the interplay of finite thickness and the in-plane component of the magnetic field. Moreover, Rezayi and Haldane [67] showed that the ground state of the Coulomb interaction for the half-filled second Landau level is very close to a transition to a compressible state: any weakening of the short-range part of the inter-electron interaction, possibly due to finite thickness or Landau level mixing, turns the state into a strongly anisotropic and compressible charge-density wave phase. They also showed that the particle-hole symmetrized version of the Pfaffian state has an improved overlap with the ground state.

Just like the ordinary CF ground states at $\nu = \frac{n}{2pn\pm1}$, the Pfaffian state can be justified as the ground state of an unphysical contact interaction (c.f. Eq. (3.8) below). Unlike for the ordinary CF states, however, this model interaction is a singular *three-body* interaction. Quasiholes states above the Pfaffian states can be introduced with reference to this model interaction. A case has been made, both from analytical arguments [77, 81, 82] and numerical calculations [83], that these Pfaffian quasiholes exhibit non-Abelian braiding statistics. However, the relevance of this result to the quasiholes of the Coulomb interaction has not been established, and there has been a debate in the literature on whether the Coulomb state is adiabatically connected to the Pfaffian state [85, 82, 81]. Recently, there have been proposals to the test non-Abelian statistics of quasiholes experimentally [88, 89, 91], and also to use it in quantum computers [88, 90, 92, 93]. Still, the only route to non-Abelions is via the three-body model interaction. This motivated our study into the adequacy of the Pfaffian model for the description of the excitations of the Coulomb interaction (Sec. 3.4). Also, it is interesting to look for possible alternative explanations for the FQHE at $\nu = \frac{5}{2}$ and $\frac{7}{2}$ (Sec. 3.5). But first the Pfaffian model is reviewed (Sec. 3.3.1) and some critical points are discussed (Sec. 3.3.2 and 3.3.3).

3.3.1 Review of the Pfaffian model

The Pfaffian wave function of Moore and Read [77, 78], which describes a paired state of composite fermions (c.f. Sec. 2.5), is given in the lowest LL by[3]

$$\Psi_0^{\rm Pf} = {\rm Pf}\left(\frac{1}{z_i - z_j}\right)\Phi_1^2, \tag{3.2}$$

The wave function for two quasiholes at η_1 and η_2 is [77]

$$\Psi_{2-{\rm qh}}^{\rm Pf} = {\rm Pf}\left(\frac{(z_i-\eta_1)(z_j-\eta_2)+(i\leftrightarrow j)}{(z_i-z_j)}\right)\Phi_1^2. \tag{3.3}$$

For two coincident quasiholes, $\eta_1 = \eta_2 \equiv \eta$, this reduces to a charge $\frac{1}{2}$ vortex:

$$\Psi_V = \prod_i (u_i - \eta)\Psi_0^{\rm Pf}. \tag{3.4}$$

Separately, each quasihole has a charge deficiency of $\frac{1}{4}$ associated with it. Unlike for the vortex, the density does not vanish at the position of a quasihole. Analogous wave functions can be written for an even number ($2m$) quasiholes. No simple wave functions presently exist for quasiparticles.

To $2m$ quasiholes several wave functions can be associated, because half of the η_k's are grouped with z_i, and the other half with z_j, in the appropriate generalization of Eq. (3.3). It has been shown [81] that only 2^{m-1} of these functions are linearly independent. Braiding quasiholes adiabatically (which is feasible in a gapped system) can take the system from one linear combination of Pfaffian quasihole states to another, which is the origin of non-Abelian statistics of quasiholes.

The wave functions in Eqs. (3.2-3.4) can be mapped to the sphere by the stereographic mapping [59], which amounts to the substitution $(z_a - z_b) \to (u_a v_b - v_a u_b)$ for all coordinate differences (electrons and intended quasihole positions) (c.f. Eq. (2.20) for u_a and v_a). The Pfaffian ground state wave function becomes

$$\Psi_0^{\rm Pf} = {\rm Pf}\left(\frac{1}{u_i v_j - v_i u_j}\right)\Phi_1^2, \tag{3.5}$$

[3] See the appendix for the definition of Pf.

while the wave function for two quasiholes at (U_1, V_1) and (U_2, V_2) is given by

$$\Psi^{\rm Pf}_{2-{\rm qh}} = {\rm Pf}\left(\frac{(u_i V_1 - v_i U_1)(U_2 v_j - V_2 u_j) + (i \leftrightarrow j)}{(u_i v_j - v_i u_j)}\right) \Phi_1^2 \,, \tag{3.6}$$

For two coincident quasiholes, $(U_1, V_1) = (U_2, V_2) \equiv (U, V)$, this reduces to a charge $\frac{1}{2}$ vortex,

$$\Psi_V = \prod_i (u_i V - v_i U) \Psi_0^{\rm Pf} \,. \tag{3.7}$$

The wave functions in Eqs. (3.5 to 3.7) are the zero-energy eigenstate of the three-body model interaction [78, 82], which in real-space takes a singular form [67]

$$V^{({\rm Pf})} = \sum_{i<j<k} \mathcal{S}_{ijk} \nabla_i^4 \nabla_j^2 \delta(\mathbf{r}_i - \mathbf{r}_j) \delta(\mathbf{r}_j - \mathbf{r}_k),$$

where $\mathcal{S}_{ijk}$ is the symmetrization, while in the spherical geometry,

$$V^{({\rm Pf})} = \frac{e^2}{\epsilon l_B} \sum_{i<j<k} P_{ijk}(L_{\rm max}), \tag{3.8}$$

where $P_{ijk}(L_{\rm max})$ is the projection operator onto a triplet of orbital angular momentum $L_{\rm max} = 3Q - 3$. Notice that $L_{\rm max}$ corresponds to the closest possible configuration of an electron triplet. $V^{({\rm Pf})}$ does not penalize the closest approach of *two* electrons, but there is an energy cost when *three* electrons are in their closest configuration. We refer to the subspace spanned by the zero energy states of $V^{({\rm Pf})}$ as the "Pfaffian quasihole (PfQH) sector." As $[V^{({\rm Pf})}, L^2] = 0$, the states spanning the PfQH sector may be chosen with a definite L.[4] If the quasiholes are spatially localized, as in $\Psi^{\rm Pf}_{2-{\rm qh}}$, the rotational invariance is broken, but the state still lives entirely in the PfQH sector.

3.3.2 Violation of particle-hole symmetry in the Pfaffian model

The exact Coulomb eigenstates in any given Landau level satisfy particle-hole (p-h) symmetry, i.e., the exact eigenstates at ν and $1-\nu$ (for the spinful case, ν and $2-\nu$) are related by p-h conjugation. The CF wave functions (Sec. 2.5) satisfy p-h symmetry to a

[4] See Ref. [82] for a thorough study of the PfQH sector on the sphere.

very good approximation, even though there is no symmetry principle that so requires. For example, the wave functions at $\nu = \frac{n}{2n-1}$, given by $\Psi_{n/(2n-1)} = \mathcal{P}_{\rm LLL}\Phi_1^2[\Phi_n]^*$, are almost identical to the those obtained by particle-hole transformation of the wave functions $\Psi_{n'/(2n'+1)} = \mathcal{P}_{\rm LLL}\Phi_1^2\Phi_{n'}$, with $n = n' + 1$.

The $V^{(\rm Pf)}$ interaction does not satisfy particle-hole symmetry. To get a feel for the extent to which this symmetry is broken, we have considered the system of $N = 8$ particles at $2Q = 15$. In this case, particle hole transformation gives eight holes (to be distinguished from *quasi*holes) at $2Q = 15$. We obtain the exact spectrum of the $V^{(\rm Pf)}$ model interaction, which is given in the upper left panel of Fig. 3.10. This system corresponds to four quasiholes, and has a number of zero energy states, which form the Pfaffian quasihole sector. We obtain the particle-hole conjugate of each eigenstate, denoted Ψ^c, and calculate its energy expectation value for the $V^{(\rm Pf)}$ interaction. When there are several degenerate Pfaffian quasihole states, we diagonalize $V^{(\rm Pf)}$ in the subspace of the p-h conjugate states to obtain the energies. The resulting spectrum is shown in the top right column of Fig. 3.10.[5] We construct symmetrized states $\Psi^s \propto (\Psi + \Psi^c)$, which satisfy particle-hole symmetry by construction; the resulting spectrum for these states is given in the lower left panel of Fig. 3.10. The lower right spectrum is for p-h antisymmetrized states $\Psi^a \propto (\Psi - \Psi^c)$.

Table 3.10 shows the squared overlaps between the original Pfaffian quasihole states with the various states obtained with the help of p-h conjugation. To handle the multiplicity of the PfQH sector for $L = 0, 2, 4, 6$ (c.f. Fig. 3.10), the overlap between two subspaces has been defined in a basis-independent manner (see caption of Table 3.10). The overlaps are not particularly high; for example, in the $L = 0$ part of the quasihole branch, which contains two states for $N = 8$, the overlap is 0.511, and deteriorates for higher L's in the PfQH sector. The near orthogonality of Ψ and Ψ^c at $L = 8$ is accompanied by a very high energy of Ψ^c.

These results demonstrate a substantial breakdown of the p-h symmetry by the $V^{(\rm Pf)}$ interaction. The Pfaffian quasihole band is absent in all of the new spectra; the states derived from the Pfaffian quasihole band are mixed up with other states. It has been shown [67] that the particle-hole symmetrization ($\Psi \to \Psi^s$) of the Pfaffian wave function

[5] For the Coulomb interaction, this exercise would produce a spectrum identical to the original one, apart from an overall energy shift.

improves the overlap with the Coulomb ground state. Our results show, however, that this also destroys the degeneracy of PfQH sector. One can ask whether the non-Abelian statistics of the Pfaffian quasiholes is robust to p-h symmetrization; we are not able resolve this question definitively by a direct calculation of the braiding phases, which requires much larger systems; but the disruption of the PfQH band is discouraging.

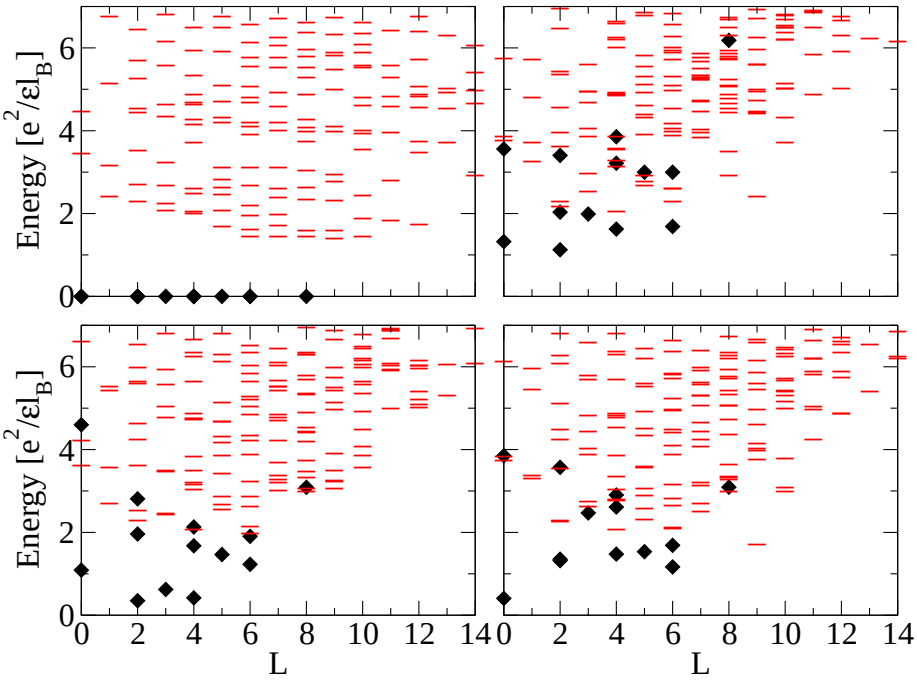

Figure 3.10: Energy of the particle-hole conjugate (Ψ^{c}), symmetrized (Ψ^{s}), and antisymmetrized (Ψ^{a}) images of the PfQH sector for $N = 8$ particles with four quasiholes. Upper left panel shows the original spectrum of $V^{(\mathrm{Pf})}$ with $N = 8, 2Q = 2N - 1$ (four quasiholes); the Pfaffian quasihole states have zero energy. Also shown are the spectra for the p-h conjugate states (top right), the p-h symmetrized states (bottom left), and p-h antisymmetrized states (bottom right). The diamonds show the states derived from the Pfaffian quasihole branch.

3.3.3 Off-diagonal long range order

We wish to stress that the Pfaffian wave function does not represent a true superconductor; the pairing of composite fermions opens a gap to produce FQHE but does not establish long range phase coherence in the electronic state. For this purpose, we calculate the

	p-h conjugate	symmetric combination	antisymmetric combination
$O(L=0)$	0.511	0.425	0.575
$O(L=2)$	0.431	0.542	0.458
$O(L=3)$	0.357	0.798	0.201
$O(L=4)$	0.255	0.641	0.359
$O(L=5)$	0.001	0.511	0.489
$O(L=6)$	0.233	0.443	0.557
$O(L=8)$	4×10^{-7}	0.500	0.500

Table 3.4: Squared overlaps between the states in the PfQH sector and the subspaces spanned by their particle-hole conjugate, particle-hole symmetrized, and particle-hole antisymmetrized images. Squared overlaps are defined as $\mathcal{O}=\sum_{i,j}^{\mathcal{N}}|\langle\Psi_{4-\mathrm{qh,i}}|\Psi'_{4-\mathrm{qh,j}}\rangle|^2/\mathcal{N}$, where $\mathcal{N}$ is the number of degenerate multiplets[82] of $V^{(\mathrm{Pf})}$ at L, and $i,j=1,\cdots,\mathcal{N}$.

off-diagonal long range order (ODLRO) parameter:

$$|G(\mathbf{r}_1,\mathbf{r}_2,\mathbf{r}'_1,\mathbf{r}'_2)|=\langle\Psi_0|\hat{\psi}^\dagger(\mathbf{r}'_1)\hat{\psi}^\dagger(\mathbf{r}'_2)\hat{\psi}(\mathbf{r}_1)\hat{\psi}(\mathbf{r}_2)|\Psi_0\rangle, \tag{3.9}$$

where $\hat{\psi}(\mathbf{r})$ and $\hat{\psi}^\dagger(\mathbf{r})$ are the usual annihilation and creation field operators. We place the primed coordinates near the north pole, separated by a distance equal to the magnetic length, and the unprimed coordinates at the south pole, also separated by a distance equal to the magnetic length. The results in Table 3.5, obtained by Monte Carlo calculation, demonstrate the absence of off-diagonal long range order in the Pfaffian wave function.

N	$\mathrm{Pf}\left(\frac{1}{z_i-z_j}\right)$	$\mathrm{Pf}\left(\frac{1}{z_i-z_j}\right)\Phi_1^2$
4	0.44(14)	0.0005(9)
6	0.47(9)	0.001(2)
8	0.46(8)	0.0000(1)
10		0.0002(5)

Table 3.5: Off-diagonal long range order $G(\mathbf{r}_1,\mathbf{r}_2,\mathbf{r}'_1,\mathbf{r}'_2)$ with $\mathbf{r}_1$ and $\mathbf{r}_2$ separated by l_B about the north pole, and $\mathbf{r}'_1$ and $\mathbf{r}'_2$ separated by l_B about the south pole for the paired CF wave function Ψ_0^{Pf}. For the electron pairing wave function $\mathrm{Pf}\left(\frac{1}{z_i-z_j}\right)$ the radius $R=\sqrt{2}$ is independent of N; we use the same *angular* separation as for the paired CF wave function.

3.4 Nature of the excitations of the at $\nu = \frac{5}{2}$

Comparisons with exact diagonalization studies on finite size systems have served as a litmus test for theoretical proposals on fractional quantum Hall effect. In this section we report on such tests for the Pfaffian model of the $\nu = \frac{5}{2}$ FQHE. We will focus on quasiparticles and quasiholes of this state. We will investigate how well the Pfaffian model represents the solutions of the Coulomb interaction $V^{(\mathrm{C})}$, with and without the presence of weak Dirac-delta impurities, which are intended to localize the quasiholes or quasiparticles.

We will work in the spherical geometry (Sec. 2.3), and study the second Landau level via effective pseudopotentials (c.f. Eq. (2.31)). Full spin polarization is assumed, LL mixing and finite thickness are neglected. The eigenstates are labeled by the orbital angular momentum L.

3.4.1 Testing the Pfaffian model for quasiholes

Figs. 3.11 to 3.13 show the spectra for states with two and four quasiholes for $N = 10$ to 14 electrons. For 10 electrons, the Pfaffian model predicts zero energy states at $L = 1, 3, 5$ and $L = 0^2, 2^4, 3^1, 4^4, 5^2, 6^3, 7^1, 8^2, 10^1$, respectively (the superscript denotes the degeneracy), for two and four quasiholes. These states form the Pfaffian quasihole band. For 12 electrons, the Pfaffian quasihole band contains states at $L = 0, 2, 4, 6$ for two quasiholes and $L = 0^3, 2^4, 3^2, 4^5, 5^2, 6^5, 7^2, 8^3, 9^1, 10^2, 12^1$ for four quasiholes. For 14 electrons, the Pfaffian quasihole band for two quasiholes has states at angular momenta $L = 1, 3, 5, 7$.

The Coulomb spectra in Figs. 3.11 to 3.13 do not show well defined bands with one-to-one correspondence to the PfQH sector. In Sec. 3.4.2 we will give overlaps between the Pfaffian and Coulomb quasihole states, which are generally worse than for the ground state. Fig. 3.14 depicts for the two quasihole state (for 14 electrons) the "total overlap," defined as $\mathcal{O} = \sum_{L=1,3,5,7} |\langle \Psi^L_{2-\mathrm{qh}} | \Psi^L_{\mathrm{coul}} \rangle|^2 / 4$ where $|\Psi^L_{2-\mathrm{qh}}\rangle$ is the two quasihole state with $L_z = L$ and $|\Psi^L_{\mathrm{coul}}\rangle$ is the Coulomb ground state with $L_z = L$. This figure shows the dependence of the overlap on the form of the interaction; by increasing the V_1 pseudopotential of the Coulomb interaction by 0.03 units, it is possible to increase the overlap from 0.3 to 0.6. For large δV_1, the solution is essentially the lowest LL Coulomb solution; Fig. 3.14 thus shows that the Pfaffian wave functions provide a comparable description of the state in the

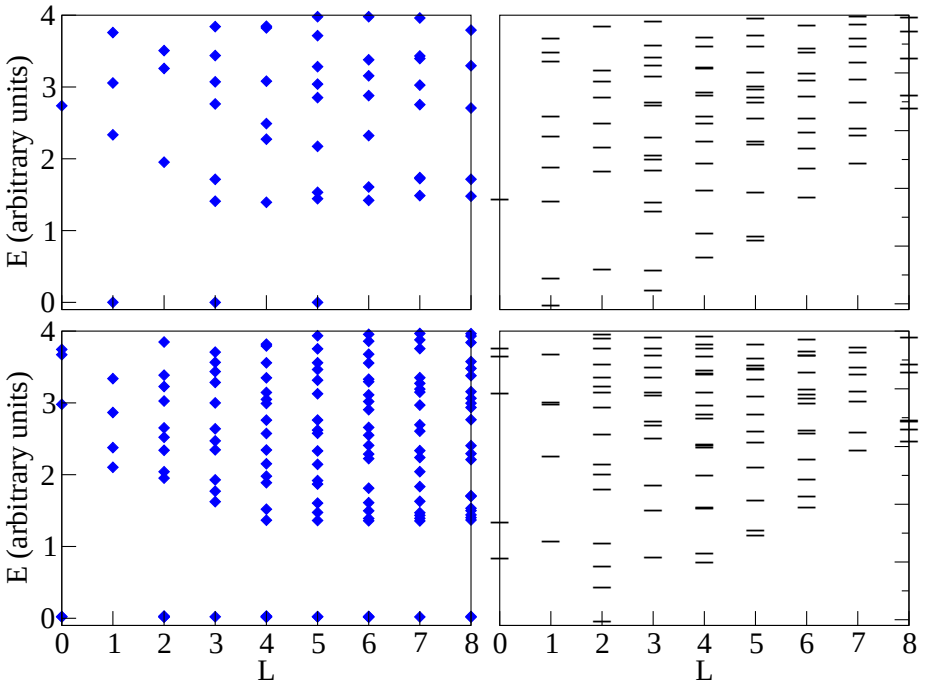

Figure 3.11: Spectra at $\nu = \frac{5}{2}$ for the model interaction $V^{(\mathrm{Pf})}$ (left column), and the Coulomb interaction (right column) for $N = 10$ particles at $2l = 18$ (two quasiholes, top row) and $2l = 19$ (four quasiholes, bottom row). For the $V^{(\mathrm{Pf})}$ interaction, two (four) quasiholes are expected for $2l = 18$ ($2l = 19$). The spectra on the left were also given in Ref. [82].

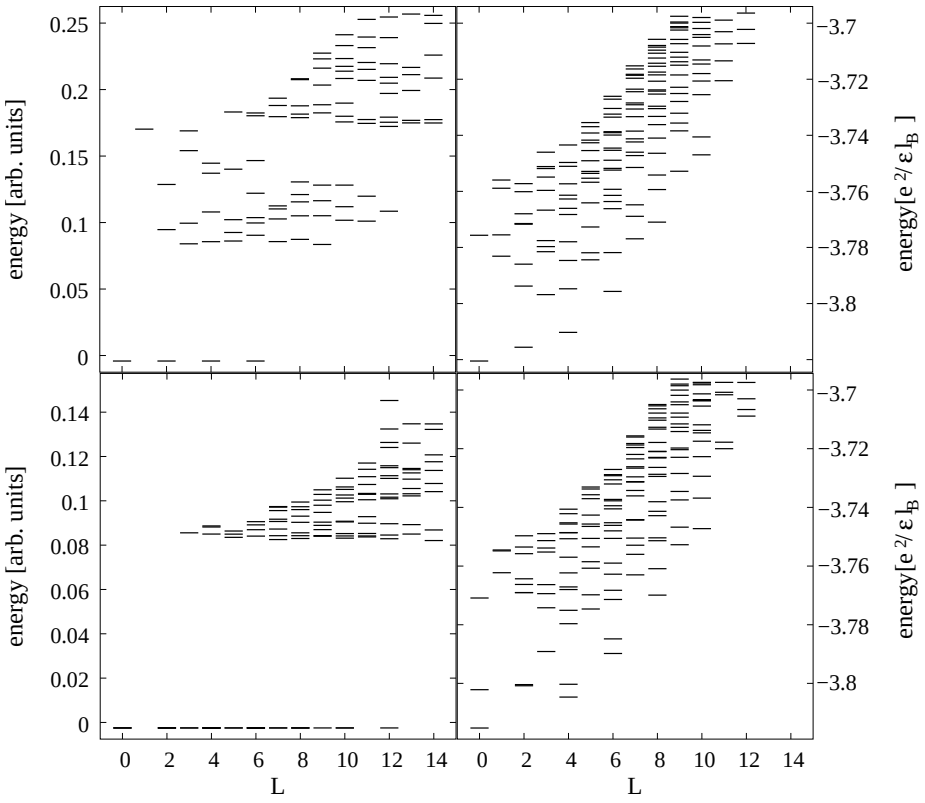

Figure 3.12: Spectra at $\nu = \frac{5}{2}$ for the model interaction $V^{(\mathrm{Pf})}$ (left column), and the Coulomb interaction (right column) for $N = 12$ particles for two (upper row) and four (lower row) quasiholes.

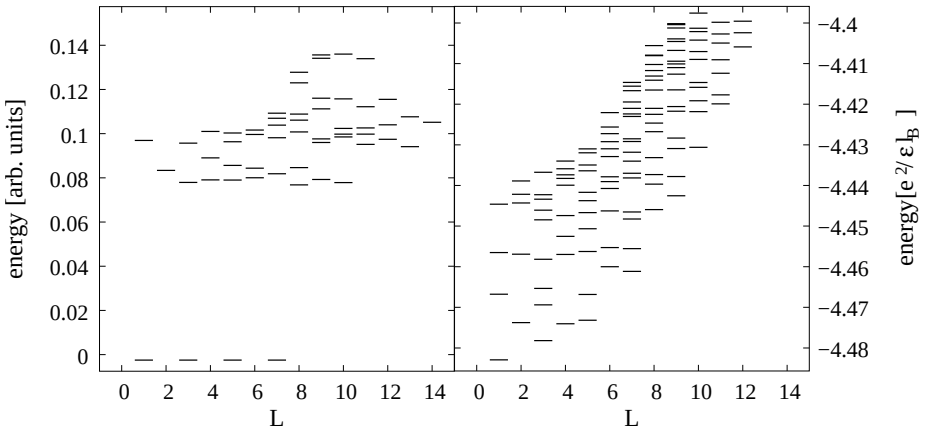

Figure 3.13: Spectra at $\nu = \frac{5}{2}$ for the model interaction $V^{(\mathrm{Pf})}$ (left column), and the Coulomb interaction (right column) for $N = 14$ particles for two quasiholes.

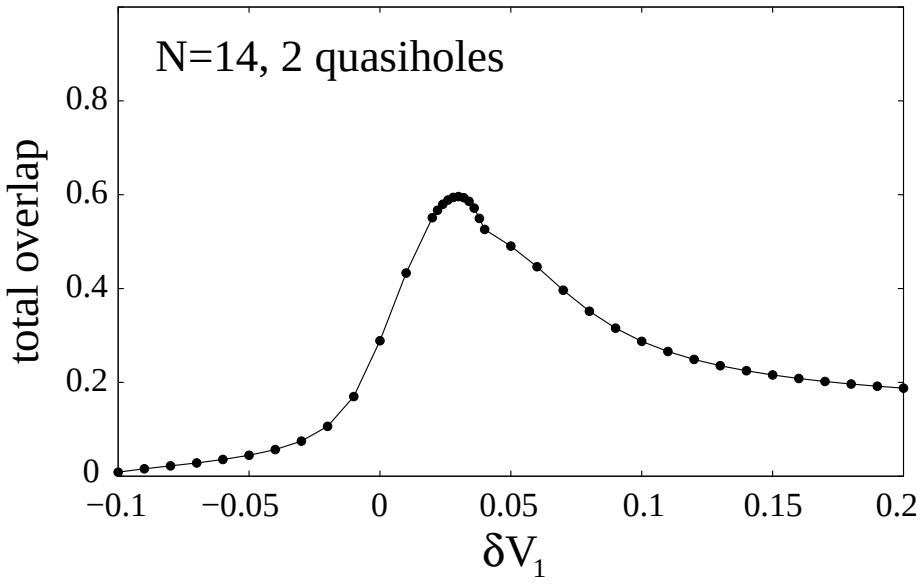

Figure 3.14: The overlap between the low-energy excitations of the second LL Coulomb and $V^{(\mathrm{Pf})}$ interactions for $N = 14$ particles as the leading pseudopotential V_1 is changed.

lowest two Landau levels. On the other hand, as finite thickness softens the short-range part of the interaction (negative δV_1), it moves the system toward the region where the excitations of $V^{(\mathrm{C})}$ and $V^{(\mathrm{Pf})}$ are not similar.

The lack of a *qualitative* correspondence between the low energy spectra of $V^{(\mathrm{Pf})}$ and the Coulomb interactions in Fig. 3.11 to 3.13 raises questions regarding the validity of the $V^{(\mathrm{Pf})}$ model, and hence of the model of quasiholes based on the Pfaffian wave function [81, 86], for the *real* quasiholes of the $\nu = \frac{5}{2}$ state. This has relevance to the issue of statistics. Non-Abelian statistics for the quasiholes of the $V^{(\mathrm{Pf})}$ model presupposes the existence of several degenerate states for a given configuration of spatially localized quasiholes, which, in turn, is closely related to the degeneracy of the angular momentum eigenstates in Fig. 3.24. The spectra in Fig. 3.11 to 3.13 demonstrate a lack of adiabatic continuity, for the systems studied, between the many quasihole states of the $V^{(\mathrm{Pf})}$ and the Coulomb models.[6]

[6]For the many quasiparticle or many quasihole states of the ordinary FQHE states in the lowest Landau level, the qualitative structure of a low-energy band predicted by the analogy to noninteracting fermions at Q^* is confirmed in similar exact spectra [54].

3.4.2 Comparison of the lowest excitations

The origin of non-Abelian statistics lies in the degeneracy of states in the PfQH sector. In this subsection we investigate how the PfQH sector, defined in terms of the model interactions $V^{(\mathrm{Pf})}$, corresponds to the low-energy excitations of the Coulomb interaction in the second Landau level.

N	$L=0$	1	2	3	4	5	6	7
8	0.64	-	0.48	-	0.52	-	-	-
10	-	0.05	-	0.56	-	0.61	-	-
12	0.59	-	0.30	-	0.49	-	0.39	-
14	-	0.39	-	0.13	-	0.39	-	0.27

Table 3.6: Squared overlaps between the PfQH basis ($\Psi^{\mathrm{Pf}}_{2-\mathrm{qh}}\rangle$) for two quasiholes and the lowest energy states of the Coulomb interaction ($\Psi^{\mathrm{C}}_{2-\mathrm{qh}}\rangle$) in the second Landau level at $2Q = 2N-2$. We note that for two quasiholes, there is a single zero energy multiplet at alternate values of L for $V^{(\mathrm{Pf})}$ ($L = 0, 2, \cdots, \frac{N}{2}$ for even $\frac{N}{2}$, and $L = 1, 3, \cdots, \frac{N}{2}$ for odd $\frac{N}{2}$).

N	$L=0$	2	3	4	5	6	7	8	9	10	12
8	0.78	0.54	0.65	0.47	0.36	0.45	-	0.21	-	-	-
10	0.67	0.48	0.49	0.47	0.21	0.34	0.26	0.32	-	0.02	-
12	0.42	0.32	0.27	0.32	0.17	0.28	0.21	0.23	0.23	0.24	0.07

Table 3.7: Overlaps between the PfQH basis for four quasiholes and the lowest energy states of the Coulomb interaction in the second Landau level at $2Q = 2N-1$. The overlap at a given L is defined as $\mathcal{O} = \sum_{i,j}^{\mathcal{N}} |\langle \Psi^{\mathrm{Pf}}_{4-\mathrm{qh,i}} | \Psi^{\mathrm{C}}_{4-\mathrm{qh,j}} \rangle|^2 / \mathcal{N}$, where $\mathcal{N}$ is the number of degenerate multiplets of $V^{(\mathrm{Pf})}$ at L [86], and $i, j = 1, \cdots, \mathcal{N}$. The states $\Psi^{\mathrm{C}}_{4-\mathrm{qh,j}}$ represent the $\mathcal{N}$ lowest energy eigenstates of the Coulomb interaction.

Tables 3.6 and 3.7 show the overlaps between the PfQH basis and the corresponding number of lowest energy states for the Coulomb interaction, for two as well as four quasiholes. The overlaps are low by the FQHE standards. As noted in Sec. 3.4.1, no distinct quasihole band analogous to the PfQH band is identifiable in the exact Coulomb spectrum. The Coulomb interaction does not simply lift the degeneracy of the PfQH states but changes the structure of the low energy sector in a fundamental manner.

3.4.3 Attempted separation of charge-$\frac{1}{4}$ quasiholes

We next investigate spatially localized quasiholes and quasiparticles, as needed for an evaluation of their braiding phases. It is natural to attempt to localize them with the help of weak delta function potentials of appropriate sign, which can serve as a model of an scanning tunneling microscope tip for manipulating them. We have studied a range of strengths for the delta function potential, but we show results below for weak delta functions of strength $(0.005/\sqrt{Q})e^2/\epsilon l_B$. We place a delta function at one or both poles of the sphere, so L_z continues to be a good quantum number.[7]

We first consider the $V^{(\mathrm{Pf})}$ model. The impurity, being weak, does not cause significant mixing with states outside the PfQH sector. A single delta function impurity in the lowest LL localizes a vortex Ψ_V rather than a Pfaffian quasihole for the following reason. The energy of a given wave function is equal to a properly weighted average of the densities at the positions of the delta functions (for weak impurity strengths). For a delta function at (U, V), the lowest energy state (which has zero energy independent of the strength of the delta impurity) is the one in which *both* quasiholes localize at (U, V), producing a vortex Ψ_V with vanishing density at (U, V). (The binding of quasiholes remains valid also for a delta function in the second LL, although the density has more complicated structure than a simple vortex, as seen in Fig. 3.15(b).) We ask if it is possible to split the vortex into two quasiholes with the help of *two* delta function impurities, placed at the two poles of the sphere. The diagonalization is performed in the *full* L_z subspace, including states within and outside the PfQH band; for sufficiently weak delta function strengths, however, the solution is essentially restricted to the PfQH sector. (For example, for $N = 14$, the overlap between the ground state with delta functions and the corresponding state in the PfQH sector is 0.999.) The lowest energy eigenstate of this model is denoted by $\Psi^{\mathrm{Pf}}_{2-\mathrm{qh}}$. Surprisingly, as seen in Fig. 3.15(b), two delta impurities fail to separate two quasiholes. The Pfaffian quasihole wave function $\Psi^{\mathrm{Pf}}_{2-\mathrm{qh}}$, in contrast, has two reasonably well separated quasiholes of charge $\frac{1}{4}$ each, as seen in Fig. 3.15(a). We also show in Fig. 3.16(a) results for two quasiparticles, and again see no indication of two separate charge-$\frac{1}{4}$ objects.

[7] The results depend slightly (though not qualitatively) on whether the impurity is a delta function in the lowest or the second LL. With the exception of Fig. 3.15(a), the results in Figs. 3.15 and 3.16 depict the electron density in the second LL for a delta function impurity in the second LL.

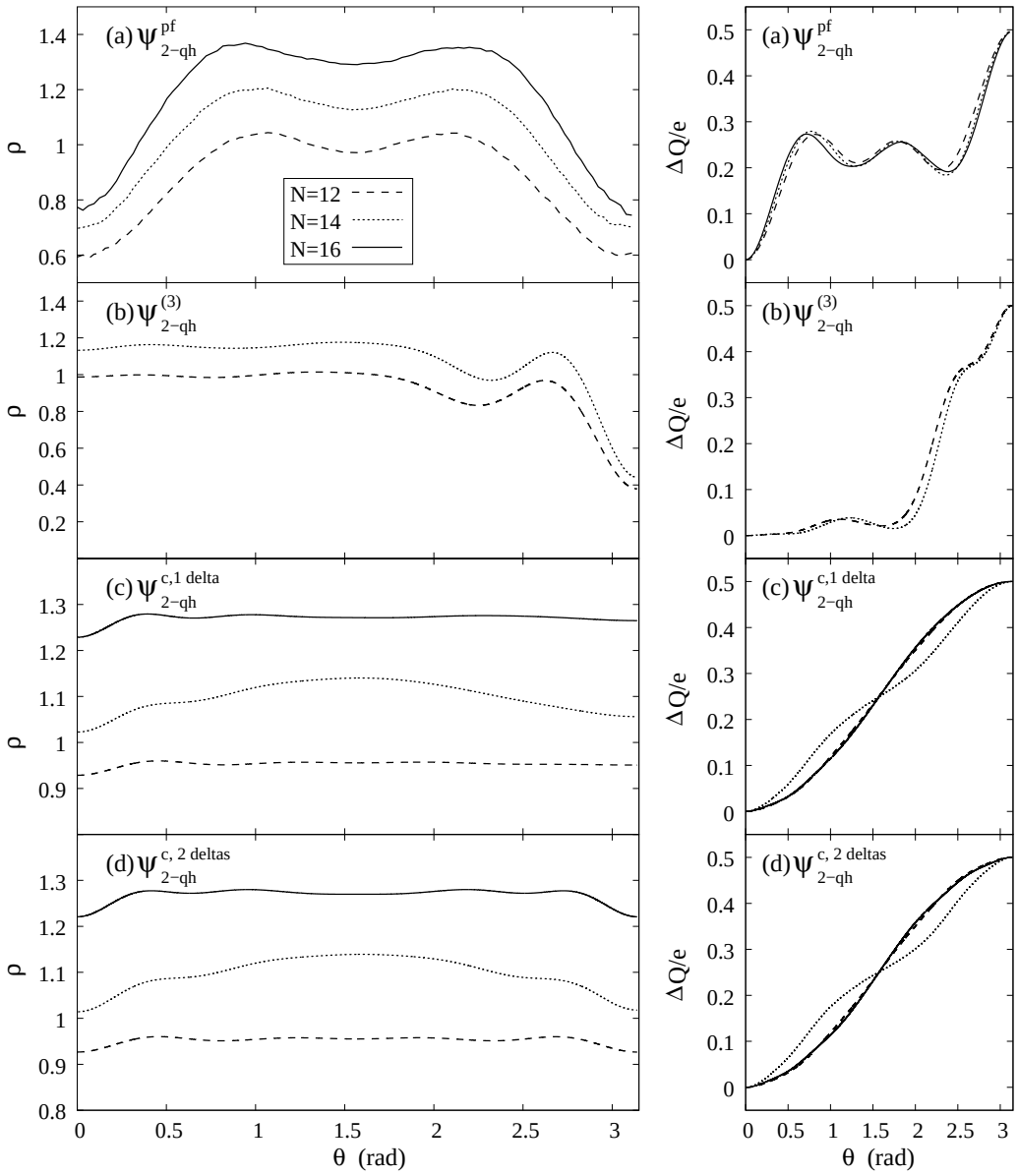

Figure 3.15: Left: Charge densities of $\Psi^{\rm Pf}_{2-{\rm qh}}$ (a) with the quasiholes placed on the two poles, and of the ground state for $\Psi^{\rm Pf}_{2-{\rm qh}}$ (b) and $\Psi^{\rm C}_{2-{\rm qh}}$ (d) in the presence of two delta function impurities at the two poles, and for $\Psi^{\rm C}_{2-{\rm qh}}$ (c) in the presence of one delta function impurity at the north pole. The results are shown for $N = 12$ (dashed lines), $N = 14$ (dotted lines) and $N = 16$ (solid lines) electrons at $2Q = 2N - 2$. When the ground state has $L_z \neq 0$, the states at $\pm L_z$ are degenerate; only one of them is shown for simplicity. The normalization ensures that the integral of the entire sphere gives N. Right: the integrated excess charge, normalized so that the total charge excess is $\frac{1}{2}$. Two spatially separated quasiholes will exhibit a step at charge $\frac{1}{4}$.

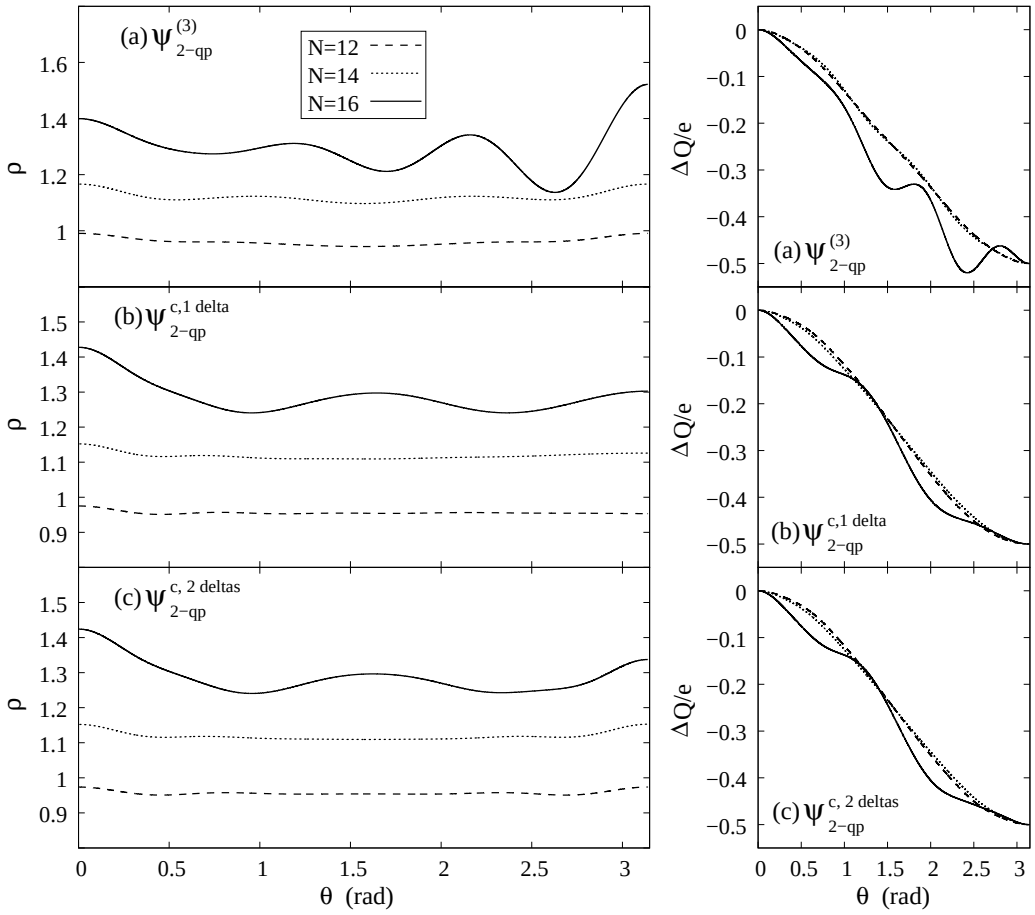

Figure 3.16: Same as in Fig. 3.15, but for quasiparticles. There are only three panels, because a Pfaffian wave function analogous to $\Psi_{2-\mathrm{qh}}$ is not known.

N	$\lvert\langle\Psi^{\rm Pf}_{2-{\rm qh}}\lvert\Psi^{\rm Pf}_{2-{\rm qh}}\rangle\rvert^2$	$\lvert\langle\Psi^{\rm Pf}_{2-{\rm qh}}\lvert\Psi^{(C)}_{2-{\rm qh}}\rangle\rvert^2$
8	0 [0.9831(1)*]	0.326(2)
10	0 [0.862(3)*]	0 [0.045(3)*]
12	0 [0.959(8)*]	0.19(2)

Table 3.8: Squared overlaps of the Pfaffian quasihole wave function $\Psi^{\rm Pf}_{2-{\rm qh}}$ (with two quasiholes located at the two poles) with the ground states of $V^{(\rm Pf)}$ and Coulomb interaction, with a delta impurity at each pole. The overlaps are identically zero when the actual ground state has $L_z \neq 0$; in those cases, the overlap of $\Psi^{\rm Pf}_{2-{\rm qh}}$ with the lowest energy state in the $L_z = 0$ sector is also given (in square brackets, marked by an asterisk).

Table 3.8 shows the overlap of the Pfaffian quasihole wave function, $\Psi^{\rm Pf}_{2-{\rm qh}}$, with two quasiholes at the two poles, with the exact ground eigenstate in the presence of two weak delta function impurities at the two poles. When the ground state has $L_z \neq 0$, the overlap of $\Psi^{\rm Pf}_{2-{\rm qh}}$ with the lowest energy state in the $L_z = 0$ sector is also shown.

Tables 3.9 and 3.10 give insight into how the exact solution of $V^{(\rm Pf)}$, with two impurities, is different from the Pfaffian wave function $\Psi^{\rm Pf}_{2-{\rm qh}}$. Table 3.9 shows the projections of $\Psi^{\rm Pf}_{2-{\rm qh}}$ with different zero-energy angular momentum eigenstates of $V^{(\rm Pf)}$. The wave function $\Psi^{\rm Pf}_{2-{\rm qh}}$ is a linear combination of PfQH states with several low angular momenta. The expectation values of L_z and L for the exact two quasihole / quasiparticle ground states of $V^{(\rm Pf)}$ are shown in Table 3.10. The actual ground state of $V^{(\rm Pf)}$ in the presence of two delta functions, $\Psi^{\rm Pf}_{2-{\rm qh}}$, has a high angular momentum in the PfQH sector, whereas $\Psi^{\rm Pf}_{2-{\rm qh}}$ predominantly contains low angular momentum components.

N	$L=0$	1	2	3	4	5	6
8	0.33	-	0.65	-	0.02	-	-
10	-	0.66	-	0.33	-	0.01	-
12	0.29(3)	-	0.57(5)	-	0.13(9)	-	0.01(1)

Table 3.9: Projections of the two quasihole wave function $\Psi^{\rm Pf}_{2-{\rm qh}}$ (with the two quasiholes located at the two poles) onto the PfQH sector, defined as $\lvert\langle\Psi^{\rm Pf}_{2-{\rm qh}}\lvert\Psi^{\rm Pf}_{2-{\rm qh,L}}\rangle\rvert^2$. The angular momentum is L, and its z component is $L_z = 0$.

We next turn to two Coulomb quasiholes or quasiparticles. Here, at first sight, one may expect that even a single delta function should produce well separated quasiholes or

N	8	10	12	14	16
$\Psi^{\rm Pf}_{2-{\rm qh}}$	(4.00,3)	(5.00,4)	(6.00,5)	(7.00,6)	-
$\Psi^{\rm C}_{2-{\rm qh}}$	(2.00,0)	(1.01,1)	(0.04,0)	(1.03,0)	(0.08,0)
$\Psi^{\rm Pf}_{2-{\rm qp}}$	(0.00,0)	(1.00,0)	(2.00,0)	(3.00,0)	(4.00,2)
$\Psi^{\rm C}_{2-{\rm qp}}$	(2.00,0)	(1.00,0)	(0.02,0)	(1.01,0)	(2.01,1)

Table 3.10: The expectation values of L and $|L_z|$, shown as $(L, |L_z|)$, for the ground states $\Psi^{\rm Pf}_{2-{\rm qh}}$, $\Psi^{\rm C}_{2-{\rm qh}}$, $\Psi^{\rm Pf}_{2-{\rm qp}}$, and $\Psi^{\rm C}_{2-{\rm qp}}$ in the presence of two weak delta function impurities at the two poles.

quasiparticles, because it can bind one of them, which then should repel the other. As seen in Figs. 3.15(c,d) and 3.16(b,c), neither one nor two delta functions produce separated quasiholes or quasiparticles. In fact, the charge profile is practically identical for the two cases. The situation is more restrictive for the Coulomb interaction because, instead of many degenerate states, we have a single ground state multiplet with a definite L. All that *weak* disorder can do is cause mixing between the different L_z components of the ground state multiplet. For the case of two delta functions at the two poles, L_z is a good quantum number, so the delta functions only lift the degeneracy of the L_z states. The lack of quasiparticle or quasihole separation in space is attributable to the fact that the ground state now has a more or less definite L. The absence of exact degeneracy, as found for the $V^{(\rm Pf)}$ model, thus inhibits quasihole localization. The overlaps of the Coulomb quasiholes with the Pfaffian quasiholes (Table 3.8) are very low and rapidly decreasing with N. (Slight modification in the pseudopotentials does not affect the picture qualitatively. For two quasiholes at $N = 14$, changing V_1 pseudopotential by $\delta V_1 = 0.03$, which results in the maximum overlap with the PfQH sector (Fig. 3.14), produces a ground state which has an overlap of 0.998 with the pure Coulomb ground state.)

While our study does not rule out well separated charge-$\frac{1}{4}$ quasiholes for the Coulomb problem for larger systems, it is rather striking that no well defined quasiholes are seen even for systems with as many as 16 electrons, which is sufficiently large at least for the *Pfaffian* quasiholes to be well separated. The Pfaffian model thus fails to capture the long-range correlations present in the true state. Eigenstates with separated quasiholes and quasiparticles do exist in some of our finite size systems, but are not the lowest energy states for our disorder potential. Separating them with more complicated impurity potentials is

thus possible, but our calculations show that it does not happen generically.

The braiding properties of the Pfaffian quasiholes have been studied numerically by Tserkovnyak and Simon [83]. In view of the above results, it is crucial to carry out similar calculations directly for the braiding properties of the Coulomb quasiholes and quasiparticles of the $\nu = \frac{5}{2}$ state. That, unfortunately, is beyond our present capabilities. The systems accessible in exact diagonalization study are too small for this purpose, as they do not even show charge-$\frac{1}{4}$ quasiholes. A computation for larger systems would require a knowledge of accurate trial wave functions for the Coulomb quasiparticles and quasiholes, not currently available. Nonetheless, to the extent that non-Abelian statistics is a consequence of the Pfaffian structure, our study questions its validity for the Coulomb problem. One may ask if the deviation between Pfaffian wave functions and the Coulomb solutions is a finite size effect and if the Pfaffian physics can be recovered in the thermodynamic limit. We see no reason for that to happen; as seen in Tables 3.6 and 3.8, the Pfaffian wave functions rapidly deteriorate with increasing N.[8] Larger systems will surely produce many *quasi* degenerate states for quasiholes, but they are unlikely to bear any relation to the states of the PfQH sector. Also, a gap separating "quasihole states" from rest of the states is crucial for maintaining their "topological" integrity; such a gap is present for the $V^{(\mathrm{Pf})}$ model, but not for the Coulomb Hamiltonian. These considerations suggest that the braiding properties of the Pfaffian quasiholes are unlikely to carry over to the Coulomb quasiholes.

The existence of charge-$\frac{1}{4}$ quasiholes is necessary (charge-$\frac{1}{2}$ vortices have Abelian braiding statistics) but not sufficient for non-Abelian braiding statistics. The braiding statistics is much more sensitive to subtle long-range correlations than the fractional charge. As an example, Laughlin's wave function for the quasiparticle at $\frac{1}{3}$ has the correct charge but an incorrect *Abelian* braiding statistics [132].

If the excitations of the $\nu = \frac{5}{2}$ state are not well described by Pfaffian wave function, what describes their physics? Further work will be needed to answer this question. The CF model may shed some light on that. It is shown in Sec. 3.5 that the residual interaction

[8] For odd-denominator FQHE states at $\nu = \frac{n}{2pn\pm1}$, similar system sizes show a separate band of states that is consistent with the effective magnetic field, and the Coulomb eigenfunctions are accurately described by CF theory. See [51, 54].

between composite fermions opens a gap at $\nu = \frac{5}{2}$. In this picture, the quasiparticles are excited composite fermions, although heavily renormalized by the interaction.

3.4.4 Energy splitting of the Pfaffian quasihole states

The Pfaffian model predicts a 2^{m-1} degenerate wave functions for any given configuration of $2m$ quasiholes, which is responsible for the emergence of non-Abelian braiding statistics. Any deviation from the model interaction $V^{(\mathrm{Pf})}$ lifts this degeneracy; but a case can be made that if the energy splitting of these states remains exponentially small as a function of the distance between the quasiholes, the idea of non-Abelian statistics remains experimentally relevant. It would be of interest to test how the energy splitting behaves in a realistic calculation. Unfortunately, a good model for the Coulomb quasiholes is not available, and it is not known how separated quasiholes can be produced in exact diagonalization studies (Sec. 3.4.3). We study how the Coulomb interaction splits the degeneracy while restricting to the PfQH sector. In light of the above comparisons, such a restriction is not necessarily a valid approximation, because the Coulomb interaction causes a substantial mixing with states outside of the PfQH sector. However, a more accurate calculation is currently not feasible.

The calculation requires at least four quasiholes, which we place on the sphere at maximal separation, i.e., at the vertices of a regular tetrahedron. The Coulomb interaction in the first and second LL's is diagonalized in the space spanned by two Pfaffian quasihole wave functions. The overlap and interaction matrices are calculated by Monte Carlo methods; an orthonormal basis is found by the standard Gram-Schmidt procedure; and the interaction is diagonalized in this basis. The Coulomb interaction in the second LL is simulated in the lowest LL by an effective interaction of the following form:

$$V^{\mathrm{eff}}(r) = \frac{1}{r} + \sum_{i=0}^{M} c_i r^i e^{-r^2}, \tag{3.10}$$

where the coefficients c_i are fixed so that the lowest LL pseudopotentials (Eq. (2.30)) of $V^{\mathrm{eff}}(r)$ reproduce the first few of the second LL Coulomb pseudopotentials $V_m^{(1)}$ (Eq. (2.31)) for odd values of m.[9]

[9]The fitting procedure of pseudopotentials is performed directly in the spherical geometry, whereas in

As apparent in Fig. 3.17, the lowest LL Coulomb interaction and the effective second LL interaction give different results for small ($N \leq 30$) systems. Because the energy splittings are very close in the $30 < N \leq 54$ range, we study larger systems ($N > 54$) with the lowest LL Coulomb interaction only. It is likely that the long distance behavior of the splitting does not depend on the Landau level index (given that the interaction at long distances is independent of the LL index). Fig. 3.18 shows the lowest LL splitting.

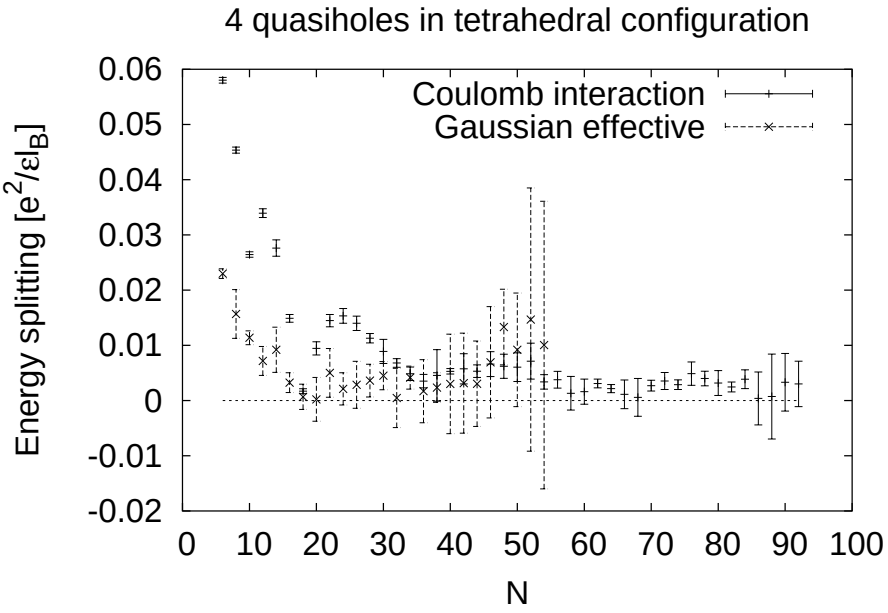

Figure 3.17: The energy splitting of the two four-quasihole wave functions on the sphere for Coulomb interaction.

The energy splitting is a nonmonotonic function of N (or R). Near the local minima the error in the logarithm of the energy splitting becomes very large. We therefore ask how the value of the ODLRO parameter at the local maxima decays with distance. While inconclusive, our results are most consistent with a power law decay of the splitting: A straight line fits at all the four bumps in the log-log plot (Fig. 3.19), but not in the semilog plot (not shown). A study of larger numbers of particles will be required for further confirmation, which is impractical at this stage, but assuming a power law, the energy

Sec. 3.2.2 the real-space effective interaction was obtained in the plane, and then used in the spherical geometry. The two procedures are equivalent in the thermodynamic limit.

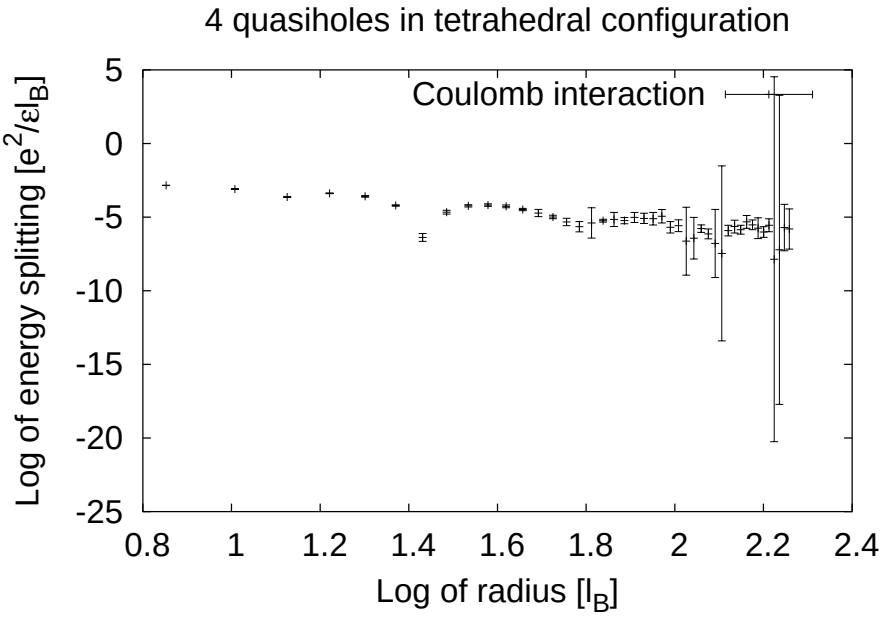

Figure 3.18: Same as Fig. 3.17, with both scales logarithmic. See line fitting on Figure 3.19.

splitting decays with an exponent $\alpha = -2.37(6)$. We stress again that the fact that the Coulomb interaction causes a substantial mixing with the non-PfQH sector diminishes the value of the calculation presented in this section.

3.5 An alternative explanation of the FQHE at $\nu = \frac{5}{2}$

Currently the best evidence in favor of the Pfaffian state comes from numerical studies, which have shown [80, 67, 76] that for small systems in the second Landau level, the Pfaffian wave function has a reasonably good overlap with the exact Coulomb ground state. On the other hand, in Sec. 3.4 we have seen evidence that the three-body interaction $V^{(\mathrm{Pf})}$ does not capture the qualitative physics of the actual excitations of the Coulomb $\nu = \frac{5}{2}$ state. Further, it is not known how the Pfaffian wave function, which does not contain any variational parameters, can be improved for the two body Coulomb interaction. The pairing of composite fermions is viewed as arising from an instability of the composite fermion Fermi sea [78, 79, 68], but the CF Fermi sea is not a limiting case of the Pfaffian wave

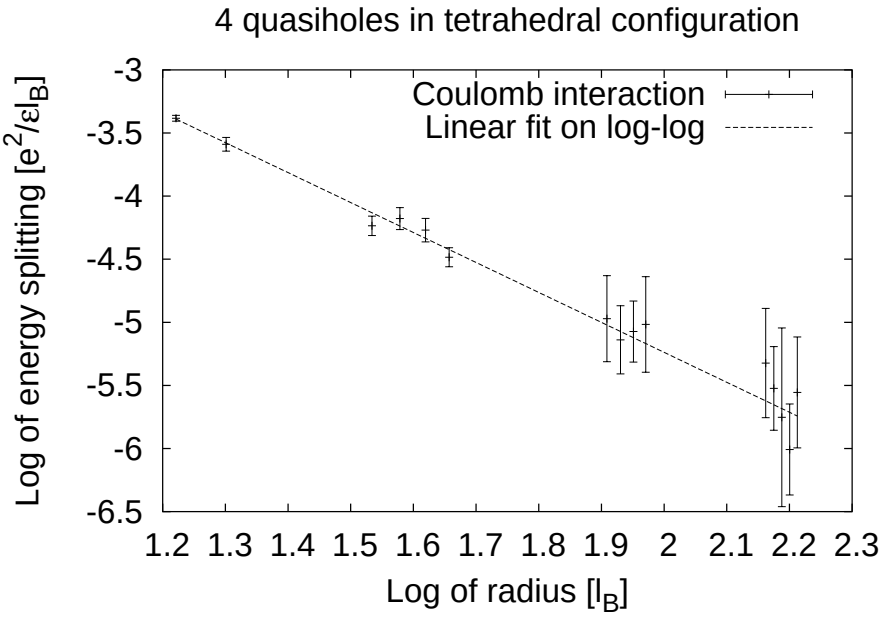

Figure 3.19: Line fitting on the log-log graph of the energy splitting as a function of the distance. A straight line fitted on the local maxima of the data is consistent with a power law decay with exponent $\alpha = -2.37(6)$.

function. Finally, the actual meaning of pairing of composite fermions remains unclear; the $\nu = \frac{5}{2}$ state has no off-diagonal long-range order (Sec. 3.3.3), and, in an operational sense, it does not appear different from other FQHE states.

These considerations have motivated us to seek another approach for describing the physics of the $\nu = \frac{5}{2}$ FQHE, on which we elaborate in this section. We still proceed within the CF framework, but without assuming any pairing at the outset. No FQHE occurs at $\nu = \frac{5}{2}$ in a model that neglects interactions between composite fermions, which predicts many degenerate ground states at this filling factor.[10] We show below that the residual interaction between composite fermions opens a gap to produce an incompressible state. Furthermore, the results can be improved systematically within a perturbative scheme. This approach produces the ground state as well as low-lying excitations.

[10] This is to be contrasted with the FQHE at $\nu = \frac{n}{2pn\pm1}$.

3.5.1 Methods

In this section the lowest LL is assumed to be full and inert; only the half-filled second LL is considered explicitly, and full spin polarization of electrons is assumed. The spherical geometry of Sec. 2.3 is employed.

Monte Carlo CF diagonalization requires a real-space interaction. The Coulomb interaction of the second LL is simulated by an effective interaction in lowest LL of the form

$$V^{\rm eff}(r) = \frac{1}{r} + \sum_{i=0}^{M} c_i r^i, \tag{3.11}$$

where the coefficients c_i are fixed so that the lowest LL pseudopotentials (Eq. (2.30)) of $V^{\rm eff}(r)$ reproduce *all* of the second LL Coulomb pseudopotentials $V_m^{(1)}$ (Eq. (2.31)) for odd values of m on the sphere.

A technical obstacle toward a quantitative study of the state at $\nu = \frac{5}{2}$, defined here through the relation $2Q = 2N - 3$, is that composite fermions experience a negative magnetic field $Q^* = -\frac{1}{2}$ by Eq. (2.34). While CF theory is known to be valid for negative B^* [118, 55], the convenient projection method developed in Ref. [54] does not apply to such situations for technical reasons.[11] One can avoid negative values of Q^* by exploiting the particle-hole symmetry of the Coulomb interaction to study

$$N_h = (2Q+1) - N = N - 2$$

holes at $2Q = 2N-3$. Composite fermions *made from holes* experience a positive monopole strength

$$Q^* = Q - (N_h - 1) = \frac{3}{2}. \tag{3.12}$$

The hole version of $\Psi_0^{\rm Pf}$ (Eq. (3.5)) is found conveniently from its second-quantized form.

3.5.2 Ground state and excitation gap

Fig. 3.20 shows the excitation spectra for $N_h = 12$, 14, 16 and 20 holes obtained by CF diagonalization at the zeroth and the first orders. ($N_h = 18$ is not considered as it aliases

[11] The projection procedure for reverse flux attachment has been elaborated recently by Möller and Simon [55], but we did not use it.

N_h	D_{ex}	$D^{(0)}$	$D^{(0)}_{L=0}$	$D^{(1)}$	$D^{(1)}_{L=0}$	$D^{(2)}$	$D^{(2)}_{L=0}$
6	151	3	1	14	2	42	3
8	1514	3	1	20	1	72	4
12	194668	4	1	37	2	205	8
14	2374753	8	1	63	3	644*	18*
16	3×10^7	4	1	52	2	495*	14*
20	5×10^9	5	1	77	2	965*	18*

Table 3.11: Dimensions of various bases for N_h particles at $2Q = 2N_h+1$. D_{ex} is the size of the Hilbert space in $L_z = 0$ sector, and $D^{(n)}$ is the dimension of the CF basis incorporating n-th order Λ-level mixing. $D^{(n)}_{L=0}$ is the number of CF states in the $L = 0$ sector. Asterisks mark the cases where we could not determine the number of linearly independent basis states.

with $\nu = \frac{3}{7}$ of holes.) The size of the correlated CF basis is compared to the dimensionality of the Hilbert space in Table 3.11, demonstrating the nontrivial nature of our results. The residual interaction between composite fermions lifts the degeneracy between various states to produce an incompressible state already at the lowest (zeroth) order, which neglects Λ-level mixing. Although the energy gaps change by up to 50% from the the zeroth to the first order, the incompressibility is preserved, indicating that while Λ-level mixing renormalizes composite fermions, it does not cause any phase transition. The overestimation of gaps at the zeroth order may be attributed to the very small dimensions of the CF basis. All CF basis states are perturbations of the noninteracting CF Fermi sea, making it explicit that a rearrangement of composite fermions near the CF Fermi level is responsible for the $\nu = \frac{5}{2}$ FQHE.[12]

Fig. 3.21 shows analogous results for the half filled *lowest* LL. Our method predicts a *compressible* state at half-filled lowest Landau level, as expected. (Recall that the half-filled lowest LL is described as a gapless Fermi sea state of CF's [130, 131], and this prediction has been confirmed by several experiments [27, 28, 29, 30].) The zeroth order CF diagonalization generates the lowest band, and the first order generates the next band. The energies of states in the lowest band do not change appreciably from zeroth to the first

[12]The Pfaffian state and the CF Fermi sea occur at different flux quanta ($2Q = 2N - 3 = 2N_h + 1$ and $2Q = 2N - 2 = 2N_h$). We chose $2Q$ as suitable for the Pfaffian. The Fermi sea state can be captured in finite systems only for $N = k^2$ particles at the neighboring monopole strength $Q = N - 1$, so there are mobile CF's in all of the systems in Fig. 3.21.

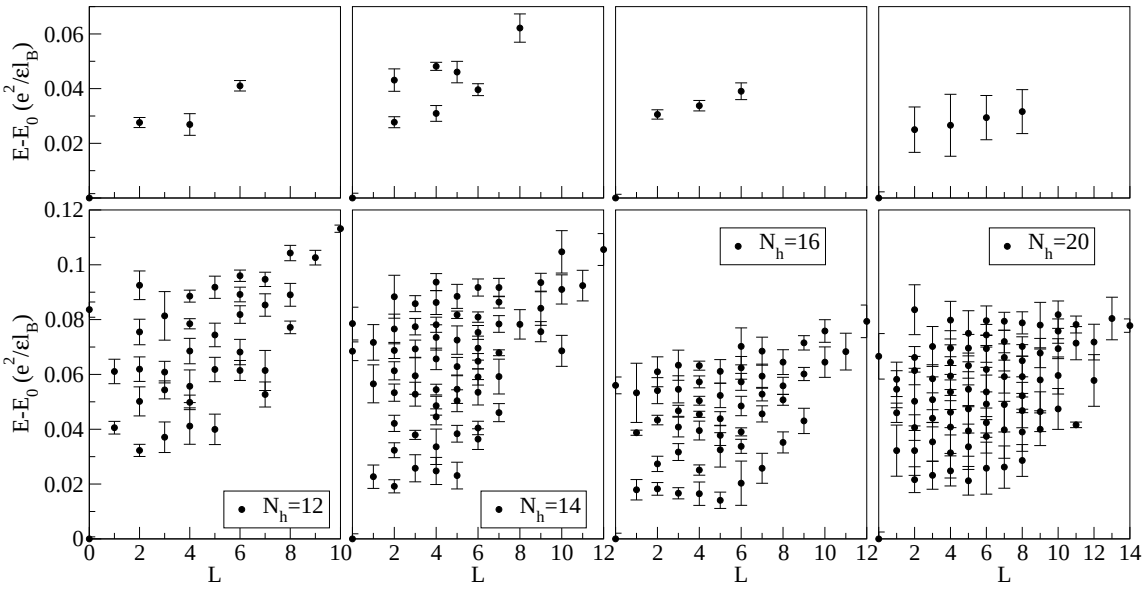

Figure 3.20: Zeroth-order (top) and first-order (bottom) CF diagonalization excitation spectra for $N_h = 12, 14, 16, 20$ holes in the second Landau level at $2Q = 2N - 3 = 2N_h + 1$ flux quanta.

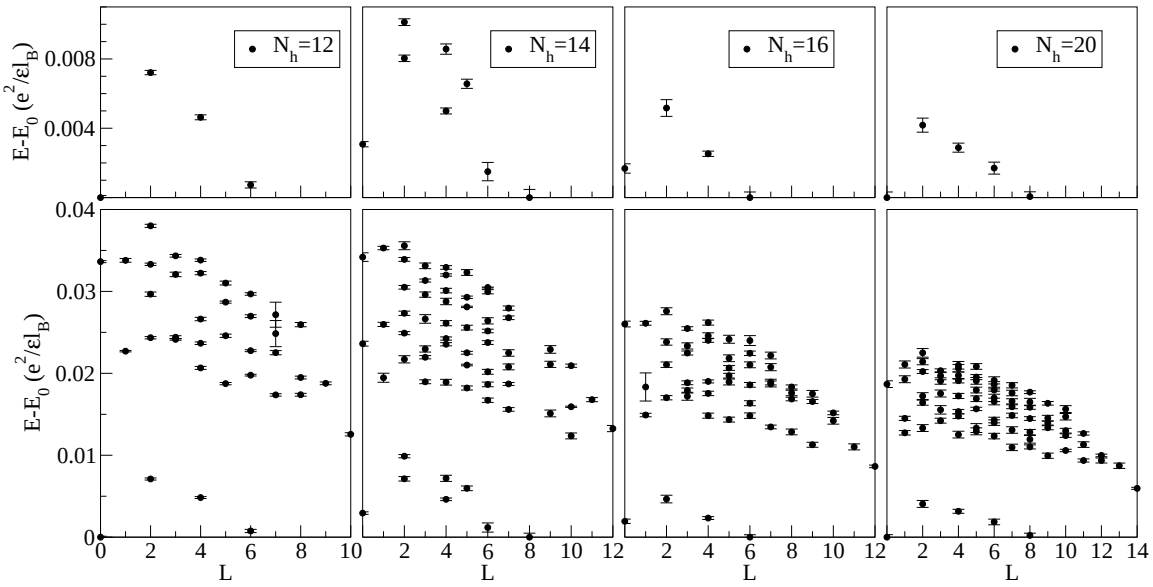

Figure 3.21: Zeroth-order (top) and first-order (bottom) CF diagonalization excitation spectra for $N_h = 12, 14, 16, 20$ holes in the lowest Landau level. The number of flux quanta $2Q$ is chosen as on Fig. 3.20.

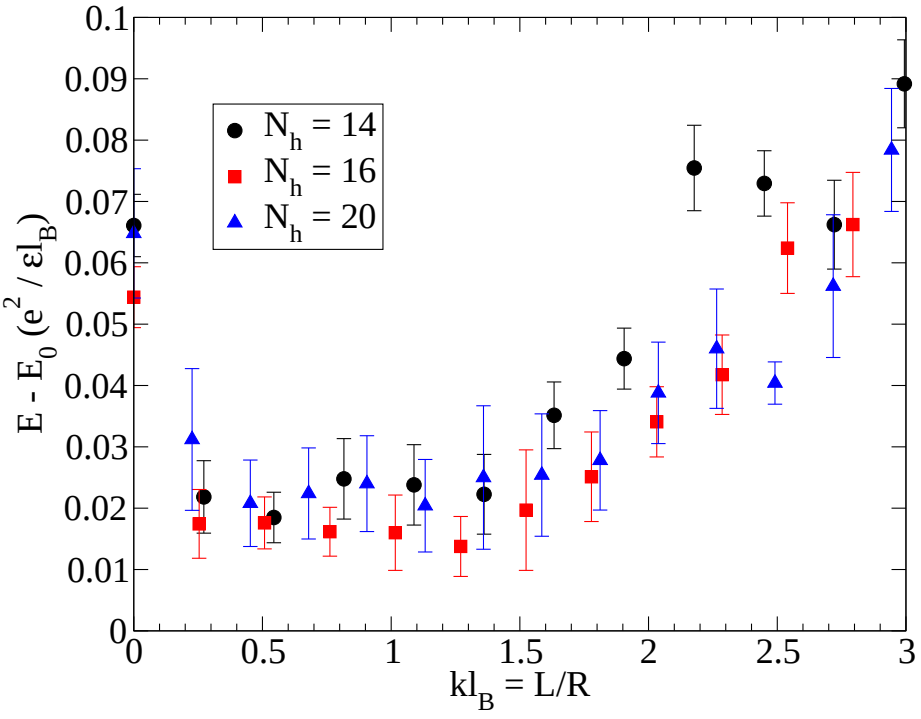

Figure 3.22: The excitation spectrum from second-order composite fermion diagonalization at $\nu = \frac{5}{2}$. The different symbols represent the excitation energy for systems sizes $N = 14, 16$, and 20 as a function of $kl_B = L/R$, where R is the radius of the sphere and L is the total orbital angular momentum.

order. The energy gap between the two lowest bands can be understood as the energy cost of exciting one more CF particle-hole pair. No such bands are seen for half filled second LL.

Returning to the second LL, when plotted as a function of $kl_B = L/R$, the lowest energy excitations for $14 \leq N_h \leq 20$ (from the first order spectra) fall on a more or less continuous curve (Fig. 3.22), which indicates that the thermodynamic behavior has been approached for $N_h \geq 14$. Finite-size effects are significant for $N_h < 14$. For $N_h > 20$ the first-order calculation is not sufficient, and the second-order CF diagonalization is computationally too time consuming. Although there is some ambiguity as to which excitation is to be identified with the transport gap (corresponding to a far separated quasiparticle-quasihole pair), the existence of an almost flat region allows us to estimate a gap of ≈ 0.02. This value is consistent with the earlier results from exact diagonalization [80, 84], and overestimates

the latest experimental figure ≈ 0.0027 (from Eisenstein *et al.* [24], whose transport gap of 0.31 K was converted with the experimental parameters they provide) by almost an order of magnitude.

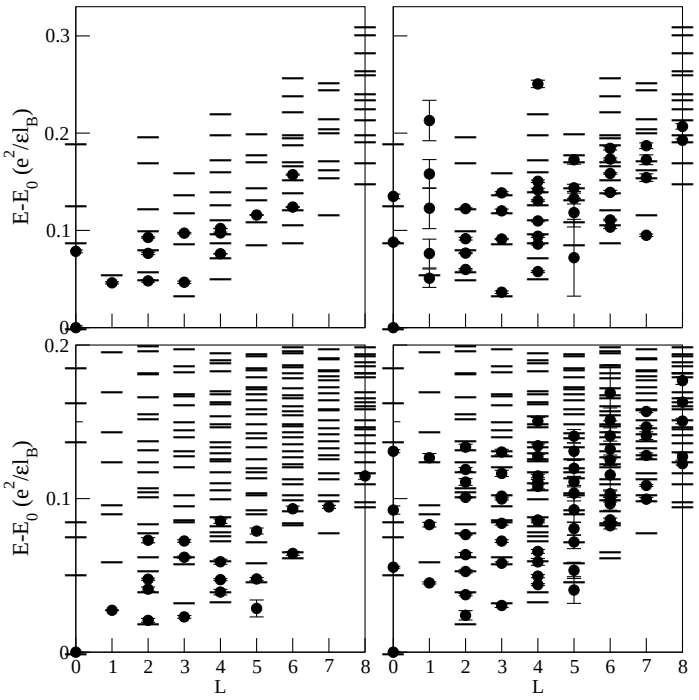

Figure 3.23: First-order (left) and second-order (right) CF diagonalization excitation spectra for $N_h = 6$ (top) and $N_h = 8$ (bottom) holes. The dashes show the exact spectrum, and the dots the CF spectrum. The exact and the CF ground state energies for $N_h = 6$ are: $E_{ex}/N = -0.415217$, $E^{(1)}/N = -0.413609$, $E^{(2)}/N = -0.415233$; those for $N_h = 8$ are: $E_{ex}/N = -0.401443$, $E^{(1)}/N = -0.395293$, $E^{(2)}/N = -0.399043$.

Fig. 3.23 shows a comparison of the CF spectra, at first- and second-order CF diagonalization, with the exact spectra for $N_h = 6$ and 8. The CF model does not provide as accurate an account of the energies as it does for the lowest LL FQHE states. However, it works reasonably well for energy differences. The CF diagonalization spectrum produces, at the first order, the energy gap to better than 25% accuracy. These comparisons thus provide credence to the semi-quantitative validity of our approach.

3.5.3 Multi-quasihole spectra

The nature of multi-quasihole states a few flux quanta away from $\nu = \frac{5}{2}$ is also interesting. Fig. 3.24 shows spectra for the $V^{(\mathrm{Pf})}$ interaction with $N = 10$ electrons at $2l = 18$ and $2l = 19$, which correspond to two and four "quasiholes" of the Pfaffian state. (We have switched back to electrons now, as these states occur at positive B^*; $l = Q + n$.) This model predicts zero energy states at $L = 1, 3, 5$ and $L = 0^2, 2^4, 3^1, 4^4, 5^2, 6^3, 7^1, 8^2, 10^1$, respectively (the superscript denotes the degeneracy). No corresponding quasi-degenerate band of states can be identified in the exact spectrum (middle column). Fig. 3.24 also shows spectra from first-order CF diagonalization. It produces a ground state at the correct quantum number but is not very successful for higher energy states. The CF spectrum can be improved systematically by incorporating higher order Λ-level mixing.

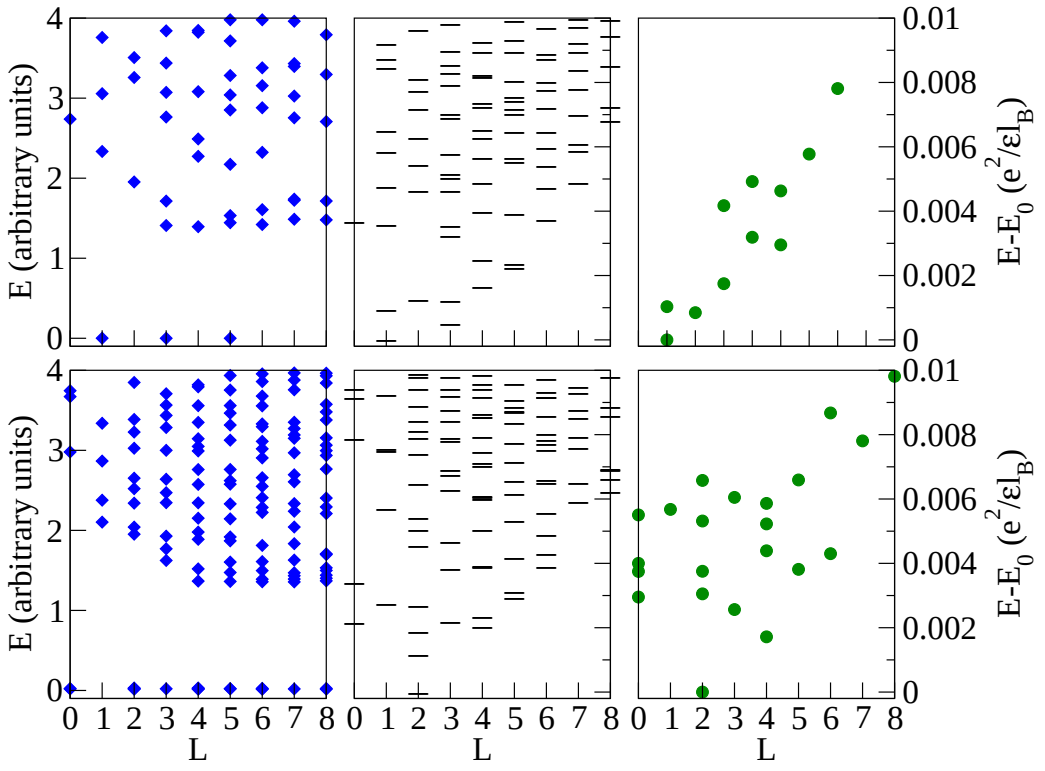

Figure 3.24: Spectra at $\nu = \frac{5}{2}$ for the model interaction $V^{(\mathrm{Pf})}$ (left column), the Coulomb interaction (central column), and the first-order CF diagonalization (right column) for $N = 10$ particles at $2l = 18$ (top row) and $2l = 19$ (bottom row). For the $V^{(\mathrm{Pf})}$ interaction, two (four) quasiholes are expected for $2l = 18$ ($2l = 19$). The ground state energies are $E_0/N = -0.415008$ (-0.40699) for exact and -0.40986 (-0.401845) for composite fermions, with $2l = 18$ ($2l = 19$). The energies in the middle column correspond to the scale shown on right. The spectra on the left were also given in Ref. [86].

Chapter 4

Interaction-induced quantum Hall effect in graphene

4.1 Introduction

Soon after the first experimental realization of graphene the integer quantum Hall effect was observed by Novoselov *et al.* [42] and Zhang *et al.* [43] at filling factors

$$\nu_n = 4n - 2. \tag{4.1}$$

The $\Delta\nu = 4$ period is understood straightforwardly as a consequence of the four-fold (near) degeneracy of Landau levels in graphene; the Zeeman energy is small in comparison to the interaction energy scale, and the pseudospin degree of freedom, which represents the two inequivalent Dirac-cones at the corners of the Brillouin zone, does not couple to external fields if the two sublattices are equivalent. The offset -2 is a consequence of a Dirac-like effective Hamiltonian, which produces a linear dispersion for low energy electronic states [103]. Recently, Zhang *et al.* [44] have observed quantum Hall plateaus at $\nu = \pm 4, \pm 1, 0$. Although external effects can surely lift the four-fold degeneracy of the low-lying LL's (see e.g. [133]), Yang, Das Sarma and MacDonald [107] have shown that the exchange interaction can break the SU(4) symmetry spontaneously, and the charged excitations are skyrmions [111, 112] in the $|n| \leq 3$ Landau levels at $\tilde{\nu} = 1$ (or, by particle-hole symmetry,

at $\tilde{\nu} = 3$) where

$$\tilde{\nu} = \nu - \nu_n \tag{4.2}$$

is the filling factor within the Landau level in question.[1]

Although the fractional quantum Hall effect has not yet been observed in graphene, it has been explored theoretically [98] assuming an SU(2) symmetry, as appropriate, for example, when the Zeeman energy is sufficiently high that only the two-fold pseudospin degeneracy remains. In this situation, the graphene FQHE problem formally maps into the well studied problem of FQHE in GaAs in the zero Zeeman energy limit [118, 119], with the pseudospin of the former playing the role of the spin of the latter. In the $n = 0$ graphene LL, the interaction pseudopotentials [58] are identical to those in GaAs, so the mapping is perfect, and the earlier composite-fermion results of Refs. [118, 119] carry over to graphene with minimal change (spin replaced by pseudospin). In particular, it follows that FQHE occurs at fractional fillings given by $\frac{n}{2pn\pm1}$, with pseudospin singlet states at even n and pseudospin polarized states at odd n (fully pseudospin polarized for $n = 1$), terminating into a pseudospin singlet composite fermion Fermi sea in the limit of $n \to \infty$ ($\tilde{\nu} = \frac{1}{2p}$). The effective interaction in the $n \neq 0$ LL's in graphene (Eq. (2.33)) interpolates between those of the $|n|$-th and $(|n| - 1)$-st LL's for the quadratic dispersion (Fig. 2.3 in Sec. 2.4.3 and [96, 97, 98]); composite fermion formation (Sec. 2.5), and therefore the FQHE, must be almost as strong in the $|n| = 1$ LL in graphene as in the lowest LL of GaAs.

4.2 SU(2) symmetric limit

4.2.1 FQHE in the $n = 0$ Landau level

The unusual electronic dispersion of graphene around $E = 0$ is reflected in the structure of Landau levels (Eq. (2.18)), which causes an offset of the IQHE staircase (Eq. (4.1)). Nonetheless, the actual wave functions of electrons in the $n = 0$ manifold (Eq. (2.15)) are identical to those in the conventional lowest Landau level of GaAs. Consequently, the FQHE in the $n = 0$ Landau level of graphene at a high magnetic field maps onto FQHE of electrons in GaAs in the zero Zeeman energy limit [118], as corroborated and extended by

[1] I can confirm this by exact diagonalization for $n \leq 2$ with $N \leq 9$ particles.

the numerical results described below.

ν	N	$2Q$	D	D_0	$L^{(0)}$	$S^{(0)}$	GaAs		graphene		overlap
							$L^{(1)}$	$S^{(1)}$	$L^{(1)}$	$S^{(1)}$	
1/3	4	9	145	5	0	2	0	2	0	2	0.99932
	5	12	1106	10	0	5/2	2	3/2	0	5/2	0.99998
	6	15	11588	50	0	3	0	3	0	3	0.99875
	7	18	109138	290	0	7/2	0	7/2	0	7/2	0.99974
2/3	4	5	29	3	0	0	0	2	0	0	0.99968
	6	8	500	10	0	0	1	3	0	0	0.98887
	8	11	11483	91	0	0	2	4	0	0	0.97482
2/5	4	7	72	4	0	0	0	0	0	0	0.99248
	6	12	3796	28	0	0	1	3	0	0	0.93622
	8	17	274842	768	0	0	0	4	0	0	0.95578
3/5	5	8	226	5	0	3/2	0	5/2	0	3/2	1.00000
	8	13	39131	205	0	2	0	4	0	0	0

Table 4.1: Orbital angular momentum $L^{(n)}$ and spin/pseudospin $S^{(n)}$ of the ground states of finite systems on a sphere at $\nu = \frac{1}{3}, \frac{2}{3}, \frac{2}{5}$ and $\frac{3}{5}$ in the $n = 0$ and $n = 1$ Landau levels of graphene and GaAs. D is the dimension of the Hilbert space in the $L_z = S_z = 0$ sector; D_0 is the dimension of the $L = 0$ sector. The last column gives the overlaps between the $n = 0$ and $n = 1$ graphene ground states.

The basic physics in the $n = 0$ graphene LL, therefore, is the same as in GaAs heterostructures; the major incompressible and compressible states are understood by composite fermion formation (Sec. 2.5). The IQHE of composite fermions for $\nu^* = n$ produces sequences of fractions:

$$\tilde{\nu} = \frac{n}{2pn \pm 1}.$$

(The index n is used for both electron and CF Landau levels; the meaning should be clear from the context.) The origin of gap, i.e. the energy required to promote a composite fermion into a higher Λ-level, is different for even and odd values of n. For even n, the ground state is a pseudospin singlet, with $\frac{n}{2}$ Λ-levels for each component of the pseudospin occupied. For odd n, the ground state is partially pseudospin polarized; no quantum Hall effect would occur here if the composite fermions did not interact, but the residual interaction between composite fermions opens a gap. To the extent the residual interaction is weak, one expects fractions with even numerators to be more robust than those with odd numerators. The excitation energies for the GaAs FQHE in the zero Zeeman energy

limit apply to graphene FQHE within the $n = 0$ level. Calculated gaps to creation of a far-separated charged quasiparticle/quasihole pair at $\nu = \frac{1}{3}$ and (unpolarized) $\nu = \frac{2}{5}$ are 0.07 and 0.04 $e^2/\epsilon l_B$, respectively [99]; the larger gap at $\frac{1}{3}$ indicates the significance of inter-CF interactions.

So long as electrons are confined to the $n = 0$ Landau level, they have no memory of the Dirac nature of the zero-field dispersion, with some surprising consequences for the FQHE. The CF-cyclotron energy opens up approximately linearly with B^*, as expected for composite fermions with a parabolic dispersion, even though the cyclotron energy of *electrons* in graphene scales anomalously with B.

In GaAs, the sequence of FQHE states at $\nu = \frac{n}{2pn\pm1}$ terminates as $n \to \infty$ in a composite fermion Fermi sea at $\nu = \frac{1}{2p}$, where the reduced magnetic field B^* vanishes [130, 131, 27]. For zero Zeeman energy, variational calculations favor the spin singlet Fermi sea [101], so graphene should have a pseudospin-singlet CF Fermi sea at $\nu = \frac{1}{2p}$. The CF Fermi sea in GaAs has been successfully modeled as an ordinary Fermi sea with parabolic dispersion, which allows one to deduce an effective mass for composite fermions. The same should be true of the CF Fermi sea in graphene, in spite of the fact that electrons in graphene make a Dirac sea at zero magnetic field and have no effective mass. The singlet nature of the CF Fermi sea can be ascertained through a measurement of the Fermi wave vector, as was accomplished in GaAs systems by various geometric means [27].

4.2.2 FQHE in the $|n| = 1$ Landau level

The nature of FQHE depends on the Haldane pseudopotentials. In GaAs, the FQHE is essentially restricted to the lowest LL: very few fractions are seen in $n = 1$, and almost none in higher LL's. The mapping between GaAs and graphene does not hold in higher Landau levels, so different behavior is expected. The graphene pseudopotentials $V_m^{(n)\mathrm{gr.}}$ of Eq. (2.33) typically interpolate between the convential $V_m^{(n-1)}$ and $V_m^{(n)}$. In particular, Fig. 2.3 shows that $V_m^{(1)\mathrm{gr.}}$ lies between $V_m^{(0)}$ and $V_m^{(1)}$, except for $m = 1$. To see what FQHE this interaction implies, we have numerically diagonalized finite systems in the spherical geometry (c.f. Sec. 2.3). We have used the pseudopotentials $V_m^{(n)\mathrm{gr.}}$ for the *planar* (disk) geometry; this gives the exact result for very large systems and is generally a reasonable approximation.

We first compare ground states for graphene systems including the pseudospin degree of freedom (but with the real spin frozen), to GaAs systems with zero Zeeman splitting. Table 4.1 shows the ground state quantum numbers, orbital angular momentum L and spin or pseudospin S, for the $n = 0$ and $|n| = 1$ LLs at several fractions. The $n = 0$ results are identical for GaAs and graphene. The near perfect overlaps in the last column of the table indicate that the FQHE in the $n = 1$ graphene LL also strongly resembles that in the $n = 0$ (lowest) graphene LL.[2] The $\frac{1}{3}$ state is fully polarized, whereas the $\frac{2}{5}$ and $\frac{2}{3}$ are (pseudo)spin singlet. At $\frac{3}{5}$ the spin of the ground state differs from that of the lowest LL for $N = 8$; the existence or the nature of FQHE at this fraction remains unclear at the moment.

4.2.3 Pseudoskyrmions

In GaAs quantum wells, the excitations of the $\nu = 1$ state for exactly zero Zeeman splitting are not simple particle-hole excitations but spin textures called skyrmions [106, 111, 112], in which half of the spins are reversed. However, the skyrmion size rapidly decreases with increasing Zeeman energy; experimentally, skyrmions typically have 3 to 5 flipped spins [113, 34]. No skyrmions occur at $\nu = 3, 5, \ldots$. CF skyrmions are believed to be relevant near $\nu = \frac{1}{3}$ at very small Zeeman energies [102, 114, 39].

In contrast, for the state in which one of the two degenerate levels of the $n = 0$ graphene manifold is fully occupied (which produces zero Hall conductance), the excitations ought to be large pseudoskyrmions. In exact diagonalization studies, we find pseudoskyrmions also in the $n = 1, 2$ graphene LL's, where the addition of one particle or hole to the fully pseudospin polarized state produces a pseudospin singlet state. No such behavior is seen for $n \geq 3$; here the excitation is fully pseudospin-polarized ($S = \frac{N}{2}$) on the quasihole side and has a single pseudospin reversed ($S = \frac{N}{2} - 1$) on the quasiparticle side. Fig. 4.1(a) depicts the N dependence of the gap to creating a pair of pseudoskyrmion and anti-pseudoskyrmion, computed by exact diagonalization. (We follow the convention of Ref. [111] to define the pseudoskyrmion gap in terms of "neutral" quasiparticle/quasihole

[2] The analogous overlaps are rather low for the FQHE states in the $n = 0$ and $n = 1$ LLs in GaAs [62].

energies [100].) Extrapolation to the thermodynamic limit yields

$$\Delta_1^{(0)} = 0.606(15), \quad \Delta_1^{(1)} = 0.126(7), \quad \text{and} \quad \Delta_1^{(2)} = 0.18(1).$$

The gap in the $n = 0$ LL is consistent with $\sqrt{\pi/8}\,(e^2/\epsilon l_B)$, half the energy required to create an ordinary particle-hole pair excitation [111]. We note that the pseudospin texture in the $n = 0$ graphene LL can be imaged directly by scanning tunneling microscopy, since an electron's pseudospin determines on which sublattice it resides.

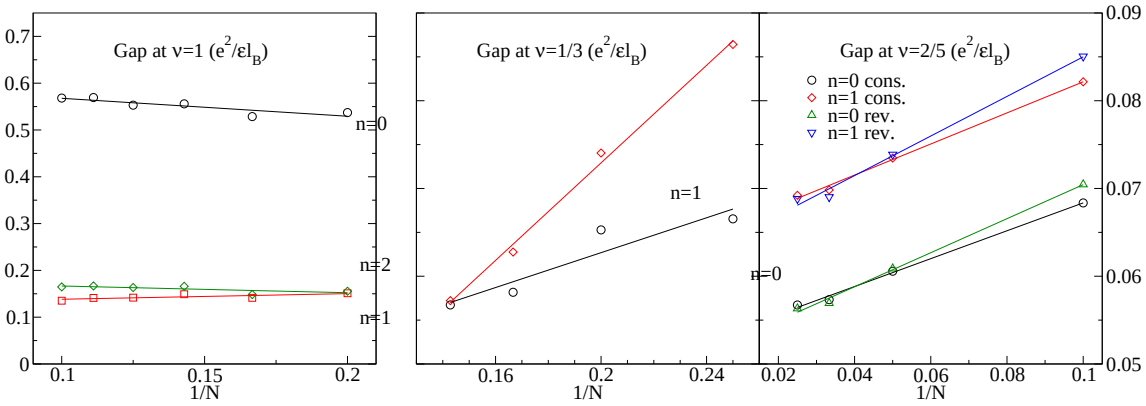

Figure 4.1: Activation gaps at $\nu^{(n)} = 1, \frac{1}{3}$ and $\frac{2}{5}$ in several graphene Landau levels. The gaps in (a) and (b) refer to the energy required to create a pseudoskyrmion-antiskyrmion pair. Gaps to pseudospin conserving (cons.) and pseudospin reversed (rev.) excitations are given in (c).

Fig. 4.1 shows the gaps as a function of the number of particles for several fractional filling factors in the n-th graphene LL. The lowest-energy charged excitations at $\nu^{(1)} = \frac{1}{3}$ are CF pseudoskyrmions (pseudo-spin singlet state), with an excitation energy of

$$\Delta_{1/3}^{(0)} = 0.043(5)e^2/\epsilon l_B \quad \text{and} \quad \Delta_{1/3}^{(1)} = 0.017(3)e^2/\epsilon l_B, \tag{4.3}$$

to be compared to 0.096 for a (pseudospin reversed) particle-hole pair of composite fermions (lowest LL). The gaps at filling factors $\frac{2}{5}$ and $\frac{2}{3}$ involve pseudospin reversal for composite fermions. For $\nu = \frac{2}{5}$ the gaps,

$$\Delta_{2/5}^{(0)} = 0.051(1) \quad \text{and} \quad \Delta_{2/5}^{(1)} = 0.062(1),$$

were obtained from the trial wave functions of the CF theory, evaluated with the simple $\frac{1}{r}$ interaction in the $n = 0$ LL, and with an effective real-space interaction described in Sec. 4.3.3 below in the $|n| = 1$ LL.

4.3 SU(4) symmetric limit

It is natural to wonder if FQHE with *new* structure appears in graphene. For this purpose, we explore in this section the FQHE including the full SU(4) symmetry, which is exact in the $g \to 0, \Delta \to 0$ limit, when the four vectors (c.f. Eqs. (2.15) to (2.17))

$$\Psi^{(n,m,1/2,1/2)}, \quad \Psi^{(n,m,1/2,-1/2)}, \quad \Psi^{(n,m,-1/2,1/2)}, \quad \Psi^{(n,m,-1/2,-1/2)}$$

are degenerate.

The SU(4) approximation is valid if $E_Z = g\mu_B B$ and Δ are small in comparison to the scale of the interactions, $e^2/(\epsilon l_B)$. While Δ is not easy to estimate, it is generally believed to be much smaller than E_Z. One can check that

$$E_Z \Big/ \left(\frac{e^2}{\epsilon l_B}\right) = 0.00103131 \epsilon g \sqrt{B[\mathrm{T}]}.$$

Obviously, both ϵ and g depend strongly on the interaction with environment in which the graphene sheet is placed. As two extremes, one can take $\epsilon_{\min} = (\epsilon_{\mathrm{air}} + \epsilon_{\mathrm{SiO_2}})/2 = 2.75$ and $\epsilon_{\max} = 15$ (the graphite value). On the other hand, Zhang *et al.* [44] found $1.7 \le g \le 2.0$. With these extreme values, assuming an extremely high field $B = 45$ T,

$$\begin{aligned} \left(E_Z \Big/ \left(\frac{e^2}{\epsilon l_B}\right)\right)_{\min} &= 0.032, \\ \left(E_Z \Big/ \left(\frac{e^2}{\epsilon l_B}\right)\right)_{\max} &= 0.208. \end{aligned}$$

Thus the SU(4) symmetric approximation is valid unless ϵ is close to the highest estimation.

By a combination of exact diagonalization and the CF model, we find new FQHE states which result from an essential interplay between the spin and the pseudospin degrees of freedom; such states occur at $\tilde{\nu} = \frac{n}{2n+1}$ for $n \ge 3$. For other states, the energy spectrum of the SU(4) problem matches with that of the SU(2) problem, although the multiplicities

are vastly different. We show by exact diagonalization that the SU(4) symmetry is spontaneously broken at $\tilde{\nu} = \frac{1}{3}$ just as at $\tilde{\nu} = 1$, i.e., the orbital part of the ground state is antisymmetric and the excitations are skyrmionic. At $\tilde{\nu} = \frac{1}{3}, \frac{2}{3}$ and $\frac{2}{5}$, the orbital part of ground state is the same as in the SU(2) symmetric system, but the state is now a highly degenerate SU(4) multiplet.

We will compare the exact diagonalization results to the composite fermion model (Sec. 2.5), and also use this theory to explore the thermodynamic limit. (Exact diagonalization can be performed only for very small systems for SU(4) symmetry.) Within the CF model, incompressible ground states are constructed by completely filling the lowest few Λ-levels in one or more spin bands. In the spherical geometry, the explicit relation between the monopole strength Q, the filling factor $\tilde{\nu}$ and the particle number N follows by this condition and Eq. (2.36); it is given in Eq. (4.4) below.

4.3.1 New FQHE states

The SU(n) generalization of the composite fermion model (Sec. 2.5.2) enables us to construct variational wave functions for $\tilde{\nu} = \frac{m}{2pm\pm1}$. For $m = 1$, a single filled Λ-level (in one of the α^t spin bands) is the only candidate for an incompressible ground state; the SU(4) multiplet is $[N]$.[3] For $m = 2$, the two Λ-levels are filled with particles of identical or different spin state; the multiplet is $[N]$ or $[N/2, N/2]$, respectively. As the restriction on the orbital part of the CF wave functions (c.f. Eq. (2.42)) is identical to the SU(2) case, we expect the latter is prefered in the absence of a symmetry-breaking field.

For $m \geq 3$, however, the SU(4) internal degree of freedom allows new ground state candidates. Let (l_1, l_2, l_3, l_4) denote a trial wave functions that fills $l_1, \ldots, l_4$ Λ-levels of the different single particle spin states with $m = \sum_i l_i$. Fig. 4.2 demonstrates this idea by collecting all such states for $m = 4$. This state is a candidate for the ground state at $\tilde{\nu} = \frac{m}{2pm\pm1}$ with $m \sum_i l_i$. It is straightforward to check that this state occurs at the flux values

$$2Q = 2p(N-1) \pm \left(\frac{N - \sum_i l_i^2}{m} \right), \tag{4.4}$$

Which of the different (l_1, l_2, l_3, l_4) states with fixed $m \sum_i l_i$ will be the ground state will

[3] Recall the Young tableau notation of SU(n) multiplets from Sec. 2.5.2.

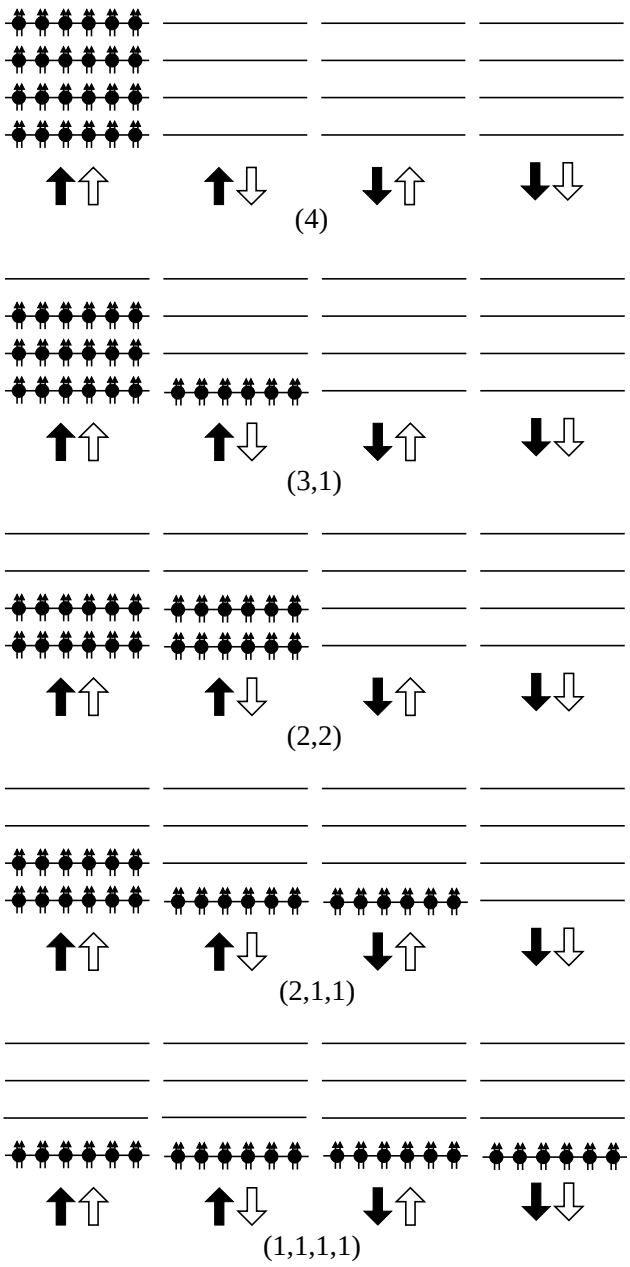

Figure 4.2: The construction of composite fermion ground states for fractions where four Λ-levels are filled ($\tilde{\nu} = \frac{4}{9}, \frac{4}{7}$, etc). While the top three states are possible in SU(2) systems, the lowest two require an SU(4) symmetric internal degree of freedom. The filled and empty arrows indicate the z-component of the spin S_z and the pseudospin P_z, respectively. This construction remains valid when S'_z and P'_z replace S_z and P_z (c.f. Eq. (4.5)).

be determined only by detailed calculations (to be described in Sec. 4.3.3 below). A mean field approximation, which has been found to be successful for SU(2) electrons [118, 119], predicts that the state with the lowest "CF kinetic energy" is the ground state. This approximation, however, neglects the residual interaction between composite fermions, which favors the maximally polarized state due to exchange contribution.

4.3.2 Exact diagonalization results

Ground states

Table 4.2 shows the angular momentum and the SU(4) multiplet of the ground state in the $|n| = 0, 1$ Landau levels at flux values given by Eq. (4.4). The following observations are consistent with CF theory:

1. All ground states at the N and $2Q$ values satisfying Eq. (4.4) have rotational symmetry ($L = 0$), consistent with the CF theory expectation of incompressibility and translational invariance for these parameters. These systems therefore are finite size representations of incompressible states at $\tilde{\nu} = \frac{m}{2pm\pm1}$.

2. As the filling $\tilde{\nu} = \frac{1}{3}$ corresponds to $m = 1$, a single filled Λ-level (in one of the α^t spin bands) is the only candidate for an incompressible ground state. The SU(4) multiplet is $[N]$, which is consistent with Table 4.2. The energy is identical to the SU(2) case, but the multiplicity[4] of the ground state is different ($\approx N^3/6$). Analogous to $\tilde{\nu} = 1$, the ground state is a completely symmetric $[N]$ multiplet, which has a fully antisymmetric orbital wave function associated with it, in accordance with the Pauli's principle. This is the SU(4) equivalent of the well-known ferromagnetic behavior in systems with quadratic dispersion relation (GaAs heterostructures and quantum wells) in the vanishing Zeeman energy limit. Unlike in the SU(2) symmetric case, however, the spins are not aligned in the same direction: in the $[N]$ multiplet spin and pseudospin are equal, but they can take all of the possible values [109, 110]: $S = P = 0, 1, \ldots, \frac{N}{2}$ if N is even, and $S = P = \frac{1}{2}, \frac{3}{2}, \ldots, \frac{N}{2}$ if N is odd. (The total

[4] Obtained by the hook length formula.

multiplicity comes from these choices combined with the choice of P_z and S_z.) Any weak perturbation that polarizes the spin should also polarize the pseudospin.

3. For $m = 2$, two Λ-levels are filled with particles of identical or different spin state; the multiplet is $[N]$ or $[N/2, N/2]$, respectively. As the orbital part of the CF wave functions is identical to the SU(2) case, it is no surprise that the latter is prefered in the absence of a symmetry-breaking field (c.f. the $\nu = \frac{2}{3}, \frac{2}{5}$ data in Table 4.2). (The multiplicity of $[\frac{N}{2}, \frac{N}{2}]$ is $\approx N^4/96$.) The ground state energy is the same as in the SU(2) symmetric case. In Sec. 2.5.2 it was shown that the maximal weight state is a product of two Slater determinants just as for an SU(2) singlet. Because the SU(2) systems already find the lowest energy state in this class, the orbital part of the wave function remains the same. However, the ground state is neither a spin nor a pseudospin singlet; all spin S and pseudospin P combinations occur with $(S + P) = 0, 2, \ldots, \frac{N}{2}$ for $\frac{N}{2}$ even, and $(S + P) = 1, 3, \ldots, \frac{N}{2}$ for $\frac{N}{2}$ odd.

4. At $\tilde{\nu} = \frac{3}{7}$ and $\tilde{\nu} = \frac{4}{9}$, the $n = 0$ LL ground state multiplets are consistent with three and four copies of completely filled lowest Λ-levels, respectively.[5] This seems to fail in the $|n| = 1$ LL. In Sec. 4.3.1, however, we have seen that new composite fermion ground states become possible at these fractions; the small system calculations we can perform at $\tilde{\nu} = \frac{3}{7}$ and $\tilde{\nu} = \frac{4}{9}$ are unable to determine the true nature of the ground states at these fractions.

Charged excitations: SU(4) composite fermion skyrmions

For SU(2) symmetry and vanishing Zeeman energy, the charged excitations at $\nu = \frac{1}{3}$, which map into filling factor one of composite fermions, are skyrmions of composite fermions [115, 39, 116]. These are analogous to skyrmions of electrons [111, 112, 34, 35, 36, 37, 38] at $\nu = 1$. The skyrmions at these fillings are obtained as the ground states with the monopole strength Q changed by ± 1 relative to the Q of the sequence representing the state at $\tilde{\nu}$. As Tables 4.3 and 4.4 testify, near $\tilde{\nu} = \frac{1}{3}$, these states belong to an $\left[\frac{N}{2}, \frac{N}{2}\right]$ or an $\left[\frac{N+1}{2}, \frac{N-1}{2}\right]$ multiplet, depending on whether N is even or odd. (The degeneracies of these

[5] Notice that $[N/3, N/3, N/3]$ and $[N/4, N/4, N/4, N/4]$ are conjugate representations to $[N/3]$ and $[0]$, respectively, which cannot be distinguished by their (S, P) quantum numbers.

$\tilde{\nu}$	N	$2Q$	D	$L^{(0)}$	SU(4) m.	$L^{(1)}$	SU(4) m.
$\frac{1}{3}$	4	9	960	0	[4]	0	[4]
	5	12	12934	0	[5]	0	[5]
	6	15	282824	0	[6]	0	[6]
$\frac{2}{3}$	4	5	204	0	[2,2]	0	[2,2]
	6	8	14464	0	[3,3]	0	[3,3]
$\frac{2}{5}$	4	7	488	0	[2,2]	0	[2,2]
	6	12	97316	0	[3,3]	0	[3,3]
$\frac{3}{7}$	3	4	27	0	[1]	0	[1]
	6	11	64392	0	[2]	0	[4]
$\frac{4}{9}$	4	6	325	0	[0]	0	[4]

Table 4.2: Orbital angular momentum $L^{(n)}$ and SU(4) multiplet of the ground states of finite systems on a sphere at the most prominent fractions in the $n = 0$ and $|n| = 1$ Landau levels of graphene. The quantity $\tilde{\nu}$ (c.f. Eq. (4.2)) is the filling factor within the Landau level; Q is the monopole strength; N is the number of electrons; and D is the dimension of the Hilbert space in the $L_z = S_z = P_z = 0$ sector.

multiplets are $\approx N^4/96$ and $\approx N^4/48$, respectively.) We identify these states with SU(4) composite fermion skyrmions. The energies of these states are identical to the familiar SU(2) skyrmions, as these spinors enforce (c.f. Sec. 2.5.2) exactly the same partition of the wave function into antisymmetric factors as the SU(2) singlet (N even) or spin-$\frac{1}{2}$ (N odd). Consequently, the gaps at $\tilde{\nu} = \frac{1}{2p+1}$ are identical to those calculated with SU(2) symmetry [115, 39, 116] (see Eq. (4.3)).

A technical remark: The Hilbert space in the calculations leading to the results of Tables 4.2-4.4 can be further reduced by exploiting the existence of a third SU(4) generator, traditionally called E_{00}, that commutes with the Hamiltonian. We identify SU(4) multiplets only by their (S, P) quantum numbers [110, 109], and do not implement this simplification.

4.3.3 Thermodynamic limit

Because of the four-fold degeneracy of the graphene Landau levels, exact diagonalization studies are possible only for very small systems. Having established the regime of validity of the CF model, we now use the variational wave functions of Eq. (2.34) to study large systems by the Monte Carlo method, and obtain thermodynamic limits for the energies of

$\tilde{\nu}$	N	$2Q$	D	$L^{(0)}$	SU(4) m.	$L^{(1)}$	SU(4) m.
1	4	2	25	0	[2,2]	0	[0,0]
	5	3	92	$\frac{1}{2}$	[3,2]	$\frac{1}{2}$	[3,2]
	6	4	644	0	[3,3]	0	[3,3]
	7	5	3236	$\frac{1}{2}$	[4,3]	$\frac{1}{2}$	[4,3]
	8	6	24483	0	[4,4]	0	[4,4]
	9	7	142587	$\frac{1}{2}$	[5,4]	$\frac{1}{2}$	[5,4]
$\frac{1}{3}$	4	8	697	0	[2,2]	0	[2,2]
	5	11	9296	$\frac{1}{2}$	[3,2]	$\frac{1}{2}$	[3,2]
	6	14	203132	0	[3,3]	0	[3,3]

Table 4.3: Orbital angular momentum $L^{(n)}$ and SU(4) multiplet of the ground states of finite systems on the sphere on the *quasiparticle* side of $\tilde{\nu} = 1$ and $\frac{1}{3}$ in the $n = 0$ and $|n| = 1$ Landau levels of graphene. D is the dimension of the Hilbert space in the $L_z = S_z = P_z = 0$ sector.

various candidate states.

For the $n = 0$ Landau level the computation is straightforward. In the $|n| = 1$ Landau levels the calculation of the energy expectation value by the Monte Carlo method requires a knowledge of the real-space interaction corresponding to the effective pseudopotentials $V_m^{(1)\mathrm{gr.}}$ given in Eq. (2.33).[6] Following the procedure of Sec. 3.2.2, we use an effective real-space interaction of the form in Eq. (3.1), and fit the coefficients c_i to reproduce the first $M + 1$ pseudopotentials $V_m^{(1)\mathrm{gr.}}$ by Eq. (2.22). The coefficients c_i thus obtained are given in Table 4.5. Our effective interaction produces the $V_0^{(n)\mathrm{gr.}}, \ldots, V_6^{(n)\mathrm{gr.}}$ pseudopotentials exactly. We have checked that the relative error in the remaining pseudopotentials is very small and does not affect our conclusions.

We have studied composite fermion wave functions for $\tilde{\nu} = \frac{m}{2pm\pm1}$. Fig. 4.3 shows the energies as a function of $1/N$ for all ground state candidates at these fractions, and the thermodynamic limits of the energies are given in Table 4.6.

For the sequences $\tilde{\nu} = \frac{m}{2m+1}$, which represent the integer quantum Hall effect of ^{2}CF's (composite fermions carrying two vortices), the ground state is consistent with the prediction of the mean-field approximation: it is the one that best exploits the SU(4) spin bands to minimize the CF kinetic energy. The examples are: the state $(1, 1, 1)$ at $\tilde{\nu} = \frac{3}{7}$; the

[6] I will have to use an effective interaction derived from the planar pseudopotentials, as the solutions of the massless Dirac equation on the sphere is not known to me.

$\tilde{\nu}$	N	$2Q$	D	$L^{(0)}$	SU(4) m.	$L^{(1)}$	SU(4) m.
1	4	4	117	0	[2,2]	0	[2,2]
	5	5	521	$\frac{1}{2}$	[3,2]	$\frac{1}{2}$	[3,2]
	6	6	3868	0	[3,3]	0	[3,3]
	7	7	21170	$\frac{1}{2}$	[4,3]	$\frac{1}{2}$	[4,3]
	8	8	165992	0	[4,4]	0	[4,4]
$\frac{1}{3}$	4	10	1281	0	[2,2]	0	[2,2]
	5	13	17490	$\frac{1}{2}$	[3,2]	$\frac{1}{2}$	[3,2]

Table 4.4: Orbital angular momentum $L^{(n)}$ and SU(4) multiplet of the ground states of finite systems on the sphere on the *quasihole* side of $\nu = 1$ and $\frac{1}{3}$ in the $n = 0$ and $|n| = 1$ Landau levels of graphene. D is the dimension of the Hilbert space in the $L_z = S_z = P_z = 0$ sector.

Coefficient	Value
c_0	-11.1534
c_1	24.9078
c_2	-18.6461
c_3	6.63657
c_4	-1.221097
c_5	0.112068
c_6	-0.00404269

Table 4.5: Coefficients in Eq. (3.1), which reproduce the effective interaction for the $|n| = 1$ LL of graphene. See Table 3.1 for analogous parameters for the $n = 1$ LL of GaAs. Here, however, both the odd and the even pseudopotentials had to be fitted because full spin polarization is not assumed.

SU(4) singlet state $(1, 1, 1, 1)$ at $\tilde{\nu} = \frac{4}{9}$; state $(2, 1, 1, 1)$ at $\tilde{\nu} = \frac{5}{11}$; and state $(2, 2, 1, 1)$ at $\tilde{\nu} = \frac{6}{13}$.

For the sequence $\tilde{\nu} = \frac{m}{4m+1}$, appropriate for ^{4}CF's, the mean-field approximation is not always valid. The ferromagnetic CF ground states are competitive even when they do not have the lowest CF kinetic energy, as seen in Fig. 4.4 and Table 4.7. The ground state at $\tilde{\nu} = \frac{3}{13}, \frac{5}{21}$ and $\frac{6}{25}$ are found to be fully polarized; the state with the least possible CF kinetic energy per particle has slightly higher energy. At $\tilde{\nu} = \frac{4}{17}$ state $(1, 1, 1, 1)$, the compact SU(4) singlet state has the lowest energy. (This state was energetically favored at $\tilde{\nu} = \frac{4}{9}$ by a large margin.) Apparently, the gain from CF kinetic energy minimization is on the same order as that from exchange maximization; which state becomes the ground state

is determined by their competition. Our results demonstrate that the inter-CF interaction is stronger for ^{4}CFs than for ^{2}CFs.

Similar behavior had earlier been found for the SU(2) case [119, 69]. For $\nu = \frac{m}{2m+1}$ the model of noninteracting composite fermions predicts the ground state quantum numbers correctly, which are also confirmed extensively through several experiments. For $\nu = \frac{m}{4m+1}$, on the other hand, a fully spin polarized state is found to have the lowest energy in detailed calculations with CF theory [69].

The data in Tables 4.6 and 4.7 include the ground states that are available in SU(2) symmetric systems. Our results are consistent with those of Ref. [119] for the SU(2) case, although the values differ slightly; the current results are more accurate. The extrapolation to the theormodynamic limit in our work is based on $N = 36 - 104$ particles, with linear functions fitted on the $E(1/N)$ curve under the condition $\chi^2 \lesssim N - 2$.

It is in principle possible to apply similar methods to the states at $\tilde{\nu} = \frac{m}{2pm-1}$, where the effective magnetic field B^* felt by composite fermions is antiparallel to the real external field B. The projection procedure for CF wave functions has been elaborated by Möller and Simon [55], but its implementation is impractical for the number of Λ-levels and effective monopole strengths Q^* that are of interest.[7] Therefore, we do not pursue that direction in the present work.

4.3.4 Zero-temperature phase transitions

Either or both of the Zeeman energy $E_Z^S = q\mu_B \vec{B} \cdot \vec{S}$ and the pseudo-Zeeman energy $E_Z^P = \Delta P_z$ will break the SU(4) symmetry. Assuming the symmetry-breaking fields are weak, the effect will be to select the most favorable member of the ground state multiplet. (Notice that P_z, S_z, as well as the third member E_{00} of the Cartan subalgebra of SU(4) generators, commute with the Hamiltonian of Eq. (2.14) in the SU(4) symmetric $\Delta \to 0, g \to 0$ limit.) Slightly stronger fields may drive zero-temperature phase transitions between the possible CF ground states at a fixed filling factor. It is convenient to change to new quantum

[7] The maximal degree of derivatives for negative-B^* states is [55] $2|Q^*| + m$, while for parallel flux attachment it is only m.

[9] When writing these lines I found an error in the Monte Carlo program I used for evaluating the energies. Therefore, the data presented in this figure as well as Fig. 4.4 and Tables 4.6, 4.7, and 4.8 contains a small systematic error of about 1%. According to my preliminary calculations at $\tilde{\nu} = \frac{3}{7}, \frac{4}{9}, \frac{3}{13}$ and $\frac{4}{17}$, these results are qualitatively correct. The correct numbers will be presented in the final version of Ref. [6].

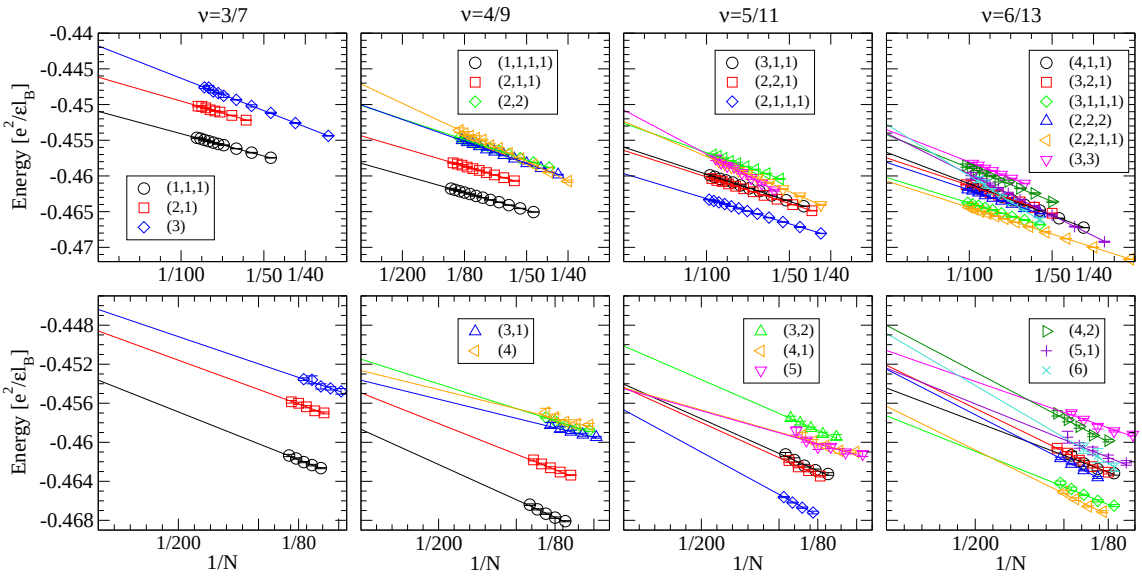

Figure 4.3: Energy per particle[9] for the novel incompressible composite fermion ground state wave functions for the sequence $\tilde{\nu} = \frac{m}{2pm+1}$. The states are denoted by (l_1, l_2, l_3, l_4), explained in the text. The upper panels are for the $n = 0$ Landau level, and the lower panels for the $|n| = 1$ Landau level. The thermodynamic limits of the ground state energies are given in Table 4.6.

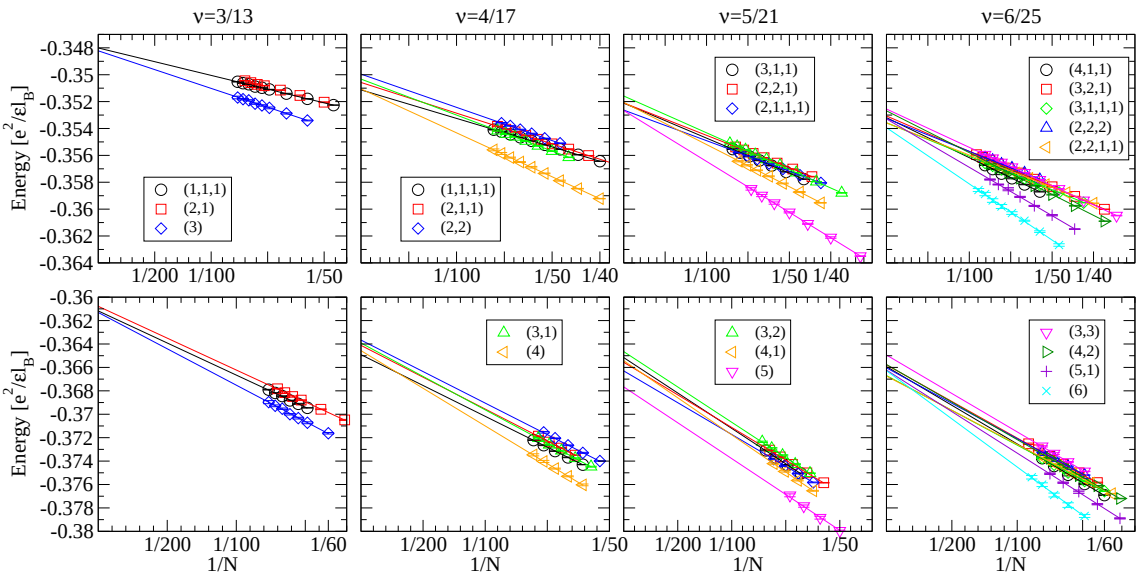

Figure 4.4: Same as in Fig. 4.3, but for the sequence $\tilde{\nu} = \frac{m}{4m+1}$, corresponding to the integer quantum Hall effect of ^{4}CFs. The thermodynamic limits of the the ground state energies are given in Table 4.7.

$\tilde{\nu}$	State	Energy $n=0$	Energy $n=1$	$\hbar\omega_c^*/N$
$\frac{3}{7}$	(3)	-0.44178(8)	-0.4463(14)	1
	(2,1)	-0.4463(1)	-0.4486(9)	1/3
	(1,1,1)	-0.45095(8)	-0.4536(6)	0
$\frac{4}{9}$	(4)	-0.4471(2)	-0.4527(15)	3/2
	(3,1)	-0.4500(1)	-0.4536(11)	3/4
	(2,2)	-0.4501(1)	-0.4515(6)	1/2
	(2,1,1)	-0.4544(1)	-0.4549(4)	1/4
	(1,1,1,1)	-0.45823(5)	-0.4596(3)	0
$\frac{5}{11}$	(5)	-0.4508(4)	-0.4545(9)	2
	(4,1)	-0.4524(1)	-0.4544(8)	6/5
	(3,2)	-0.4526(1)	-0.4501(12)	4/5
	(3,1,1)	-0.4560(1)	-0.4540(9)	3/5
	(2,2,1)	-0.45641(7)	-0.4544(8)	2/5
	(2,1,1,1)	-0.45966(4)	-0.4567(7)	1/5
$\frac{6}{13}$	(6)	-0.4527(4)	-0.4488(19)	5/2
	(3,3)	-0.4535(2)	-0.4511(7)	1
	(5,1)	-0.4540(1)	-0.4524(15)	5/3
	(4,2)	-0.4542(3)	-0.4480(9)	7/6
	(4,1,1)	-0.4567(1)	-0.4544(18)	1
	(3,2,1)	-0.45746(8)	-0.4521(5)	2/3
	(2,2,2)	-0.45809(8)	-0.4525(7)	1/2
	(3,1,1,1)	-0.46021(9)	-0.4573(6)	1/2
	(2,2,1,1)	-0.46071(4)	-0.4563(1)	1/3

Table 4.6: Energy per particle for incompressible composite fermion ground state candidates of different SU(4) symmetries at $\tilde{\nu} = \frac{m}{2m+1}$, corresponding to the integer quantum Hall effect of ^{2}CF's. For each fraction $\tilde{\nu}$ the states are listed in decreasing order of energy. The last column gives the CF kinetic energy ($\hbar\omega_c^*$) per particle in the thermodynamic limit, measured relative to the energy of the lowest Λ-level.

numbers S_z', P_z' by

$$\begin{pmatrix} S_z' \\ P_z' \end{pmatrix} = U \begin{pmatrix} S_z \\ P_z \end{pmatrix}, \tag{4.5}$$

with a unitary U to eliminate one kind of Zeeman energy. Choosing

$$U = \frac{1}{\sqrt{1+\lambda^2}} \begin{pmatrix} 1 & \lambda \\ -\lambda & 1 \end{pmatrix}, \tag{4.6}$$

$\tilde{\nu}$	State	Energy $n=0$	Energy $n=1$	$\hbar\omega_c^*/N$
$\frac{3}{13}$	(2,1)	-0.34752(7)	-0.36078(14)	1/3
	(1,1,1)	-0.34801(3)	-0.36118(10)	0
	(3)	-0.34822(12)	-0.36131(29)	1
$\frac{4}{17}$	(2,2)	-0.34995(9)	-0.3637(2)	1/2
	(3,1)	-0.35033(8)	-0.3639(2)	3/4
	(2,1,1)	-0.35057(3)	-0.3641(2)	1/4
	(4)	-0.35106(5)	-0.3646(3)	3/2
	(1,1,1,1)	-0.35113(2)	-0.3649(1)	0
$\frac{5}{21}$	(3,2)	-0.35158(4)	-0.3646(2)	4/5
	(4,1)	-0.35206(7)	-0.3654(3)	6/5
	(2,2,1)	-0.35209(4)	-0.3656(1)	2/5
	(3,1,1)	-0.35211(6)	-0.3652(2)	3/5
	(2,1,1,1)	-0.35263(3)	-0.3663(1)	1/5
	(5)	-0.35266(10)	-0.3677(3)	2
$\frac{6}{25}$	(3,3)	-0.35255(3)	-0.3649(2)	1
	(4,2)	-0.35269(3)	-0.3658(1)	7/6
	(3,2,1)	-0.35307(3)	-0.3658(1)	2/3
	(4,1,1)	-0.35319(7)	-0.3659(1)	1
	(2,2,2)	-0.35326(5)	-0.3660(1)	1/2
	(5,1)	-0.35329(6)	-0.3662(2)	5/3
	(3,1,1,1)	-0.35357(3)	-0.3666(1)	1/2
	(2,2,1,1)	-0.35358(3)	-0.3667(1)	1/3
	(6)	-0.35394(18)	-0.3663(6)	5/2

Table 4.7: Same as in Table 4.6 for $\tilde{\nu} = \frac{m}{4m+1}$, corresponding to the integer quantum Hall effect of ^{4}CF's. Energies per particle for incompressible composite fermion ground state candidates with different SU(4) symmetries are shown in decreasing order. For each fraction $\tilde{\nu}$ the states are in decreasing order of energy.

with $\lambda = E_Z^P/E_Z^S$ yields

$$\begin{aligned} E_Z^{S'} &= \frac{1}{\sqrt{1+\lambda^2}} E_Z^S + \frac{\lambda}{\sqrt{1+\lambda^2}} E_Z^P, \\ E_Z^{P'} &= 0. \end{aligned} \tag{4.7}$$

The phase transitions driven by the effective Zeeman energy $E_Z^{S'}$ are given in Table 4.8. Here we assume a sufficiently weak field that does not mix the low-lying states, but only selects the most favorable member of the ground state multiplet. In state (l_1, l_2, l_3, l_4) the with $l_i \geq l_{i+1}$, this means filling $l_1 + l_2$ Λ-levels of the favorable S' spin, and $l_3 + l_4$

levels of the unfavorable S' spin. This results in an effective Zeeman energy difference per particle. Notice that no value of E_Z^P and E_Z^S will drive the system at $\tilde{\nu} = m/(2pm+1)$ to a completely antisymmetric orbital state (m). This is a consequence of our freedom to choose a basis P'_z, S'_z in the Cartan subalgebra of SU(4) (Eq. (4.5)), which eliminates one kind of Zeeman energy; the states where the two unfavorable bands of the S' spin are emptied will already have the lowest possible effective Zeeman energy $E_Z^{S'}$.

Tilting the magnetic field is often used as a means to tune the Zeeman energy. (By Eq. (4.7), this will also tune the effective Zeeman energy $E_Z^{S'}$.) Unlike in GaAs/AlGaAs heterostructures, the in-plane magnetic field is unlikely to change the single-particle states in any significant manner, because the transverse thickness of the two dimensional electron system is graphene ($\sim$ 2Å) is much smaller than the typical magnetic lengths ($\sim$100Å). The most favorable parameter space for the observation of these transitions occurs for very low values of the static dielectric constant ϵ and the sublattice asymmetry Δ. The value of ϵ depends on the interaction with the substrate on which the graphene sheet is placed.

$\tilde{\nu}$	Transition	$\left(\frac{E_Z^{S'}}{e^2/\epsilon l_B}\right)_c$	Change of $\langle S' \rangle$
$\frac{3}{7}$	$(1,1,1) \to (2,1)$	0.0170(7)	$\frac{1}{6} \to \frac{1}{2}$
$\frac{4}{9}$	$(1,1,1,1) \to (2,1,1)$	0.0153(7)	$0 \to \frac{1}{4}$
	$(2,1,1) \to (2,2)$	0.0172(9)	$\frac{1}{4} \to \frac{1}{2}$
$\frac{5}{11}$	$(2,1,1,1) \to (2,2,1)$	0.0163(5)	$\frac{1}{10} \to \frac{3}{10}$
	$(2,2,1) \to (3,2)$	0.019(1)	$\frac{3}{10} \to \frac{1}{2}$
$\frac{6}{13}$	$(2,2,1,1) \to (3,2,1)$	0.0195(7)	$\frac{1}{6} \to \frac{1}{3}$
	$(3,2,1) \to (5,1)$	0.021(1)	$\frac{1}{3} \to \frac{1}{2}$

Table 4.8: Zero temperature phase transitions[11] driven by the effective Zeeman energy in the $n = 0$ Landau level. The last column gives the expectation value of the transformed spin S' (Eq. (4.5)), which coincides with the ordinary spin in the case of perfect sublattice symmetry ($\Delta = 0$). The quantity $\left(E_Z^{S'}/(e^2/\epsilon l_B)\right)_c$ give the value of the parameters where the transition is predicted to take place.

[11] See footnote 9.

Chapter 5

Conclusion

The FQHE in the second Landau level of the 2DEG with quadratic dispersion has been explored by means of the composite fermion model. The residual interaction between CF's has proved to be essential for an understanding of the observed FQHE states. At $\nu = \frac{7}{3}$ and $\frac{8}{3}$, this interaction has to be taken into account to obtain reliable variational wave functions. At $\nu = \frac{5}{2}$ and $\frac{7}{2}$, it has been found that the origin of incompressibility is inter-composite-fermion interaction; the estimate of the activation energy from the first-order treatment of this interaction is consistent with earlier exact diagonalization results. The perturbative inclusion of the residual interaction between composite fermions directly connects the $\nu = \frac{5}{2}$ state to the Fermi sea, yields a qualitatively correct picture of the excitations at $\nu = \frac{5}{2}$ and of the states slightly away from $\nu = \frac{5}{2}$, and it is amenable to systematic improvement. Thus the model of interacting composite fermions is a feasible alternative of the Pfaffian theory of the $\nu = \frac{5}{2}$, whose weaknesses (inaccuracy in the description of excitations, a violation of the particle-hole symmetry) have also been remarked. Other nonstandard states have also been proposed for fractions observed in the second Landau level; the most interesting examples are the parafermionic states [86, 87] at $\nu = \frac{12}{5}$ and $\frac{13}{5}$. It would be interesting to test the validity of these theories as well as the existence of alternatives by the methods we have developed.

The physics in the lowest Landau level of graphene in the large Zeeman energy limit is equivalent to the that of the lowest LL of GaAs in the zero Zeeman energy limit. Therefore, FQHE states with partial polarization and skyrmionic excitations are expected to occur

here; the FQHE states should terminate in a pseudospin-singlet Fermi sea at half filling. On the other hand, the different matrix elements in higher LL's cause difference physics in graphene and GaAs. In the IQHE regime skyrmionic excitations have been found at $\nu^{(n)} = 1, 3$ in the $|n| = 0, 1, 2$ LL's of graphene. We have also found that the effective interaction is more favorable to CF formation in the $|n| = 1$ LL of graphene than in the $n = 1$ LL of GaAs. Using the noninteracting composite fermion model, the gaps at $\nu^{(1)} = \frac{1}{3}, \frac{2}{5}$ were calculated. The residual interaction between CF's may cause qualitative corrections to the FQHE in the $|n| = 1$ LL of graphene, but due to the similarity of the effective interaction to the lowest LL interaction these corrections are expected to be of minor importance.

A large range of possible FQHE states are allowed in graphene by SU(4) symmetry, including new states, which have no analog in GaAs, at filling factors $\tilde{\nu} = \frac{m}{2pm \pm 1}$ for $m \geq 3$ in the $|n| = 0$ and $|n| = 1$ Landau levels of graphene. For ^{2}CF's, the ground states are those for which the composite fermion kinetic energy is minimum; these states spread out maximally in spin space. For ^{4}CF's the fully polarized ground state wins, with the exception of $\tilde{\nu} = \frac{4}{17}$, where very compact SU(4) singlet structures are possible. The ordering of these states is similar in the $n = 0$ and $|n| = 1$ Landau levels. We have also estimated the parameter regimes where these states should occur; if the SU(4) symmetry is only slightly broken, zero temperature phase transitions are driven by an effective Zeeman energy that accounts for the combined effect of the Zeeman energy and the sublattice symmetry breaking field. The existence of an effective Zeeman energy is related to our freedom to choose a basis in the SU(4) spin space; this is also the reason why certain states with high CF kinetic energy are not accessible in the SU(4) system.

At $\tilde{\nu} = \frac{1}{3}$ we found SU(4) skyrmions to be the lowest energy charged excitations. The nature of the excitations at fractions with a greater numerator is an issue that has not been explored. The collective modes of the SU(4) symmetric case, as well as the nature of the possible compressible states might be subject matter of future research.

Appendix: the Pfaffian

The Pfaffian $\mathrm{Pf}(A)$ is defined for a $2n \times 2n$ antisymmetric matrix A as

$$\mathrm{Pf}(A) = \sum_{\pi} \mathrm{sgn}(\pi) a_{i_1,j_1} a_{i_2,j_2} \cdots a_{i_n,j_n},$$

where π runs over all partitions $\{(i_1,j_1),(i_2,j_2),\ldots,(i_n,j_n)\}$ of $\{1,2,\ldots,2n\}$, and $\mathrm{sgn}(\pi)$ is the sign of π. The most important properties of the Pfaffian are [135]:

$$\begin{aligned}
\mathrm{Pf}(A^{\mathrm{T}}) &= (-1)^n \mathrm{Pf}(A) \\
\mathrm{Pf}(A)^2 &= \det(A) \\
\mathrm{Pf}\begin{pmatrix} A_1 & 0 \\ 0 & A_2 \end{pmatrix} &= \mathrm{Pf}(A_1)\mathrm{Pf}(A_2) \\
\mathrm{Pf}(BAB^{\mathrm{T}}) &= \det(B)\mathrm{Pf}(A) \\
\mathrm{Pf}\begin{pmatrix} 0 & M \\ -M^{\mathrm{T}} & 0 \end{pmatrix} &= (-1)^{\frac{n(n-1)}{2}} \det(B).
\end{aligned}$$

Bibliography

[1] C. Tőke, M. R. Peterson, G. S. Jeon, and J. K. Jain, Phys. Rev. B **72**, 125315 (2005).

[2] C-C. Chang, C. Tőke, G. S. Jeon, and J. K. Jain, Phys. Rev. B **73**, 155323 (2006).

[3] C. Tőke and J. K. Jain, Phys. Rev. Lett. **96**, 246805 (2006).

[4] C. Tőke, P. E. Lammert, J. K. Jain, and V. H. Crespi, Phys. Rev. B **74**, 235417 (2006).

[5] C. Tőke, N. Regnault, and J. K. Jain, Phys. Rev. Lett., **98**, 036806 (2007).

[6] C. Tőke and J. K. Jain, submitted to Phys. Rev. B. See cond-mat/0701026 (2007).

[7] C. Tőke, N. Regnault, and J. K. Jain, submitted to Solid State Communications (2007).

[8] K. von Klitzing, G. Dorda, and M. Pepper, Phys. Rev. Lett. **45**, 494 (1980).

[9] M. A. Paalanen, D. C. Tsui, and A. C. Gossard, Phys. Rev. B **25**, 5566 (1982).

[10] D. C. Tsui, H. L. Stormer, and A. C. Gossard, Phys. Rev. Lett. **48**, 1559 (1982).

[11] H. L. Stormer, Rev. Mod. Phys. **71**, 875 (1999).

[12] J. P. Eisenstein, H. L. Stormer, L. N. Pfeiffer, and K. W. West, Phys. Rev. Lett. **62**, 1540 (1989).

[13] M. E. Cage, in *The Quantum Hall Effect*, edited by R. E. Prange and S. M. Girvin (Springer, New York, 1987).

[14] R. Dingle, H. L. Störmer, A. C. Gossard, and W. Wiegmann, Appl. Phys. Lett. **33**, 665 (1978).

[15] S. Wang, *Fundamentals of Semiconductor Theory and Device Physics*, Prentice Hall, Englewood Cliffs, 1989.

[16] J. H. Davies, *The Physics of Low-Dimensional Semiconductors*, Cambridge University Press, Cambridge, 1998.

[17] W. Pan, H. L. Stormer, D. C. Tsui, L. N. Pfeiffer, K. W. Baldwin, and K. W. West, Phys. Rev. Lett. **90**, 016801 (2003).

[18] W. Pan, H. L. Stormer, D. C. Tsui, L. N. Pfeiffer, K. W. Baldwin, and K. W. West, Phys. Rev. Lett. **88**, 176802 (2002).

[19] R. Willett, J. P. Eisenstein, H. L. Stormer, D. C. Tsui, A. C. Gossard, and J. H. English, Phys. Rev. Lett. **59**, 1776 (1987).

[20] J. P. Eisenstein, R. Willett, H. L. Stormer, D. C. Tsui, A. C. Gossard, and J. H. English, Phys. Rev. Lett. **61**, 997 (1988).

[21] W. Pan, R. R. Du, H. L. Stormer, D. C. Tsui, L. N. Pfeiffer, K. W. Baldwin, and K. W. West, Phys. Rev. Lett. **83**, 820 (1999).

[22] M. P. Lilly, K. B. Cooper, J. P. Eisenstein, L. N. Pfeiffer, and K. W. West, Phys. Rev. Lett. **83**, 824 (1999).

[23] W. Pan, J. S. Xia, V. Shvarts, D. E. Adams, H. L. Stormer, D. C. Tsui, L. N. Pfeiffer, K. W. Baldwin, and K. W. West, Phys. Rev. Lett. **83**, 3530 (1999).

[24] J. P. Eisenstein, K. B. Cooper, L. N. Pfeiffer, and K. W. West, Phys. Rev. Lett. **88**, 076801 (2002).

[25] J. S. Xia, W. Pan, C. L. Vicente, E. D. Adams, N. S. Sullivan, H. L. Stormer, D. C. Tsui, L. N. Pfeiffer, K. W. Baldwin, and K. W. West, Phys. Rev. Lett. **93**, 176809 (2004).

[26] G. Gervais, L. W. Engel, H. L. Stormer, D. C. Tsui, K. W. Baldwin, K. W. West, and L. N. Pfeiffer, Phys. Rev. Lett. **93**, 266804 (2004).

[27] R. L. Willett, R. R. Ruel, K. W. West, and L. N. Pfeiffer, Phys. Rev. Lett. **71**, 3846 (1993).

[28] W. Kang, H. L. Stormer, L. N. Pfeiffer, K. W. Baldwin, and K. W. West, Phys. Rev. Lett. **71**, 3850 (1993).

[29] V. J. Goldman, B. Su, and J. K. Jain, Phys. Rev. Lett. **72**, 2065 (1994).

[30] J. H. Smet, D. Weiss, R. H. Blick, G. Lütjering, K. von Klitzing, R. Fleischmann, R. Ketzmerick, T. Geisel, and G. Weimann, Phys. Rev. Lett. **77**, 2272 (1996).

[31] S. E. Barrett, R. Tycko, L. N. Pfeiffer, K. W. West, Phys. Rev. Lett. **72**, 1368 (1994).

[32] G. Lampel, Phys. Rev. Lett. **20**, 491 (1968).

[33] N. W.Ashcroft and N. D. Mermin, *Solid State Physics*, Thomson Learning, (1976).

[34] S. E. Barrett, G. Dabbagh, L. N. Pfeiffer, K. W. West, and R. Tycko, Phys. Rev. Lett. **74**, 5112 (1995).

[35] A. Schmeller, J. P. Eisenstein, L. N. Pfeiffer, and K. W. West, Phys. Rev. Lett. **75**, 4290 (1995).

[36] E. H. Aifer, B. B. Goldberg, and D. A. Broido, Phys. Rev. Lett. **76**, 680 (1996).

[37] S. P. Shukla, M. Shayegan, S. R. Parihar, S. A. Lyon, N. R. Cooper, and A. A. Kiselev, Phys. Rev. B **61**, 4469 (2000).

[38] Y. P. Shkolnikov, S. Misra, N. C. Bishop, E. P. De Poortere, and M. Shayegan, Phys. Rev. Lett. **95**, 066809 (2005).

[39] D. R. Leadley, R. J. Nicholas, D. K. Maude, A. N. Utjuzh, J. C. Portal, J. J. Harris, and C. T. Foxon, Phys. Rev. Lett. **79**, 4246 (1997).

[40] K. S. Novoselov, D. Jiang, F. Schedin, T. J. Booth, V. V. Khotkevich, S. V. Morozov, and A. K. Geim, Proc. Nat. Acad. Sci. USA, **102**, 10451 (2005).

[41] C. Berger, Z. Song, T. Li, X. Li, A. Y. Ogbazghi, R. Feng, Z. Dai, A. N. Marchenkov, E. H. Conrad, P. N. First, W. A. de Heer, J. Phys. Chem. B, **108**, 19912 (2004).

[42] K. S. Novoselov, A. K. Geim, S. V. Morozov, D. Jiang, M. I. Katsnelson, S. V. Dubonos, and A. A. Firsov, Nature **438**, 197 (2005).

[43] Y. Zhang, Y.-W. Tan, H. L. Stormer, and P. Kim, Nature **438**, 201 (2005).

[44] Y. Zhang, Z. Jiang, J. P. Small, M. S. Purewal, Y.-W. Tan, M. Fazlollahi, J. D. Chudow, J. A. Jaszczak, H. L. Stormer, and P. Kim, Phys. Rev. Lett. **96**, 136806 (2006).

[45] F. Stern and W. E. Howard, Phys. Rev. **163**, 816 (1967).

[46] F. Stern and S. Das Sarma, Phys. Rev. B **30**, 840 (1984).

[47] F. C. Zhang and S. Das Sarma, Phys. Rev. B **33**, 2903 (1986).

[48] R. B. Laughlin, Phys. Rev. B **23**, R5632 (1981).

[49] B. I. Halperin, Phys. Rev. B **25**, 2185 (1982).

[50] R. B. Laughlin, Phys. Rev. Lett. **50**, 1395 (1983).

[51] J. K. Jain, Phys. Rev. Lett. **63**, 199 (1989); Physics Today **53**(4), 39 (2000); Physics E **20**, 79 (2003).

[52] J. K. Jain, Phys. Rev. B **41**, 7653 (1990).

[53] G. S. Jeon, J. K. Jain, Phys. Rev. B **68**, 165346 (2003).

[54] J. K. Jain and R. K. Kamilla, Int. J. Mod. Phys. **B11**, 2621 (1997); Phys. Rev. B **55**, R4895 (1997).

[55] G. Möller and S. H. Simon, Phys. Rev. B **72**, 045344 (2005).

[56] J. K. Jain, *Composite Fermions*, Cambridge University Press (2007).

[57] F. D. M. Haldane, Phys. Rev. Lett. **51**, 605 (1983)

[58] F. D. M. Haldane, in *The Quantum Hall Effect*, ed. by R. E. Prange and S. M. Girvin (Springer, New York, 1987).

[59] G. Fano, F. Ortolani, and E. Colombo, Phys. Rev. B **34**, 2670 (1986).

[60] P. A. M. Dirac, Proc. R. Soc. London, Ser. A **133**, 60 (1931).

[61] T. T. Wu and C. N. Yang, Nucl. Phys. B **107**, 365 (1976); Phys. Rev. D **16**, 1018 (1977).

[62] N. d'Ambrumenil and A. M. Reynolds, J. Phys. C: Solid State Phys. **21**, 119 (1988).

[63] V. W. Scarola, K. Park, and J. K. Jain, Phys. Rev. B **62**, R16259 (2000).

[64] A. A. Koulakov, M. M. Fogler, and B. I. Shklovskii, Phys. Rev. Lett. **76**, 499 (1996); M. M. Fogler, A. A. Koulakov, and B. I. Shklovskii, Phys. Rev. B **54**, 1853 (1996).

[65] A. H. MacDonald, Phys. Rev. B **30**, 3550 (1984).

[66] A. Wójs, Phys. Rev. B **63**, 125312 (2001); A. Wójs and J. J. Quinn, Physica E **12**, 63 (2002).

[67] E. H. Rezayi and F. D. M. Haldane, Phys. Rev. Lett. **84**, 4685 (2000).

[68] V. W. Scarola, K. Park, and J. K. Jain, Nature **406**, 863 (2000).

[69] K. Park, V. Melik-Alaverdian, N. E. Bonesteel, and J. K. Jain, Phys. Rev. B **58**, R10167 (1998).

[70] M. O. Goerbig, P. Lederer, and C. Morais-Smith, Phys. Rev. B **69**, 115327 (2004).

[71] G. S. Jeon, C-C. Chang, and J. K. Jain, Phys. Rev. B **69**, 241304(R) (2004); J. Phys: Condens. Matter **16**, L271 (2004).

[72] A. H. MacDonald and S. M. Girvin, Phys. Rev. B **33**, 4009 (1986).

[73] J. K. Jain and T. Kawamura, Europhys. Lett. **29**, 321 (1995).

[74] S.-Y. Lee, V. W. Scarola, and J. K. Jain, Phys. Rev. B **66**, 085336 (2002).

[75] G. Dev and J. K. Jain, Phys. Rev. Lett. **69**, 2843 (1992).

[76] V. W. Scarola, J. K. Jain and E. H. Rezayi, Phys. Rev. Lett. **88**, 216804 (2002).

[77] G. Moore and N. Read, Nucl. Phys. B **360**, 362 (1991).

[78] M. Greiter, X. G. Wen, and F. Wilczek, Phys. Rev. Lett. **66**, 3205 (1991); Nucl. Phys. B **374**, 567 (1992).

[79] M. Greiter, X. G. Wen, and F. Wilczek, Phys. Rev. B **46**, 9586 (1992).

[80] R. H. Morf, Phys. Rev. Lett. **80**, 1505 (1998).

[81] C. Nayak and F. Wilczek, Nucl. Phys. B **479**, 529 (1996).

[82] N. Read and E. Rezayi, Phys. Rev. B **54**, 16864 (1996).

[83] Y. Tserkovnyak and S. H. Simon, Phys. Rev. Lett. **90**, 016802 (2003).

[84] R. H. Morf, N. d'Ambrumenil, and S. Das Sarma, Phys. Rev. B **66**, 075408 (2002).

[85] T.-L. Ho, Phys. Rev. Lett. **75**, 1186 (1995).

[86] N. Read and E. Rezayi, Phys. Rev. B **59**, 8084 (1999).

[87] E. Rezayi and N. Read, cond-mat/0608346 (2006).

[88] S. Das Sarma, M. Freedman, and C. Nayak, Phys. Rev. Lett. **94**, 166802 (2005).

[89] A. Stern and B. I. Halperin, Phys. Rev. Lett. **96**, 016802 (2006).

[90] M. Freedman, C. Nayak, and K. Walker, Phys. Rev. B **73**, 245307 (2006).

[91] P. Bonderson, A. Kitaev, and K. Shtengel, Phys. Rev. Lett. **96**, 016803 (2006).

[92] P. Bonderson, K. Sthengel, and J. K. Slingerland, Phys. Rev. Lett. **97**, 016401 (2006).

[93] C. Bena and C. Nayak, Phys. Rev. B **73**, 133335 (2006).

[94] S. Das Sarma, E. H. Hwang, and W. K. Tse, cond-mat/0610581 (2006).

[95] V.P. Gusynin and S.G. Sharapov, Phys. Rev. Lett. **95**, 146801 (2005).

[96] K. Nomura and A. H. MacDonald, Phys. Rev. Lett. **96**, 256602 (2006);

[97] M. O. Goerbig, R. Moessner, and B. Douçot, Phys. Rev. B **74**, 161407 (2006).

[98] V. M. Apalkov and T. Chakraborty, Phys. Rev. Lett. **97**, 126801 (2006).

[99] E. H. Rezayi, Phys. Rev. B **36**, 5454 (1987); S. S. Mandal and J. K. Jain, *ibid.* **63**, 201310 (2001).

[100] A. H. MacDonald and S. M. Girvin, Phys. Rev. B **34**, 5639 (1986).

[101] K. Park and J. K. Jain, Phys. Rev. Lett. **80**, 4237 (1998).

[102] R. K. Kamilla, X. G. Wu, and J. K. Jain, Phys. Rev. Lett. **76**, 1332 (1996).

[103] G. W. Semenoff, Phys. Rev. Lett. **53**, 2449 (1984).

[104] F. D. M. Haldane, Phys. Rev. Lett. **61**, 2015 (1988).

[105] D. P. DiVincenzo and E. J. Mele, Phys. Rev. B **29**, 1685 (1984); N. H. Shon and T. Ando, J. Phys. Soc. Jpn. **67**, 2421 (1998).

[106] D.-H. Lee and C. L. Kane, Phys. Rev. Lett. **64**, 1313 (1990);

[107] K. Yang, S. Das Sarma, A. H. MacDonald, **74**, 075423 (2006).

[108] M. Hamermesh, *Group Theory and its Application to Physical Problems* (Addison-Wesley, Reading MA, 1962).

[109] C. Quesne, J. Math. Phys. **17**, 1452 (1976).

[110] K. T. Hecht and S. C. Pang, J. Math. Phys. **10**, 1571 (1968).

[111] S. L. Sondhi, A. Karlhede, S. A. Kivelson, and E. H. Rezayi, Phys. Rev. B **47**, 16419 (1993).

[112] K. Moon, H. Mori, K. Yang, S. M. Girvin, A. H. MacDonald, L. Zheng, D. Yoshioka, S-C. Zhang, Phys. Rev. B **51**, 5138 (1995).

[113] H. A. Fertig, L. Brey, R. Cote, A. H. MacDonald, Phys. Rev. B **50**, R11018 (1994).

[114] A. Wójs and J. J. Quinn, Phys. Rev. B **66**, 045323 (2002).

[115] R. K. Kamilla, X. G. Wu, and J. K. Jain, Solid State Commun. **99**, 289 (1996).

[116] A. F. Dethlefsen, R. J. Haug, K. Výborný, and O. Čertík, Phys. Rev. B **74**, 195324 (2006).

[117] J. K. Jain and X. G. Wu, Phys. Rev. B **49**, 5085 (1994).

[118] X. G. Wu, G. Dev, and J. K. Jain, Phys. Rev. Lett. **71**, 153 (1993).

[119] K. Park and J. K. Jain, Solid State Comm. **119**, 291 (2001).

[120] K. Park and J. K. Jain, Phys. Rev. B **62**, R13274 (2000).

[121] C-C. Chang and J. K. Jain, Phys. Rev. Lett. **92**, 196806 (2004).

[122] A. Lopez and E. Fradkin, Phys. Rev. B **69**, 155322 (2004).

[123] M. O. Goerbig, P. Lederer, and C. Morais-Smith, Phys. Rev. B **69**, 155324 (2004).

[124] S. S. Mandal and J. K. Jain, Phys. Rev. B **66**, 155302 (2002).

[125] S. S. Mandal and J. K. Jain, Solid State Commun. **118**, 503 (2001); Phys. Rev. Lett. **89**, 096801 (2002).

[126] T. Seki, Y. Kuramoto and T. Nishino, J. Phys. Soc. Jpn. **65**, 3945 (1996).

[127] P. A. Maksym, Phys. Rev. B **53**, 10879 (1996).

[128] W. Y. Ruan, Y. Y. Liu, C. G. Bao and Z. Q. Zhang, Phys. Rev. B **51**, R7942 (1995).

[129] C. Yannouleas and U. Landman, Phys. Rev. B **68**, 035326 (2003).

[130] V. Kalmeyer and S. C. Zhang, Phys. Rev. B **46**, R9889 (1992).

[131] B. I. Halperin, P. A. Lee, and N. Read, Phys. Rev. B **47**, 7312 (1993).

[132] H. Kjønsberg and J. Myrheim, Int. J. Mod. Phys. A **14**, 537 (1999).

[133] J.-N. Fuchs and P. Lederer, cond-mat/0607480 (2006).

[134] W. Ludwig and C. Falter, *Symmetries in Physics* (Springer, 2nd ed., 1995).

[135] M. Bajdich, L. Mitas, L. K. Wagner, and K. E. Schmidt, cond-mat/0610850 (2006).

Index

Vita

Name	Csaba Tőke
Date of Birth:	April 8, 1974
Place of Birth	Székesfehérvár, Hungary
Address:	Department of Physics
	104 Davey Lab, # 156
	The Pennsylvania State University
	University Park, PA 16802-6300
Telephone:	(814)8652811
E-mail:	tcs@phys.psu.edu
Webpage:	http://www.phys.psu.edu/~tcs

Education:	PhD candidate, The Pennsylvania State University, 2003 to 2007
	Master of Science, Eötvös University, Budapest, Hungary, 1992 to 1998
Employment:	Graduate Assitant, The Pennsylvania State University, 2003 to 2007
	Software Engineer, Ericsson Telecommunication Hungary Kft. 2000 to 2003
	Software Engineer, 3C Hungary Kft. 1999 to 2000
	Software Engineer, TCL Kft. 1998
Associations:	American Physical Society
	Referee for Phys. Rev. Lett. and Phys. Rev. B
Scholarships:	Duncan Fellowship (Spring 2004, Spring 2005, Spring 2006)
	Bradock Fellowship (Fall 2003)
Publications:	Refs. [1, 2, 3, 4, 5, 6, 7] in the Bibliography
	Gy. Szabó, Cs. Tőke, Phys. Rev. E, **58**, 69 (1998).